UNIVERSIDADE FEDERAL DO RIO GRANDE DO NORTE - UFRN

PROGRAMA DE PÓS-GRADUAÇÃO EM CIÊNCIAS E ENGENHARIA DE MATERIAIS - PPGCEM

Doctoral Thesis

Microscale evaluation of epoxy matrix composites containing thermoplastic healing agent

Érick Stéfano Silveira Guerra

Academic advisor:

Prof. Dr. José Daniel Diniz Melo

Academic co-advisor:

Prof. Dr. Ana Paula Cysne Barbosa

December 2022

Natal – RN – Brazil

ÉRICK STÉFANO SILVEIRA GUERRA

Microscale evaluation of epoxy matrix composites containing thermoplastic healing agent

Tese apresentada ao Programa de Pós-Graduação em Ciências e Engenharia de Materiais da Universidade Federal do Rio Grande do Norte como pré-requisito para a obtenção de Título de Doutor em Ciências e Engenharia de Materiais.

Orientador: Prof. Dr. José Daniel Diniz Melo

Coorientadora: Prof.ª Dr.ª Ana Paula Cysne Barbosa

COMISSÃO EXAMINADORA

Prof. Dr. José Daniel Diniz Melo - UFRN

Prof.ª Dr.ª Ana Paula Cysne Barbosa - UFRN

Prof.ª Dr.ª Laura Hecker de Carvalho - UFCG

Prof. Dr. Pedro Dolabella Portella - BAM

Dr. Gerhard Kalinka - BAM

Natal – RN

Dezembro 2022

Universidade Federal do Rio Grande do Norte - UFRN
Sistema de Bibliotecas - SISBI
Catalogação de Publicação na Fonte. UFRN - Biblioteca Central Zila Mamede

Guerra, Érick Stéfano Silveira.
Microscale evaluation of epoxy matrix composites containing thermoplastic healing agent / Érick Stéfano Silveira Guerra. - 2022.
97 f.: il.

Tese (doutorado) - Universidade Federal do Rio Grande do Norte, Centro de Tecnologia, Programa de Pós-graduação em Ciência e Engenharia de Materiais. Natal, RN, 2022.
Orientador: Prof. Dr. José Daniel Diniz Melo.
Coorientadora: Profa. Dra. Ana Paula Cysne Barbosa.

1. Compósitos de matriz epóxi - Tese. 2. Resistência interfacial - Tese. 3. Ligação fibra-matriz - Tese. 4. Autorreparo - Tese. I. Melo, José Daniel Diniz. II. Barbosa, Ana Paula Cysne. III. Título.

RN/UF/BCZM CDU 620.1(043.2)

Elaborado por Fernanda de Medeiros Ferreira Aquino - CRB-15/301

DEDICATED TO THE MEMORY OF

Alice Medeiros de Oliveira

☆ 1931 · ✝ 2021

ACKNOWLEDGMENTS

Gratitude is recognizing that this life is a present. So, full of this feeling, I come here to thank each one of the hands that helped me to make this work come true.

I would first like to thank my academic advisor, Professor José Daniel, for his inspirational way of doing science and also for coordinating so brilliantly the PRINT collaboration project between the Federal University of Rio Grande do Norte (UFRN – Brazil) and the Federal Institute for Materials Research and Testing (BAM – Germany), without which this study would not have even been imaginable.

Secondly, I would like to thank my academic co-advisor, Professor Ana Paula, whose expertise in formulating the research path of this work was invaluable. Her insightful feedback and precise supervision in Brazil and in Germany played a key role in the development of this Doctoral thesis.

I would also like to thank Dr. Gerhard Kalinka for his conspicuous and generous spirit of helping, which so many times brought light to uncleared questions and issues during the development of this work.

In Brazil, I would like to thank the technical support gently offered by Igor Zumba and José Roberto Filho. Their readily way of aiding and solving problems was vital to realize the laboratory activities. I would also like to thank the PRINT project assistance, represented by Professor Rubens Maribondo and the technical crew, represented by Márcia Aratusa and Mauriceia Medeiros.

In Germany, I would like to thank the welcoming assistance kindly offered by Professor Pedro Dolabella Portella, whose genuine devotion to the science is undoubtedly notorious by his acts. Moreover, his readiness to integrate both office and outland activities was fundamental to the progress of this work. Technical support offered by Martina Bistritz is something to always remember because of her unbelievable kindness and patience to try to overpass the speak barrier between us. In fact, *sie war meine beste Deutschlehrerin*.

I would also like to thank my doctoral colleague, Allana Azevedo, for all the moments we shared in laboratory experiments, foreign life experiences, and productive talks, which many times were a relief during this academic trajectory.

Furthermore, I would also like to thank Bruna Louise and Alexander Funk for their essential help in the kinetics of curing and microtomography analyses, respectively.

Last but not least, I would also like to thank my family and friends, especially my father, who spared no effort to help me achieve this stage of my life. I love you, Mr. Guerra.

ABSTRACT

Epoxy matrix composites are often subjected to adverse service conditions leading to the formation of microcracks. Microcracks are of great concern because they can act as nucleation sites for more prejudicial types of damage, such as delamination. Among the solutions to mitigate the deleterious effect of matrix microcracking is the use of thermoplastic healing agents. Poly(ethylene-co-methacrylic acid) (EMAA) has been particularly used as a thermoplastic healing agent because of its suitable chemical and physical properties. When the material is heated, the thermoplastic phase dispersed in the epoxy matrix is allowed to flow into microcracks and restore mechanical properties. The addition of EMAA particles, however, may alter chemical and thermomechanical properties of epoxy composites. These changes may also affect other fundamental features of epoxy composites, such as their fiber-matrix interfacial properties. Therefore, the objectives of this work are: (1) study the effects of EMAA addition on epoxy formation, (2) investigate the effect of EMAA addition on fiber-matrix interfacial properties, and (3) study the potential for self-healing through micromechanical testing. The effect of a 10 wt.% EMAA modified epoxy was investigated through infrared spectroscopy and differential scanning calorimetry (DSC) experiments. The results suggested that EMAA addition may cause changes during the epoxy network formation. Then, single fiber pull-out tests were used to characterize the fiber interfacial shear strength (IFSS) of pure and modified epoxy systems, as well as between fiber and pure EMAA. IFSS results of pure and modified epoxy were quite similar, revealing that epoxy modification did not significantly alter fiber-matrix interfacial properties. On the other hand, IFSS measurements of fiber-EMAA presented considerably lower values than fiber-epoxy, suggesting that healing is most likely held by fiber-epoxy or EMAA-epoxy interactions. A novel method to assess the healing efficiency (η) using optically monitored single fiber pull-out testing was proposed. According to the data obtained, healing efficiency of EMAA modified epoxy was lower than that of pure epoxy systems. The attenuated matrix shrinkage effect due to the addition of rubbery EMAA particles, along with the lower IFSS results of EMAA-fiber are proposed to explain the observed low η values. Complementary tests investigated thermomechanical properties and the curing of the EMAA modified epoxy, along with the effect of healing on the chemical structure and its IFSS properties.

Key words: Epoxy matrix composites, Interfacial strength, Fiber-matrix bond, Self-healing.

RESUMO

Compósitos de matriz epóxi estão regularmente submetidos a condições de trabalho adversas levando à formação de microtrincas. A presença de microtrincas é preocupante porque elas podem servir de sítios de nucleação para formas de danos mais prejudiciais, como delaminação. O uso de agentes de reparo termoplásticos está entre as principais soluções usadas para mitigar o efeito deletério das microtrincas. Poli(etileno-co-ácido metacrílico) (EMAA) tem sido particularmente usado como agente de reparo termoplástico em função de suas adequadas propriedades químicas e físicas. Quando calor é aplicado ao material, a fase termoplástica dispersa flui e preenche as microtrincas, assim recuperando as propriedades mecânicas. A adição de partículas de EMAA, no entanto, pode causar alterações nas propriedades químicas e termomecânicas do compósito epoxídico. Essas mudanças podem também afetar outras características fundamentais dos compósitos epoxídicos, como as propriedades interfaciais fibra-matriz. Os objetivos desse trabalho são, portanto, (1) estudar os efeitos da adição de EMAA na formação do epóxi, (2) investigar os efeitos da adição de EMAA nas propriedades interfaciais fibra-matriz e (3) estudar o potencial de autorreparo através de testes micromecânicos. O efeito da adição de 10% em peso de EMAA em epóxi foi investigado através das técnicas de espectroscopia do infravermelho e calorimetria diferencial exploratória (DSC). Os resultados sugerem que a adição de EMAA pode causar alterações na formação da rede epoxídica. Em seguida, testes de puxamento de fibra única foram usados para caracterizar a resistência ao cisalhamento interfacial (IFSS) entre fibra e os sistemas epoxídicos (puro e modificado), além de entre fibra e EMAA puro. Resultados de IFSS dos sistemas epoxídicos foram bastante similares, revelando que a modificação do epóxi não altera significantemente as propriedades interfaciais fibra-matriz. Contudo, medidas de IFSS entre fibra-EMAA apresentaram valores consideravelmente menores do que fibra-epóxi, sugerindo que a habilidade de reparo é provavelmente realizada pelas interações fibra-epóxi ou EMAA-epóxi. Um novo método para avaliar a eficiência de reparo (η) usando testes de puxamento de fibra única monitorados opticamente foi proposto. Resultados revelaram que o epóxi modificado com EMAA apresentou menores valores de η do que para o epóxi puro. As principais razões sugeridas para são a atenuação da contração de cura da matriz devido à presença das partículas borrachosas de EMAA e os baixos valores de IFSS obtidos entre fibra-EMAA. Testes complementares investigaram as propriedades termomecânicas e a cura do epóxi modificado com EMAA, assim como o efeito do reparo na estrutura química e nas propriedades IFSS.

Palavras-chave: Compósitos de matriz epóxi, Resistência interfacial, Ligação fibra-matriz, Autorreparo.

LIST OF FIGURES

Figure 1 - Schematic of curing and post-curing processes of an epoxy matrix. 3

Figure 2 - Epoxy employed as: (a) paints and coatings, (b) domestic repair adhesives, (c) electronic components, and (d) aerospace structures [15]. 5

Figure 3 - Schematic of the curing process in an epoxy-amine system [22]. 6

Figure 4 - Spectra of different epoxy monomers using (a) NIR [23] and (b) FTIR (adapted from [20]) techniques. 7

Figure 5 - Spectra of amine hardeners using (a) NIR and (b) FTIR techniques [20]. 8

Figure 6 - Epoxy curing monitoring using (a) NIR [27] and (b) FTIR (adapted from [25]) techniques. In (a) lighter curves indicate shorter times of curing. 8

Figure 7 - Standard procedure for characterization of the glass transition region of an hypothetical polymer [45]. 9

Figure 8 - DSC runs of dynamic heating ramps in an epoxy system [38]. 10

Figure 9 - Arrhenius curves of (a) Kissinger and (b) Ozawa-Flynn-Wall methods from a dynamic DSC runs of two different epoxy systems [39]. 10

Figure 10 - Hypothetical DSC curve showing the degree of curing of an isothermal scan [41]. 11

Figure 11 - Comparison between two typical models of degree of curing of an epoxy resin obtained from (a) non-isothermal and (b) isothermal scans [41]. 11

Figure 12 - Oscillating stress-strain curves for different mechanical behavior of: (a) a perfectly elastic material; (b) a perfectly viscous liquid; and (c) a viscoelastic material (Adapted from [47]). 12

Figure 13 - Typical DMA curves of epoxy composites: Storage modulus (*E'*), Loss modulus (*E''*), and damping factor (*tan δ*) [48]. 12

Figure 14 - Examples of microcracks after (a) fatigue test (adapted from [65]) and (b) hygrothermal aging (adapted from [33]). 13

Figure 15 - Crack density of epoxy composites and epoxy modified with different thermoplastics [66]. 14

Figure 16 - The main intrinsic mechanisms using thermoplastic healing agents: (a) viscous flow [76]; (b) molecular interdiffusion [100]; thermally reactive flow with (c1) poly (ε-caprolactone) (PCL) [84] and; with (c2) poly (ethylene-co-methacrylic acid) (EMAA) [86]. 17

Figure 17 - Test specimens configuration of epoxy polymer: (a) SENB [101] and (b) TDCB [102]. 18

Figure 18 - Schematic configuration of double cantilever beam testing [93]. 20

Figure 19 - (a) Schema of the X-ray microtomography technique, (b) 2D projections throughout the sample height and (c) Images obtained according to the number of angle views. (Adapted from [109]). 22

Figure 20 - X-Ray Microtomography of an EMAA modified epoxy showing the matrix (light gray regions), particles (dark gray regions) and bubbles (black regions) [89]. 22

Figure 21 - NIR spectra of thermoplastic healing agents dissolved in epoxy resin [83]. 23

Figure 22 - FTIR spectra of different microscopic regions of two given epoxy/PCL formulations [85]. 23

Figure 23 - (a) FTIR and (b) NIR spectra of EMAA modified epoxy with varying post-curing times [89]. 24

Figure 24 - FTIR spectra of EMAA films exposed to DGEBA (ED-50) and TETA (ET-50) at 50˚C [88] 25

Figure 25 - FTIR spectra of EMAA films exposed to DGEBA/TETA at 50˚C (EDT-50) and at 150˚C (EDT-150) [88] 25

Figure 26 - Main chemical interactions between carboxylic acid from EMAA and epoxy resin network [88]. 26

Figure 27 - Schema of EMAA-epoxy interphase according to EMAA particle size: (a) ≤ 125 μm and (b) ≤ 425 μm [110]. 26

Figure 28 - Examples of DMA curves of PBE modified epoxy with (a) non-functionalized PBE (adapted from [82]) and (b) PBE-Na ionomer [83]. 27

Figure 29 - DMA results of unmodified and PCL modified epoxy resin: (a) varying temperature runs [84] and isothermal results with varying PCL volume fraction (Adapted from [85]). 28

Figure 30 - DMA curves of modified epoxy systems with different thermoplastic healing agents: (a) storage modulus (E '), (b) tan δ [79]. 28

Figure 31 - Schematic illustration showing the difference between a three-dimensional interphase region (left) and a two-dimensional interface (right) [112]. 29

Figure 32 - Main interface bonding mechanisms: (a) chain entanglement; (b) electrostatic attraction; (c) interdiffusion; (d) chemical bonding; (e) reacting bonding and; (f) mechanical interlocking [111]. 30

Figure 33 - Schematic configuration of different pull-out tests: (a) restrained top fiber; (b) fixed bottom fiber and; (c) double pull-out with multiple embedded fibers [111]. 31

Figure 34 - Representative curve of a single fiber pull-out test (adapted from [111]). 31

Figure 35 - Effect of the embedded fiber length on interface bond strength in a carbon fiber-acrylic matrix composite [111]. 32

Figure 36 - Schematic illustration of deformation around a fiber embedded in a matrix under longitudinal tension [111]. 32

Figure 37 - Variations of fiber axial tension stress and interface shear strength (τ) throughout the embedded fiber length (l_i) [113]. 33

Figure 38 - Relationship between the embedded fiber length and the load to detach [113]. 33

Figure 39 - Topography of a glass fiber microindented [117] 34

Figure 40 - (a) Stages of a push-in test and (b) the resulting load-displacement curve [117]. 34

Figure 41 - Scanning electron micrographs of pushed-out glass fibers. (a) bottom surface, (b) top surface of the sheet [117]. 35

Figure 42 - (a) Stages of a push-out test and (b) the resulting load-displacement curve [117]. 36

Figure 43 - Single fiber push-in: (a) load-displacement curves of a pure epoxy sample, along with the fitting curve; and (b) corresponding image of the indented test specimen [99]. 37

Figure 44 - IFSS results of pure and different PCL modified epoxy systems [99]. 37

Figure 45 - Storage Modulus and *tan* δ curves of cured (a,b) and post-cured (c,d) of epoxy systems (preliminary studies). 41

Figure 46 - FTIR spectra of epoxy formulations, along with spectrum of pure EMAA thermoplastic: (a) full spectral range and (b) (1800-1400) cm^{-1} interval range (preliminary studies). 42

Figure 47 - DMA curves of pure and modified epoxy systems: (a) Storage Modulus and (b) Loss Modulus (complementary tests). 56

Figure 48 - Non-isothermal DSC curves for (a) pure epoxy and (b) modified epoxy systems (complementary tests). 57

Figure 49 - Slopes of $-ln(\beta/T_p^2)$ vs $1/T_p$ for pure and modified epoxy (complementary tests). 58

Figure 50 – Normalized curing conversion (α) over temperature for pure and modified epoxy (complementary results). 58

Figure 51 - FTIR spectra of all samples: (a) full range spectra and (b) 1800-1550cm^{-1} interval (complementary tests). 59

Figure 52 - Single fiber pull-out force-displacement curves: (a) pure epoxy, (b) 10 wt.% EMAA modified epoxy, (c) pure epoxy healed, and (d) modified epoxy healed (complementary tests). 60

Figure 53 - Analyses of pull-out test results for epoxy systems: (a) Average and standard deviation of IFSS values, (b) Maximum force (F_{max}) *vs* Embedded fiber area and (c) Embedded fiber length plot (complementary tests). 61

Figure 54 - Arrangement and dimensions of a single-lap shear specimen test. 63

LIST OF TABLES

Table 1 - Main effects of epoxy and hardener monomer structure [4–7]. 4

Table 2 - Main chemical groups mapped by infrared spectroscopy. 7

Table 3 - Main thermoplastic healing agents. 16

Table 4 - Main mechanical tests used to assess healing efficiency in epoxy polymers. 19

Table 5 - Main mechanical tests used to assess healing efficiency in epoxy composites. 21

Table 6 – Formulations of epoxy samples (preliminary studies). 40

Table 7 - Glass transition temperature (*Tg*) obtained from *tan δ* peaks of cured and post-cured epoxy formulations (preliminary studies). 42

Table 8 - Sample designations for FTIR measurements (complementary tests). 55

Table 9 - Number of IFSS samples for each condition tested (complementary tests). 55

Table 10 - DSC data of pure and modified epoxy systems (complementary tests). 57

LIST OF ABBREVIATIONS AND SYMBOLS

α	Curing conversion
β	Heating rate
ΔH	Heat of reaction
η	Healing efficiency
τ	Interfacial shear strength (IFSS)
χ	Degree of curing
ABS	Acrylonitrile butadiene styrene
ATR	Attenuated Total Reflectance
d, d_{fiber}	Fiber diameter
DCB	Double cantilever beam
DDS	4,4'-diaminodiphenyl sulfone
DETDA	Diethyl toluene diamine
DGEBA	Diglycidyl ether of Bisphenol A
DMA	Dynamic mechanical analysis
DSC	Differential scanning calorimetry
E'	Storage Modulus
E''	Loss Modulus
E_a	Activation energy
EMA	Poly(ethylene-co-methyl acrylate)
EMAA	Poly(ethylene-co-methacrylic acid)
EVA	Ehylene-vinyl acetate
F_{healed}	Maximum load after healing
F_{max}	Maximum load reached
$F_{original}$	Maximum load before healing
FTIR	Fourier transform infrared
G	Strain energy to failure, fracture toughness
H	Thickness of composite sheet
IFSS	Interfacial shear strength (τ)
ILSS	Interlaminar shear strength
k_1, k_2	Rate constant of curing kinetics
l, l_e	Embedded fiber length
m, n	Kinetics exponents constants
MW	Molecular weight
NIR	Near infrared
P	Generic mechanical property
PBE	Poly(bisphenol A-co-epichlorohydrin)
PCL	Poly(ε-caprolactone)
PEGMA	Poly(ethylene-co-glycidyl methacrylate)
PIPS	Polymerization-induced phase separated
PVB	Polyvinyl butyral
R	Ideal gas constant
SBS	Short beam shear
SEBS	Styrene-ethylene-butylene-styrene
$tan\ \delta$	Damping factor
TDCB	Tapered Double Cantilever Beam
TETA	Triethylenetetramine
Tg	Glass transition temperature
T_p	Temperature of exothermic peak

TABLE OF CONTENTS

ABSTRACT ..... **V**

RESUMO ..... **VI**

LIST OF FIGURES ..... **VII**

LIST OF TABLES ..... **XI**

LIST OF ABBREVIATIONS AND SYMBOLS ..... **XII**

1. Introduction **1**

2. Literature Review **3**

Epoxy matrix 3

Self-healing 14

Effect of thermoplastic healing agent addition on epoxy 21

Fiber-matrix interactions 29

Measuring fiber-matrix interfacial properties (micromechanical tests) 30

3. Objectives **38**

4. Preliminary studies **39**

Experimental 39

Preliminary results 40

Conclusions of the preliminary work 43

5. Paper: Microscale evaluation of epoxy matrix composites containing thermoplastic healing agent **44**

7. Complementary tests **53**

Experimental 53

Results 55

8. Conclusions **62**

9. Suggestions for future works **63**

Single-lap shear test: EMAA-epoxy interaction 63

Effect of multiple healings on epoxy 63

Effect of multiple healings on interfacial properties 63

Appendix A – Supporting information 64

References 72

1. Introduction

Epoxy matrix composites are among the most employed fiber-reinforced polymers in industry and academic research. Excellent mechanical properties, good chemical resistance, great versatility of composition and processing routes are the main characteristics that explain their wide application. Wind turbine blades, sporting goods, aerospace and transportation structures are among the applications of this material in primary structures.

Epoxy matrices are produced using a mixture of two chemical reactants – epoxy resin and hardener. When combined, the chemical reactants produce a solid highly crosslinked molecular structure. Due to this molecular network arrangement, epoxy matrices are brittle, which facilitates the nucleation of microcracks into their structure. The formation of microcracks may lead to more critical types of damage, such as delamination, thus decreasing the lifetime and reliability of epoxy-based components. Furthermore, these microcracks are typically difficult to be observed by non-destructive testing techniques, becoming hard to predict and, consequently, to be repaired by traditional repair methods.

The use of thermoplastic healing agents is one of the alternatives able to mitigate the microcrack problem in epoxy matrix composites. The method consists of adding thermoplastic healing agents to the epoxy chemical reactants during processing, allowing it to curing sequentially. The result is a solid epoxy network containing thermoplastic distributed throughout the epoxy structure. This way, when microcracks are formed, the thermoplastic healing agent can flow under high temperatures and infill damaged areas. When the system is cooled down, the thermoplastic mends the fractured surfaces, partially recovering the mechanical integrity of the material.

Poly(ethylene-co-methacrylic acid) (EMAA) is one of the most used thermoplastic healing agents reported in the literature. Low melting temperature and viscosity, high chemical affinity with epoxy network and thermally triggered mechanism of flow are some of the characteristics that favor the use of EMAA as a thermoplastic healing agent. However, adding EMAA into an epoxy matrix may lead to changes in the network formation, which, consequently, may change their properties. Alterations in chemical network, curing kinetics and thermomechanical properties are among the main changes thermoplastic addition may cause to the epoxy matrix.

In fiber reinforced epoxy composites, characteristics of the epoxy matrix are combined with fiber reinforcement properties to develop a synergy among the constituent materials. The result is a material with high specific properties such as elastic modulus, strength and toughness. These superior mechanical properties may be explained in part by the transfer of loads between fibers and matrix across the interface between these phase components. Therefore, the interfacial properties – along

with other properties – perform a decisive role in the mechanical response of epoxy matrix composites. Fiber-matrix interfacial properties may be evaluated by interfacial shear strength (IFSS) tests, in which single fibers are employed in micromechanical tests.

Considering that EMAA addition may affect the epoxy matrix properties and consequently change the fiber-matrix interface, this work investigates the effect of EMAA addition on IFSS properties of epoxy matrix composites. For this reason, alterations on an EMAA modified epoxy were first investigated using infrared spectroscopy, dynamic mechanical analysis (DMA) and differential scanning calorimetry (DSC) techniques. Then, the effect of EMAA addition on IFSS properties of epoxy is investigated using single fiber pullout tests. Finally, the effect of EMAA addition on healing ability of epoxy is investigated using a novel test method based on monitored single-fiber pull-out tests.

This work is divided in eight chapters, including this introductory Chapter 1. In Chapter 2, a literature review will be presented on topics such as epoxy matrices, self-healing in epoxy, effects of thermoplastic healing agent addition on epoxy, fiber-matrix interactions and interfacial properties. In Chapter 3, the objectives of this research are presented. In Chapter 4, preliminary results of prospecting tests are introduced. In Chapter 5, a journal paper containing the main research object of this doctoral thesis is presented. Complementary results are presented in Chapter 6 . Finally, Chapter 7 and Chapter 8 present the overall conclusions and suggestions for future works. The document also includes References and an Appendix with supporting information for the journal paper.

2. Literature Review

Epoxy matrix

Epoxies are polymers produced by a condensation reaction between an epoxy monomer and a hardener [1,2] (Figure 1). The epoxy monomer contains necessarily a minimum of two epoxide rings (Figure 1a). An epoxide ring is composed by a three-atoms (R'–O–R") cyclic ether. The hardener (Figure 1b) is also a monomer containing chemical groups that react with the epoxide ring, in a process called "curing".

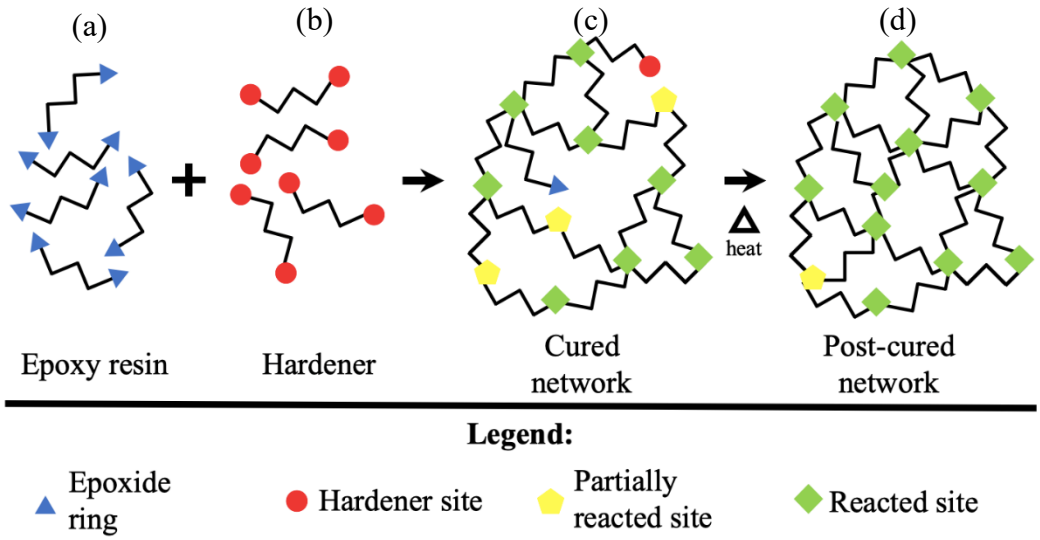

Figure 1 - Schematic of curing and post-curing processes of an epoxy matrix.

The result of the sequence of curing is a solid polymer with a three-dimensional molecular structure containing both reacted epoxy and hardener molecules forming a crosslinked network (Figure 1c). Post-curing heat treatments are normally used to allow unreacted and/or intermediate compounds promote further crosslink reactions [2] (Figure 1d). Examples of partially reacted sites can be found in Figure 3. Post-curing normally causes matrix shrinkage, as weak van der Walls bonds are converted into strong covalent bonds [3]. To avoid the deleterious consequences of matrix shrinkage, processing routes need to be planned when projecting composites goods.

Epoxy resins and hardener monomers are available in various molecular structures. Chain size (usually assigned by molecular weight – MW), the presence of aromatic groups, and the number of reactive sites are among the main criteria used to label both monomers. Table 1 summarizes the principal effects attributed by the main criteria of classification of epoxy and hardener monomers. A mixture of two or more types of resin or hardener monomers is an effective strategy to manipulate processing parameters and properties of crosslinked epoxy compounds [4,5]. In fact, many epoxy

resin systems commercially available are a mixture of different types of epoxy resins and hardeners, according to the intended application. For instance, the level of reactivity may affect the heat generated during curing and must be controlled to avoid overheat, which could be detrimental to epoxy matrix composites. Gel-time is another important parameter to ensure a satisfactory fiber impregnation, as it allows extending resin manipulation before the reacted structure makes it unfeasible.

Table 1 - Main effects of epoxy and hardener monomer structure [4–7].

Criteria	**Main effects**
Chain length	• Lower reactivity, the larger the chain • Lower crosslinking density, the larger the chain • Higher viscosity, the larger the chain • Longer gel-time, the larger the chain
Aliphatic chain	• Higher reactivity compared to aromatic • Higher density compared to aromatic • Heat-deformation at lower temperatures compared to aromatic • Lower viscosity compared to aromatic • Curing at room temperature
Aromatic groups	• Lower reactivity, steric hindrance effect • Increased gel-time compared to aliphatic • Need post-curing at high temperature • Higher glass transition temperature (*Tg*) compared to aliphatic
Number of reactive sites	• Higher reactivity, the more available reactive sites • Higher density of crosslinking, the more available reactive sites • Higher *Tg*, the more available reactive sites

The diversity of epoxy resin and hardener compositions, along with processing parameters, turn epoxy into a very versatile polymer. Epoxy products may be classified as traditional or high-performance applications. Traditional epoxies, with simpler chemical compounds, are generally designed for unsophisticated applications. On the other hand, high-performance epoxies of more complex structures exhibit better physical and chemical properties. Applications of epoxies without fiber-reinforcement include coatings (as corrosion barrier [8–10], electrical insulation [10–12] or encapsulation [10,13,14]) and domestic repair kits, adhesives or paintings [10,15]. Fiber-reinforced epoxy applications include the use of epoxy matrix in primary structures [4,6,15], such as wind turbine blades, aerospace and transportation components, and sporting goods. Examples of applications of epoxy-based components are shown in Figure 2.

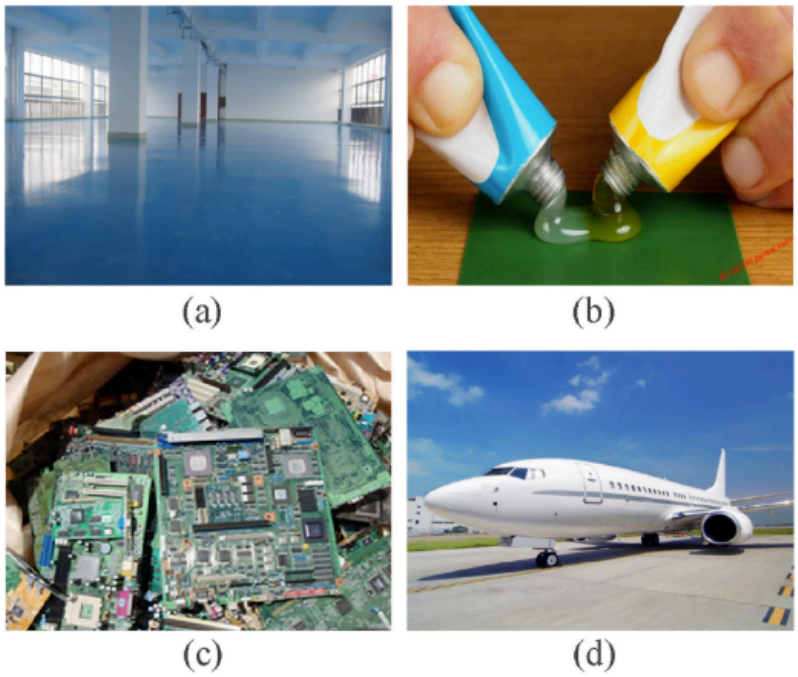

Figure 2 - Epoxy employed as: (a) paints and coatings, (b) domestic repair adhesives, (c) electronic components, and (d) aerospace structures [15].

Epoxy characterization

As previously discussed, the main characteristics of epoxy resins are driven by their crosslinked structure. Thus, monitoring the network formation – *i.e.* the curing reaction – is key to understand the properties of this material. Infrared spectroscopy, dynamic scanning calorimetry (DSC) and dynamic mechanical analysis (DMA) are among the most common techniques used to monitor curing and will be further addressed in this section. Other techniques include the use of ultrasonic spectroscopy [16], dielectric measurements [17], optical fiber strain measurements [18] and atomic force microscopy [19], to name a few.

Infrared spectroscopy

The principle of infrared spectroscopy is based on vibration of the molecules and atoms bonds in the region of infrared wavelength. Hence, infrared spectroscopy is widely used to monitor chemical groups in epoxy matrix structures [19–28]. Observing the changes in these groups gives important information of the most likely chemical reactions occurring to form the epoxy network. Epoxide rings, amine and hydroxyl groups are among the chemical groups involved in the curing process (Figure 3). Therefore, signal intensities in infrared spectra can be used to follow the progress of network formation.

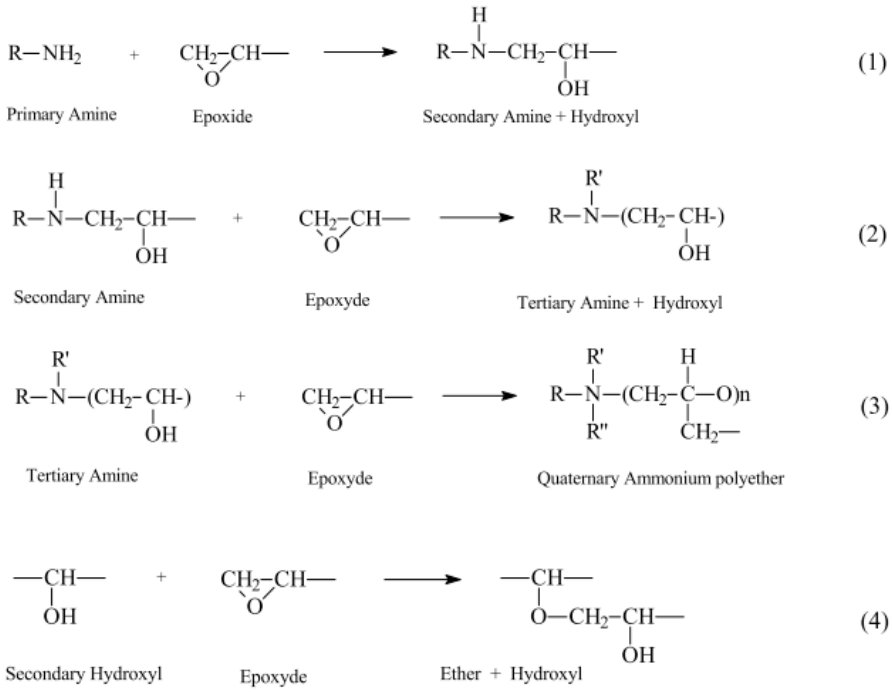

Figure 3 - Schematic of the curing process in an epoxy-amine system [22].

As shown in Figure 3, the epoxide ring initially reacts with a primary amine (1). The result is an intermediate structure containing a secondary amine group, which will further react with another epoxide ring (2). Both epoxide-primary amine or epoxide-secondary amine reactions continue until amine or epoxide are no longer able to react. Thus, more epoxy-amine consumed indicates a more crosslinked structure.

Intermediate compounds present during epoxy curing include hydroxyl (3) and secondary (2) and tertiary amine groups (Figure 3). These groups are known to participate in the latter stages of curing [22], in which normally heat is applied for molecules to react. Therefore, epoxide ring, amines (primary, secondary, and tertiary) and hydroxyl chemical groups are commonly used to investigate curing of epoxy networks using infrared spectroscopy [19–28].

Traditionally, infrared spectroscopy uses both near- and mid-infrared spectral window to observe the main chemical alterations related to the curing of epoxy. Table 2 summarizes the main chemical groups according to near-infrared (NIR) and Fourier transformed infrared (FTIR) characteristic wavenumbers. Due to the various types of monomers, some characteristic peaks may vary from one to another. For this reason, characteristic wavenumbers with large variation are presented in an interval range.

Table 2 - Main chemical groups mapped by infrared spectroscopy.

Chemical group	FTIR		NIR	
	Wavenumber (cm^{-1})	Reference	Wavenumber (cm^{-1})	Reference
Epoxide ring	910	[20,22,25]	4530	[20,24,27,28]
Primary amine	1500-1650	[20,22]	4902-4942	[20,24,27,28]
Secondary amine	1490-1580	[20,22]	6510-6525	[20,24,27,28]

Infrared spectra of different epoxy monomers are shown in Figure 4. Characteristic peaks of the epoxide ring in the resin monomers are shown using near- (Figure 4a) and mid-infrared (Figure 4b) techniques. The main bands representing the epoxide-ring in the near- and mid-infrared are 4530 cm^{-1} and 910 cm^{-1}, respectively. Among other important chemical groups present in the monomers structure are aromatic rings (NIR: 4065 cm^{-1}, 6060cm^{-1} / FTIR: 1530 cm^{-1}, 1608 cm^{-1}) and hydroxyl groups (NIR: 7028-7099 cm^{-1} / FTIR: 3500 cm^{-1}).

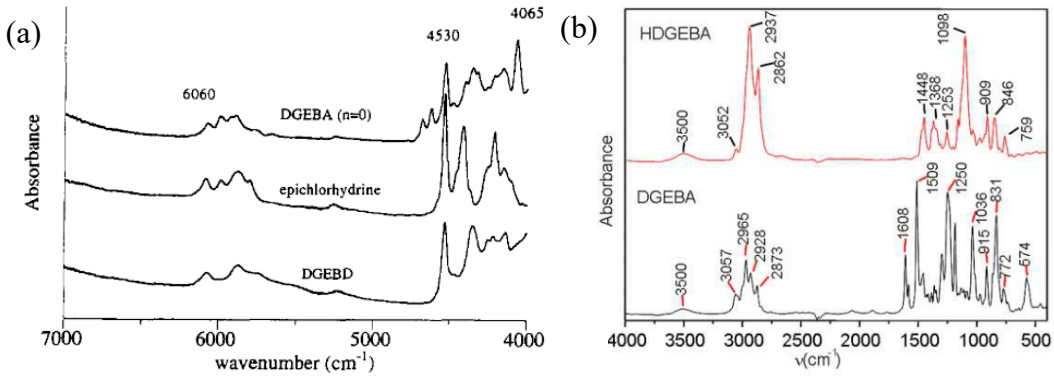

Figure 4 - Spectra of different epoxy monomers using (a) NIR [23] and (b) FTIR (adapted from [20]) techniques.

An example of an amine hardener spectrum is presented in Figure 5. In the NIR range, peaks of primary and secondary amine are located at 4935 cm^{-1} and 6510 cm^{-1}, respectively (Figure 5a). However, in FTIR spectra (Figure 5b), primary amine (1610 cm^{-1}) normally exhibit higher intensity signal as compared to the secondary amine (1490 cm^{-1}) [20]. Moreover, in FTIR, the band (3286-3354) cm^{-1} may be also related to amine groups, but in this case it can be affected by the overlap of strong hydroxyl infrared signal, limiting the use of these bands to quantitative studies [20].

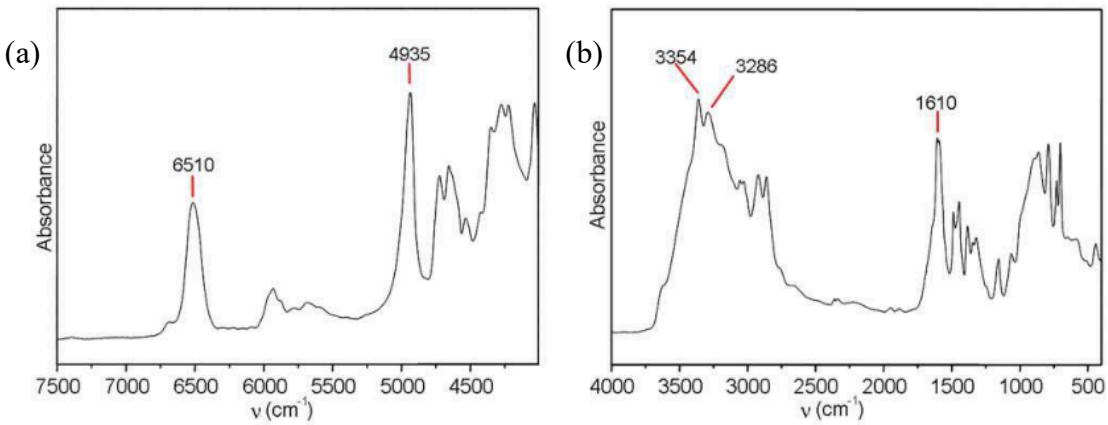

Figure 5 - Spectra of amine hardeners using (a) NIR and (b) FTIR techniques [20].

Two examples of epoxy curing monitoring using infrared spectroscopy [25,27] are presented in Figure 6. In NIR spectra (Figure 6a), the main alterations observed are the decrease in intensity of epoxy and amine peaks and an increase in intensity of hydroxyl groups. This indicates that the amount of these groups is altered during curing. On the other hand, due to the lower sensitivity to alterations in the concentration of the chemical groups, curing monitoring using FTIR spectra (Figure 6b) is more challenging. In this regard, the use of FTIR spectroscopy has been reported in literature as related to the peak band of the epoxide group (915 cm^{-1}) [20,22,25]. Traditionally, curing monitoring considers the area under of the absorption bands and a more complete understanding of this technique can be found in specialized literature [19–28].

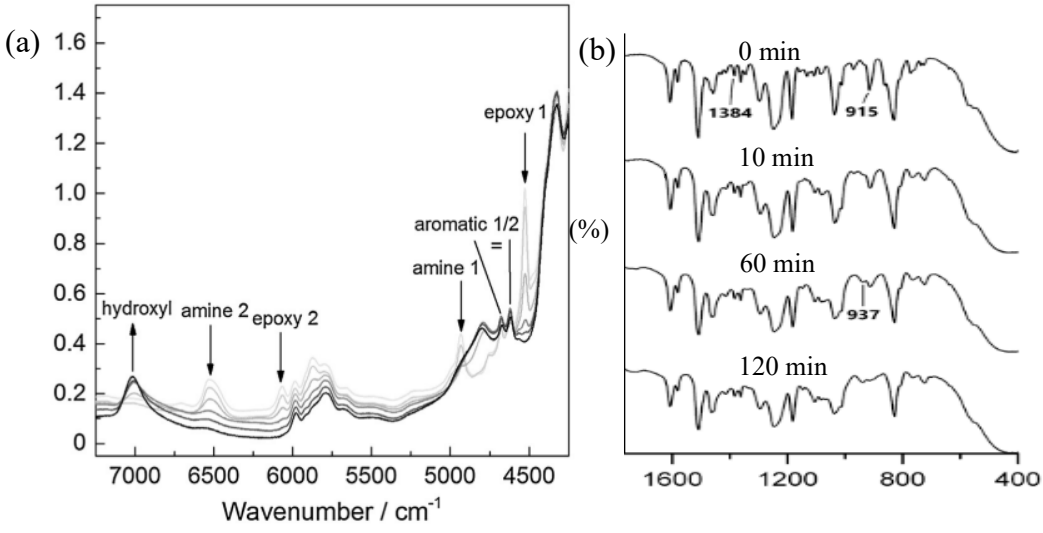

Figure 6 - Epoxy curing monitoring using (a) NIR [27] and (b) FTIR (adapted from [25]) techniques. In (a) lighter curves indicate shorter times of curing.

Infrared spectroscopy can also be used to monitor other changes occurring due to degradation of the epoxy network structure under aging conditions. Parameters used to produce accelerated aging effects can include the use of high temperature, which can be associated with others [29–31] such as

water condensation [32,33] or immersion [34]. Ultraviolet radiation can also be used to simulate aging conditions and promote photo-oxidation reactions, which can also be investigated using infrared spectroscopy [32,35].

Differential Scanning Calorimetry (DSC)

For epoxy-amine thermosets, DSC can be used to obtain information of the epoxy resin system [27,36–46] . Among the main results obtained from this technique are glass transition temperature (*Tg*) and curing characterization – such as heat of curing, maximum rate of curing, and degree of curing.

Tg characterizes the temperature range over which an amorphous material changes from a glassy state into a rubbery state as the temperature is increased. Thermal characterization of a polymer can be obtained by DSC run and its derivate (Figure 7) [45]. In this case, *Tg* is usually referred as the mid-point of the glass transition region. For a fully cured system, the glass transition temperature can be also represented by the maximum temperature over the glass transition region [27,41].

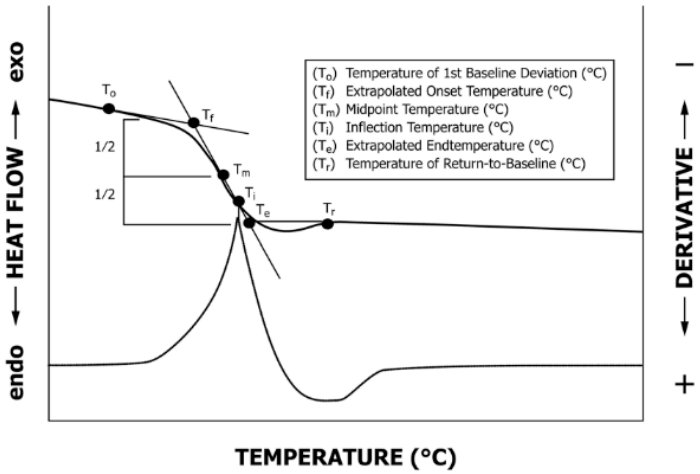

Figure 7 - Standard procedure for characterization of the glass transition region of an hypothetical polymer [45].

DSC thermal measurements of a not fully cured can also provide information regarding the degree of curing (α). This is because as curing proceeds new chemical bonds are formed, and the molecular structure becomes highly constrained, thus increasing *Tg*. In some cases, however, the determination of *Tg* of epoxy can be challenging due to endothermic relaxation events [27], such as the release of internal stresses, and the increase of molecular mobility, making the determination of *Tg* difficult.

Kinetics of curing measurements typically use two different routes: dynamic heating [27,36–44] or isothermal [41–43,46] temperature profiles. In dynamic heating routes, uncured epoxy is

subjected to various heating rates (β), from which DSC curves are plotted and the temperature of the exothermic peak (T_p) and total reaction enthalpy (ΔH, area under the exothermic peak) are obtained.

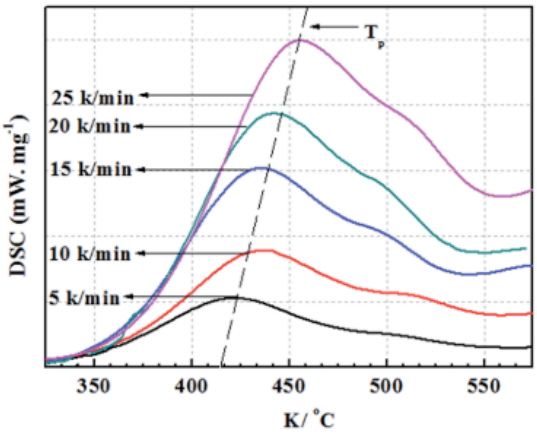

Figure 8 - DSC runs of dynamic heating ramps in an epoxy system [38].

The activation energy (E_a) is the minimum energy necessary for curing to occur. Thus, the higher the E_a, the more difficult is an epoxy system to curing. Activation energy (E_a) can be calculated from Arrhenius curves based on β, T_p and ΔH data. Kissinger and Ozawa-Flynn-Wall are among the main methods used to calculate the activation energy (E_a) of curing. Linear graphs (Figure 9) can be plotted, from which it is possible to obtain the E_a, along with the pre-exponential factor (A) of the curing [44].

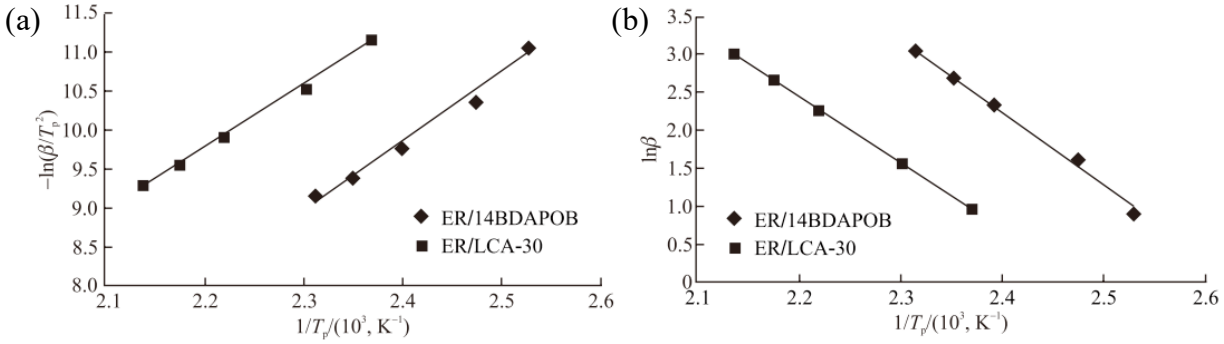

Figure 9 - Arrhenius curves of (a) Kissinger and (b) Ozawa-Flynn-Wall methods from a dynamic DSC runs of two different epoxy systems [39].

Isothermal methods [41–43,46], on the other hand, use constant temperature profiles to outline resin curing. In this case, uncured resin is placed into the DSC cell and the reaction is isothermally maintained at different temperatures until curing completion. Figure 10 shows a representative curing cycle using an isothermal run and the respective data obtained from this curve. Curing in the isothermal run is considered complete when no longer heat flow slopes are observed and the line becomes flat (horizontal). The total reaction enthalpy is obtained using a dynamic heating ramp after

isothermal measurements. In this case, the residual enthalpy is added to that obtained during the isothermal cycle.

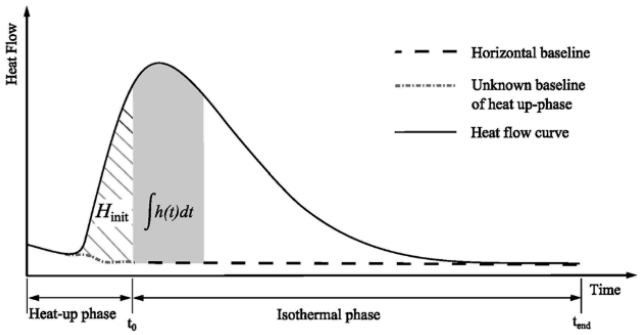

Figure 10 - Hypothetical DSC curve showing the degree of curing of an isothermal scan [41].

Kamal's method [46] is one of the most used kinetic models to describe the curing employing isothermal curves. This method has the advantage of obtaining a wider understanding of resin curing. This is because it provides more information of the curing process, such as their four fitting parameters (m and n constants, and A_1 and A_2 pre-exponential factors), and two associated activation energies (E_{a1} and E_{a2}). Therefore, relevant information of curing can be obtained, such as the description of the curing as nth order and/or autocatalytic. Figure 11 compares the isothermal and dynamic heating methods for the same epoxy systems in terms of degree of curing.

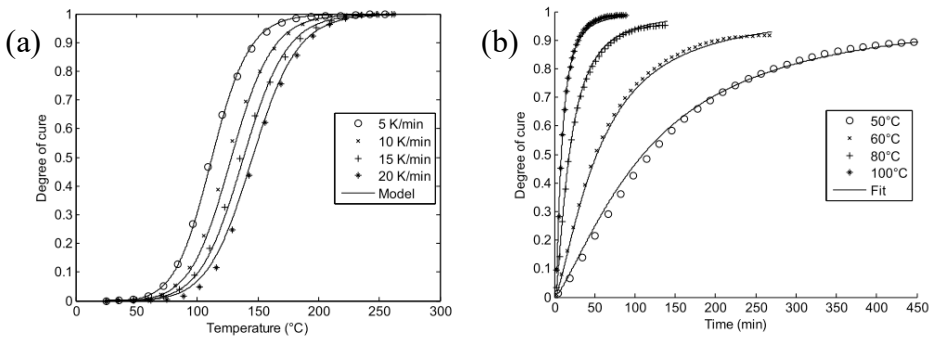

Figure 11 - Comparison between two typical models of degree of curing of an epoxy resin obtained from (a) non-isothermal and (b) isothermal scans [41].

Dynamical Mechanical Analysis (DMA)

Polymers, such as epoxy thermosets, exhibit both viscous and elastic characteristics when deformed under stress, known as viscoelastic behavior [47]. While an ideally elastic material under stress exhibits an immediate strain response following Hooke's law (Figure 12a), when a load is applied to a viscous liquid, the applied stress is proportional to the rate of strain and 90˚ out-of-phase with the strain (Figure 12b). Therefore, for a viscoelastic material, elastic and viscous components

act simultaneously and the applied excitation and the measured response are out-of-phase damp angle (δ) between 0˚ (perfectly elastic) and 90˚ (perfectly viscous) (Figure 12c).

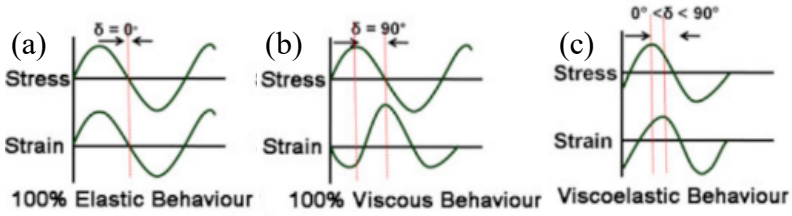

Figure 12 - Oscillating stress-strain curves for different mechanical behavior of: (a) a perfectly elastic material; (b) a perfectly viscous liquid; and (c) a viscoelastic material (Adapted from [47]).

Viscoelastic properties are often investigated as a function of temperature, frequency, and time [48]. Thus, in a typical dynamic mechanical analysis (DMA) an oscillating load or displacement is applied to a specimen and the material response is measured over ranges of temperature or frequency. Viscoelastic properties can be obtained using rheometers [49–52] or dynamic mechanical analyzers [53–59].

The material response is normally determined by measuring storage modulus (*E'*) and loss modulus (*E"*), related to the elastic and viscous behavior, respectively, and the loss factor (*tan δ*), as the ratio between loss and storage moduli (*tan δ = E"/E'*). *Tan δ* values are indicative of the energy dissipation of a material [48]. Typical DMA curves of epoxy-matrix composites are presented in Figure 13.

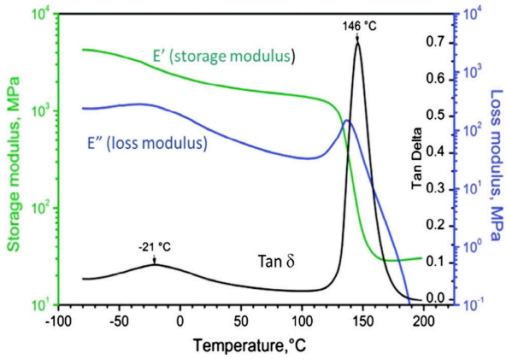

Figure 13 - Typical DMA curves of epoxy composites: Storage modulus (*E'*), Loss modulus (*E"*), and damping factor (*tan δ*) [48].

DMA curves provide important information about the main transitions a polymer can undergo. It is usually employed to characterize the glass transition temperature (*Tg*), which is directly related to the crosslink density and mobility of the network structure [51]. *Tg* is the temperature range above which the polymer network exhibits rubbery behavior. Further, DMA can also provide information of secondary transitions, which are related to a variety of movements of side chains and small groups

of backbone atoms. Thus, DMA provides important information to characterize the thermomechanical properties of epoxy-based composites and, therefore, to predict the temperature dependence of their mechanical properties. Therefore, DMA data allow the determination of optimal operational conditions, such as service temperature, applied stress and loading frequency, along with interactions between the composite constituents [47]. Studies on thermal degradation [60] are also commonly carried out in this regard.

Studies of epoxy resin using DMA also include investigations of the curing process, such as the type of epoxy or hardener used [49], the effect of the epoxy content [56], and post-curing monitoring [57]. The addition of a thermoplastic second-phase [50,52,56], the use of epoxidized resins [55,59], and the use of shape memory polymers [53] are among the investigations of epoxy modification using DMA. Regarding epoxy composites, the reinforcement content [58,61] and fiber configuration [54] are the common parameters studied using this technique. A list of DMA applications can be found in [48].

Microcracking

During service life, microcracks may be formed in epoxy matrix composites. Cyclic, static and impact loads, along with environmental conditions are among the main causes of microcracks in these materials [62]. Studies of the formation of microcracks may employ different mechanical conditions varying from fatigue to long-term loading tests. Environmental conditions used may involve moisture variation, high temperatures, chemicals, and ultraviolet radiation to simulate the effects of aging on microcracks formation. A literature review concerning matrix microcrack formation can be found in previous references [62–64]. Examples of microcracks in epoxy matrix composites are presented in Figure 14.

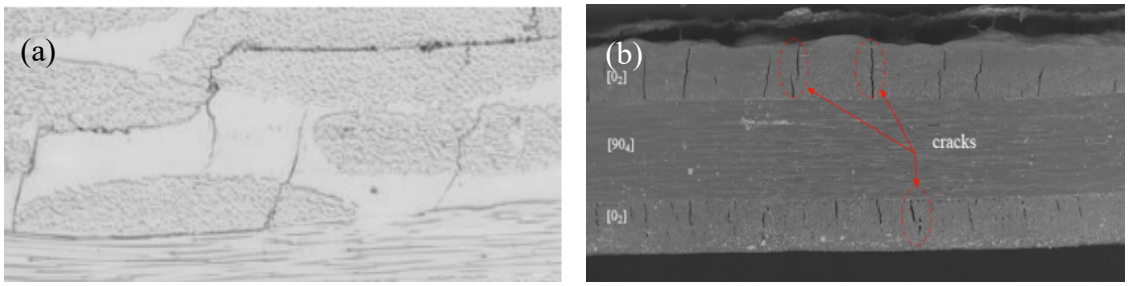

Figure 14 - Examples of microcracks after (a) fatigue test (adapted from [65]) and (b) hygrothermal aging (adapted from [33]).

The initial effects of microcrack formation may be minor and are commonly related to slight alterations in viscoelastic properties, thermal expansion coefficient, and Poisson's ratio. This means that the deleterious effects of microcracks in composites structures may be tolerable (except in

applications in which sealing is crucial) [63]. However, microcracks can be precursors of events which can ultimately lead to failure in polymer composites [62]. In fact, the coalescence of microcracks can lead to matrix macrocracks, fiber-matrix interfacial debonding, fiber breakage, and ply delamination. Due to inhomogeneity, these types of damage may occur simultaneously, randomly, or sequentially and lead to composite failure.

If microcrack formation in epoxy-based composites is not prevented, retardation of matrix cracking can be achieved through the of use of appropriate chemical reactants (epoxy monomers and hardeners), additives and thermoplastic modifiers [64]. In Figure 15, crack density of a standardized damaged sample and the use of thermoplastic modifiers is presented. Thermoplastic modification of epoxy may result in improved impact strength and lower coefficient of thermal expansion.

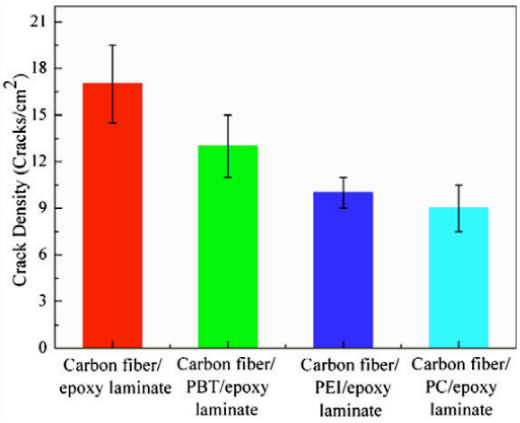

Figure 15 - Crack density of epoxy composites and epoxy modified with different thermoplastics [66].

Microcracks are difficult to be detected by non-destructive testing due to their submicroscopic dimension and the heterogeneous nature of epoxy composites [64]. Additionally, traditional repair techniques are quite ineffective for mitigating the constraints of matrix microcracks, due to the same geometric and non-homogeneous situations [67]. Therefore, the use of self-healing materials is a promising solution for matrix microcracks.

Self-healing

Self-healing composites have the inherent capacity to recover the ability to bear loads after damage [67]. The mechanisms of self-healing of thermoset polymers can be divided into two broad categories: extrinsic (or autonomic) and intrinsic (or non-autonomic) [68,69]. Extrinsic self-healing mechanisms are those where external interventions are not necessary and repair occurs autonomously. In this mechanism, reservoirs containing liquid healing agents are embedded within the thermoset matrix. When a crack in propagation meets and breaks these reservoirs, healing agent is released into

the crack plane. Then, the healing agent hardens in contact with hardeners or catalysts (also dispersed in the matrix), thereby infilling and closing the crack. Thus, mechanical properties of the damaged area are partially recovered. The main examples of extrinsic mechanisms include the use of vascular systems [70] and microcapsules [71].

On the other hand, intrinsic self-healing mechanisms have the inherent ability to repair without any addition of reservoirs containing dispersed liquid reactants in the matrix. In this case, intrinsic mechanisms require external intervention and, for this reason, they are also usually called non-autonomic mechanisms. Typically, stimuli such as heat or radiation are used to trigger the healing mechanism. Examples of intrinsic mechanisms include the use of thermoreversible reactions [72–75] and the addition of thermoplastic healing agents into the thermoset matrix [76–94]. In contrast to the extrinsic mechanisms, in the intrinsic self-healing mechanisms the matrix keeps latent the healing ability, even after multiple healing cycles. Previous studies about self-healing in epoxy composites are available in the literature [67–69,95–98].

Intrinsic self-healing mechanisms can further be subdivided into four categories: (i) thermally reversible reactions [72–75]; (ii) viscous flow [76,77,79,80]; (iii) molecular interdiffusion [81–83] and; (iv) thermally reactive flow [76–79,83–93]. Moreover, the thermally reactive flow may be categorized in two other subtypes: (a) polymerization-induced phase separation (PIPS) and (b) addition of immiscible thermoplastics.

Thermoplastic healing agents

All intrinsic self-repair mechanisms employ the addition of thermoplastic healing agents to thermosetting matrices typically used in industry, with the exception of thermoreversible reactions. Thus, the use of thermoplastic healing agents is more attractive than the use of new thermoreversible matrices, which would require new processing routes.

Table 3 lists the main thermoplastics used as healing agents. Figure 16 shows schematically the main healing mechanisms with the addition of thermoplastic agents.

Table 3 - Main thermoplastic healing agents.

Intrinsic self-healing mechanism	Thermoplastic	References
Viscous flow*	Pre-polymerized epoxy particles	[76]
	Ethylene-vinyl acetate (EVA)	[77,79,80]
	Acrylonitrile butadiene styrene (ABS)	[77,79]
	Polyvinyl butyral (PVB)	[79]
	Styrene-ethylene-butylene-styrene (SEBS)	[79]
Molecular interdiffusion	Poly(bisphenol A-co-epichlorohydrin) (PBE)	[81–83]
Thermally reactive flow	Poly(ε-caprolactone) (PCL)**	[84,85,99]
	Poly(ethylene-co-methacrylic acid) (EMAA)*	[76–87,93]
	Poly(ethylene-co-methyl acrylate) (EMA)*	[91]
	Poly(ethylene-co-glycidyl methacrylate) (PEGMA)*	[77,79,80]

* Immiscible thermoplastic.

** Polymerization-induced phase separated (PIPS) thermoplastic

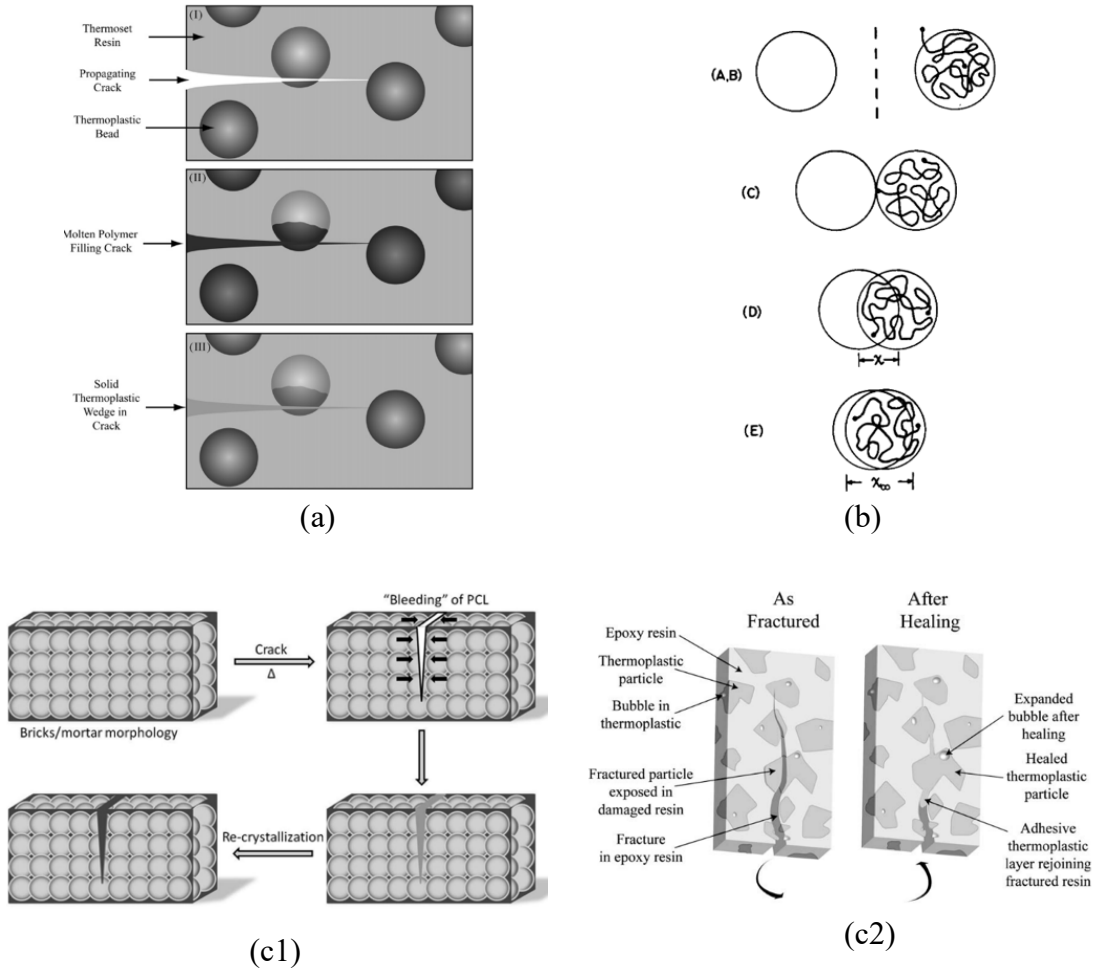

Figure 16 - The main intrinsic mechanisms using thermoplastic healing agents: (a) viscous flow [76]; (b) molecular interdiffusion [100]; thermally reactive flow with (c1) poly (ε-caprolactone) (PCL) [84] and; with (c2) poly (ethylene-co-methacrylic acid) (EMAA) [86].

Healing assessment

The healing assessment of epoxy using thermoplastic healing agents can be obtained by various test methods. Fracture toughness tests are often used for healing assessment because of the advantage of forming pre-determined and reproducible damages, which are intended to be healed. In any case, samples (damaged or not) are subjected to stress loading followed by healing cycle(s). Depending on the test, complete failure may occur and, in this case, intimate contact between the fractured surfaces is necessary, prior to healing.

Healing efficiency (η) is mostly assessed by comparing a property (P) of a healed sample to its original condition, before damage occurs, as described in Eq. 1.

$$\eta = \frac{P_{healed}}{P_{original}} \times 100\% \quad \text{(Eq. 1)}$$

Furthermore, the sequence of healing events can also be assessed in terms of healing efficiency [86,90]. In that case, $P_{1st\ heal}$, $P_{2nd\ heal}$ … P_{n-heal} are commonly compared to $P_{original}$.

The next sessions will cover the main tests used to assess the healing efficiency. Tests will be divided in two main groups according to the configuration epoxy-based materials, that is, epoxy polymers and epoxy composites.

Healing efficiency in epoxy polymers

Typical tests used in the literature for the assessment of healing efficiency in thermoset modified matrices are the Single-Edge Notched Beam (SENB) [77,79,84] and Tapered Double Cantilever Beam (TDCB) [85,86]. Specimen configurations for these tests are described in Figure 17. Both tests SENB and TDCB use principles of fracture mechanics and act in fracture mode I.

Table 4 summarizes the main tests used to assess self-healing efficiency in thermosetting matrices.

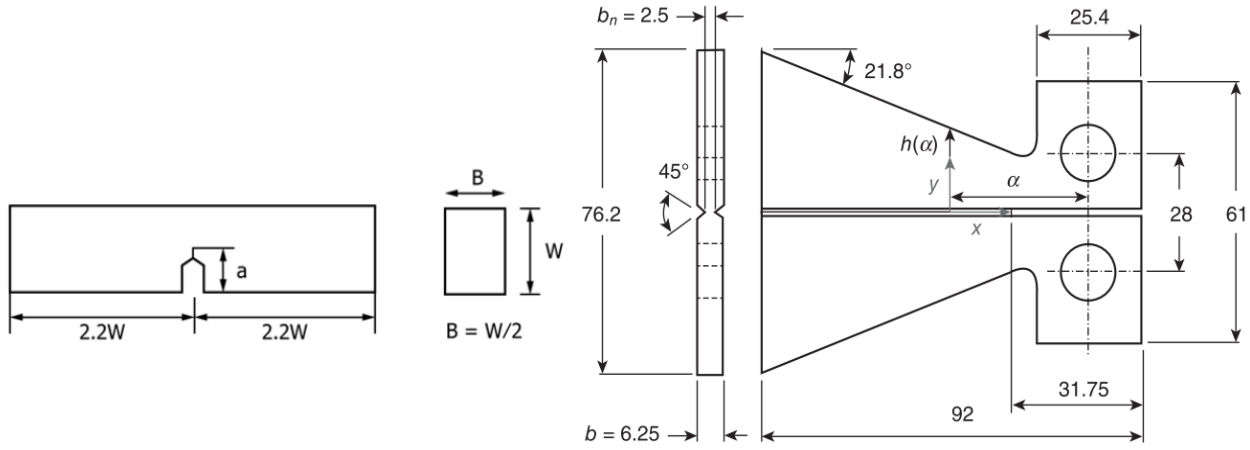

Figure 17 - Test specimens configuration of epoxy polymer: (a) SENB [101] and (b) TDCB [102].

Table 4 - Main mechanical tests used to assess healing efficiency in epoxy polymers.

Mechanical test	Healing modifier	Epoxy resin	Ref
Single edge-notched beam (SENB)	EMAA	DGEBA/TETA	[86,89]
	PCL	DGEBA/DDS	[84]
	EMAA, PEGMA, ABS and EVA	DGEBA/TETA	[77]
	EMAA, PEGMA, ABS, EVA, SEBS and PVB	DGEBA/TETA and DGEBA/DETDA	[79]
	EMAA + Low-molecular PBE	DGEBA/TETA	[103]
	Phenoxy resin + Low-molecular PBE	DGEBA/DETDA	[83]
Tapered double cantilever beam (TDCB)	EMAA	DGEBA/TETA	[86]
	PCL	DGEBA/DDS	[85]

In SENB test configuration (Figure 17a), a rectangular beam is notched and pre-cracked at the mid-plane and subjected to 3-point bending load. After a given displacement is reached, based on the point where there is a given drop in the maximum stress [84], the test is interrupted and the sample is subjected to a healing cycle. After the healing cycle, the test is repeated and strain energy to failure (G_{IC}) or peak load (P_{max}) of original and healed samples are compared.

Pre-notches of SENB specimens can be partially closed after a healing cycle, thus affecting the calculations, which can be a concern for SENB tests. However, TDCB testing configuration has the advantage of using a specimen geometry to determine fracture toughness regardless of crack length, contrasting with tensile, compression or bending sample geometries [102]. In TDCB tests, the specimen is also notched and pre-cracked, but due to its geometry (Figure 17b), the larger is the crack opening displacement, the greater is the resistance to plastic deformation [104].

Healing efficiency in epoxy composites

The main test used to assess healing efficiency in fiber reinforced epoxy is the double cantilever beam (DCB), which also uses the principles of fracture toughness, acting in fracture mode I. Among the reasons for the use of DCB test is the relative ease of sample preparation, which basically consists of adding healing agent to the mid-plane of a laminate test specimen in which

damage followed by repair will take place. Figure 18 shows schematically the mechanism of this test. Normally, a pre-crack is obtained by placing a thin film of non-adhesive material on the mid-plane of the samples, which are then loaded to obtain a controlled crack-growth. At each increment of cracking growth, its respective applied load (P), crack opening displacement (δ) and crack length (a) are recorded to obtain fracture toughness (G) measurements (Eq. 4). Healing efficiency is generally assessed by comparing values of fracture toughness before and after a healing cycle.

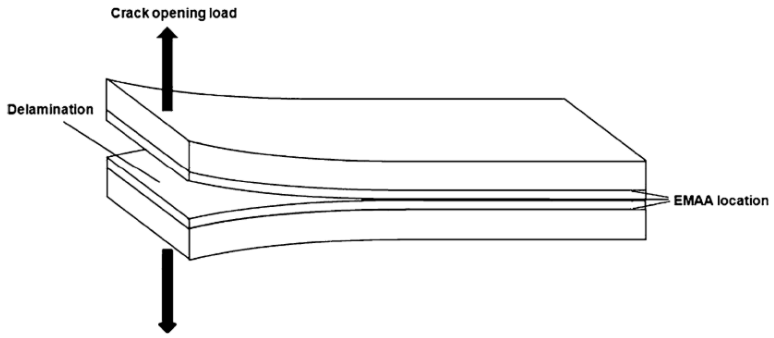

Figure 18 - Schematic configuration of double cantilever beam testing [93].

$$G = \frac{3P\delta}{2b(a + |\Delta l|)} \quad \text{(Eq. 4)}$$

where $|\Delta l|$ is a correction factor that takes into account the rotation effects in the crack-tip.

The main tests used to assess healing efficiency in polymer matrix composites with thermoplastic additions are summarized in Table 5.

Table 5 - Main mechanical tests used to assess healing efficiency in epoxy composites.

Mechanical test	Healing modifier	Composite constituents	Ref
Double cantilever beam (DCB)	EMAA particles and fibers	DGEBA/TETA + carbon fiber	[87,90,93]
	EMAA fibers	Carbon fiber-epoxy prepreg	[92,94]
	Particles of EMAA, PEGMA, EVA and ABS	DGEBA/TETA + carbon fiber	[77]
	EMAA particles	High performance epoxy + carbon fiber	[78,105]
	EMAA and EMA films	Carbon fiber-epoxy prepreg	[91]
	EMAA fabric	High performance epoxy + carbon fiber	[106]
Static three-point bending and Tensile fatigue	Epoxy pre-polymer particles	Non-specified epoxy + glass fiber	[76]
Falling weight impact	PBE	DGEBA/NMA + glass fiber	[82]
Tensile and Compression	Particles of EMAA, PEGMA and EVA	DGEBA/TETA + carbon fiber	[80]
Short beam shear (SBS)	EMAA and EMA films	Carbon fiber-epoxy prepreg	[91]
Interlaminar shear strength (ILSS)	EMAA particles	Carbon fiber-epoxy prepreg	[107]

Effect of thermoplastic healing agent addition on epoxy

Thermoplastic modified epoxy can be characterized through various techniques. In this section, the main alterations the addition of thermoplastic healing agents may cause in epoxy are addressed.

Particle distribution

X-Ray microtomography is one of the more complete non-destructive inspection techniques [108]. In this technique, a collimated X-ray beam crosses the analyzed material, and a detector on the other beam axis collects it (Figure 19a). Due to different attenuation effect according to the atomic number and density of the material [108,109], a 2D image is created on the detector. In addition, a 3D image may be obtained from two complementary sample movements: (1) through the height (Figure 19b) and (2) the rotation angle (Figure 19c).

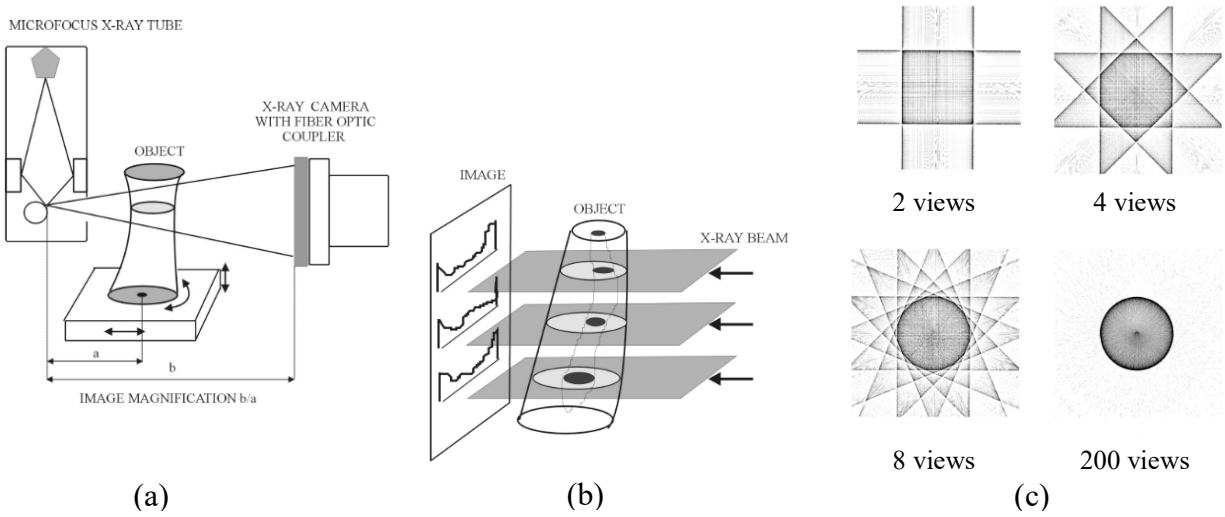

Figure 19 - (a) Schema of the X-ray microtomography technique, (b) 2D projections throughout the sample height and (c) Images obtained according to the number of angle views. (Adapted from [109]).

The technique then computes images from all planes. Finally, it creates a virtual 3D image, determining the thermoplastic particles' distribution, size, and morphology throughout the sample. An example of a 2D epoxy characterization using X-ray microtomography is shown in Figure 20.

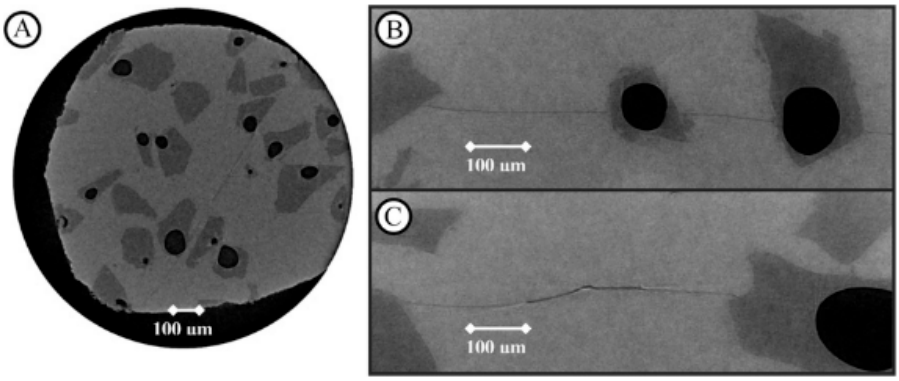

Figure 20 - X-Ray Microtomography of an EMAA modified epoxy showing the matrix (light gray regions), particles (dark gray regions) and bubbles (black regions) [89].

Chemical structure

Chemical alterations in epoxy network are mostly analyzed using infrared spectroscopy, either by (i) Fourier transformed infrared (FTIR) or (ii) near infrared (NIR). Both techniques are used to compare the concentration of epoxide and amine functional groups, as well as to examine the main alterations in functional groups of epoxy and/or thermoplastics molecules.

In the case of addition of **molecular interdiffusion thermoplastics (**Table 3), NIR was used to confirm that no relevant alterations on epoxide (band 4500-4600 cm^{-1}) or secondary amine and

hydroxyl (band 6500-7100cm^{-1}) groups are observed, indicating that the thermoplastic addition has minor effects on the formation of epoxy network [83]. An example of NIR spectra of dissolved thermoplastics is presented in Figure 21. It can be observed that even after a healing event, (orange curve) no significant alterations on spectra are observed. Furthermore, this result also confirms that healing events using dissolved thermoplastics occur most likely by physical process rather than chemical bonding.

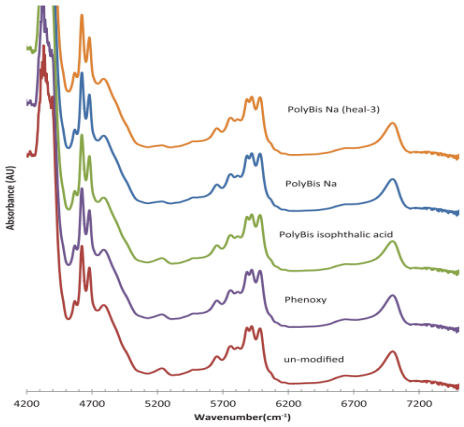

Figure 21 - NIR spectra of thermoplastic healing agents dissolved in epoxy resin [83].

In the case of modified epoxy by **polymerization-induced phase separated (PIPS) thermoplastic (**Table 3), FTIR spectroscopy was used to inspect the chemical composition of different phases in the thermoplastic-thermosetting network [85]. Therefore, morphology of the phase domains can be characterized (Figure 22). In that case, specific regions of the spectra associated to the characteristic carbonyl stretch band (1680-1780 cm^{-1}) from PCL were analyzed [85].

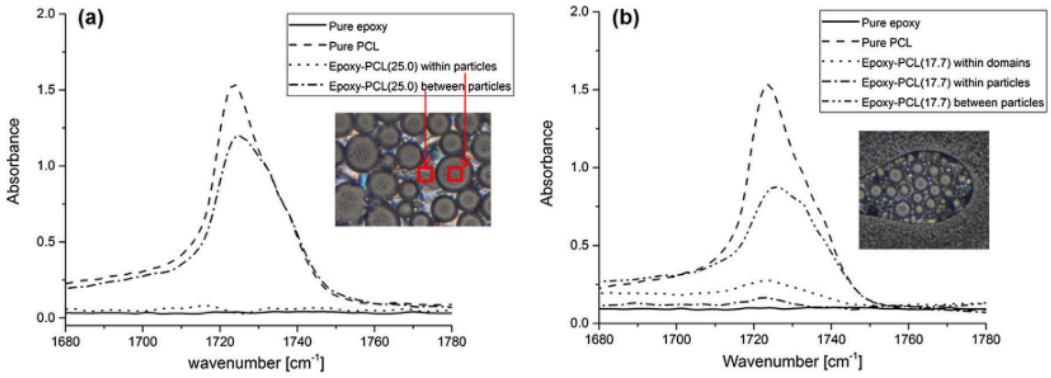

Figure 22 - FTIR spectra of different microscopic regions of two given epoxy/PCL formulations [85].

In the case of addition of **thermally reactive immiscible thermoplastics (**Table 3), a previous study [89] used both FTIR and NIR spectroscopy to monitor the interfacial strength between EMAA and epoxy, in terms of epoxide, amine and hydroxyl group concentrations. This was achieved by varying time of post-curing at 150 ˚C and inspecting alterations in these functional groups. Results

suggest that the epoxy resin has reacted with EMAA at post-curing temperature promoting a better adhesion between them (Figure 23). Similar results were found in literature, in which different molecular weight EMAA thermoplastic [103] and high-performance epoxy resins [78] were used.

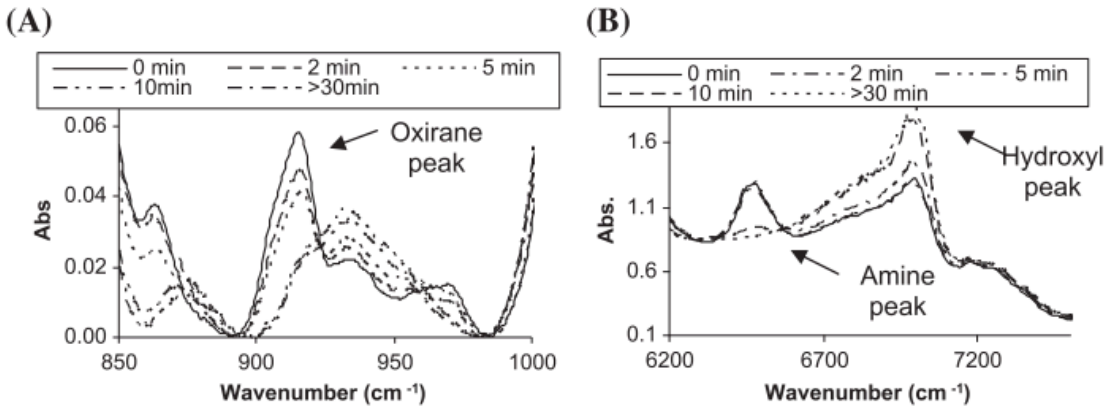

Figure 23 - (a) FTIR and (b) NIR spectra of EMAA modified epoxy with varying post-curing times [89].

In another study [88], FTIR spectroscopy was used to determine chemical reactions and interactions associated to the EMAA and epoxy resin. EMAA films were exposed to epoxy monomer (Diglycidyl ether of bisphenol A, DGEBA), hardener (Triethylenetetramine, TETA) and DEGBA/TETA systems at curing (50 ˚C) and post-curing (150 ˚C) temperatures. Results show that during curing at 50 ˚C, EMAA film was only hydrogen-bonded by DGEBA, as no relevant alterations from DGEBA peaks related to its aromatic core (peaks 830 $cm^{-1}$and 1030 cm^{-1}), aliphatic ether (1035 cm^{-1}) or epoxide (915 cm^{-1}) were observed (Figure 24). EMAA films exposed to TETA hardener, only presented ionic bonding, as shown in Figure 24 by the absence of acid dimer peaks from EMAA (920 and 1700 cm^{-1}), as long amide and amine salt formations are represented by the arising of the 1627 cm^{-1} and 1540 cm^{-1} respective peaks.

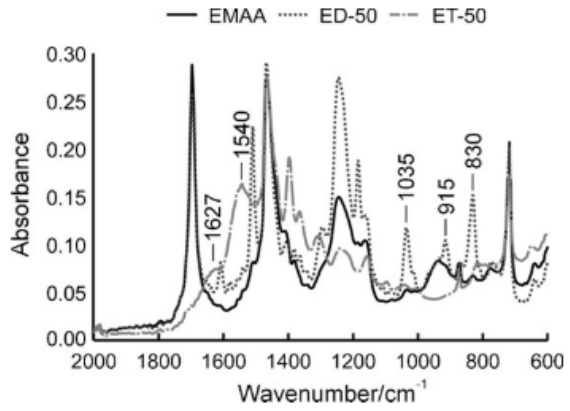

Figure 24 - FTIR spectra of EMAA films exposed to DGEBA (ED-50) and TETA (ET-50) at 50˚C [88]

EMAA films were exposed to DGEBA/TETA at different temperatures (Figure 25). It was observed that at 50 ˚C (EDT-50) in the presence of TETA a higher adsorption phenomenon was promoted. This can be observed by the increase in aromatic (830 cm^{-1}) and ether groups (1035 cm^{-1}) compared to ED-50 spectrum. Further, at 50 ˚C a small reduction on EMAA acid-dimer (1700 cm^{-1}) is also observed, revealing that, in a small extent, this functional group has reacted with DGEBA/TETA. However, considerable alterations are presented when EMAA films are subjected to DGEBA/TETA at 150 ˚C, indicating that covalent bonds have been promoted, as shown by the presence of an ester peak at 1710 cm^{-1} (Figure 25).

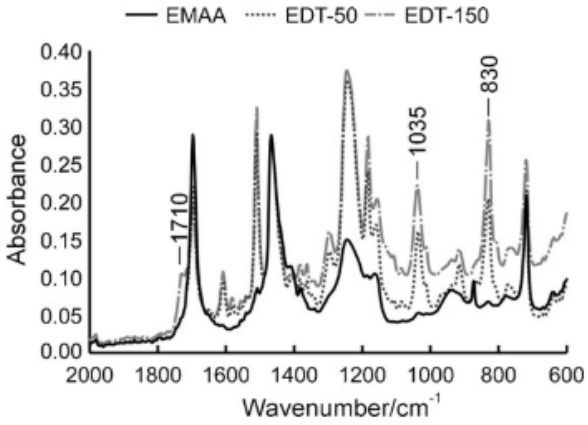

Figure 25 - FTIR spectra of EMAA films exposed to DGEBA/TETA at 50˚C (EDT-50) and at 150˚C (EDT-150) [88]

The main chemical reactions between EMAA acid-dimer and epoxy resin components are described in Figure 26.

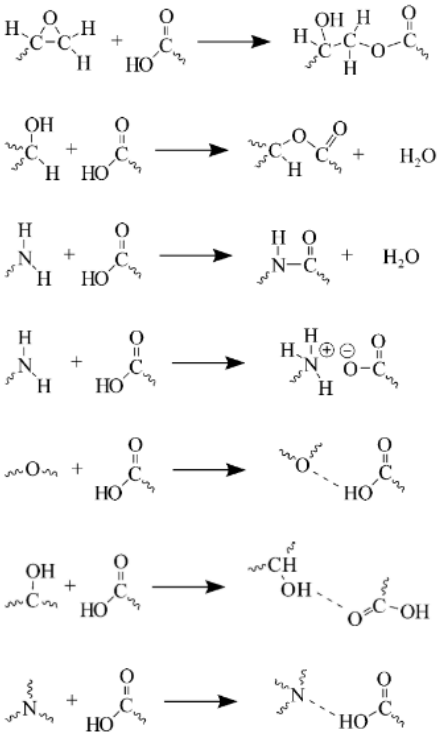

Figure 26 - Main chemical interactions between carboxylic acid from EMAA and epoxy resin network [88].

Curing kinetics of epoxy modified with healing agent particles also provide relevant information of the chemical alterations occurring due to the thermoplastic addition. In a previous work [110], curing kinetics of modified epoxy with different particle size of EMAA was investigated. Results suggest that during processing EMAA particles react with epoxy resin forming an interphase (Figure 27). Moreover, it was also observed that smaller thermoplastic particles tend to slow the curing process, whilst larger particles tend to accelerate them.

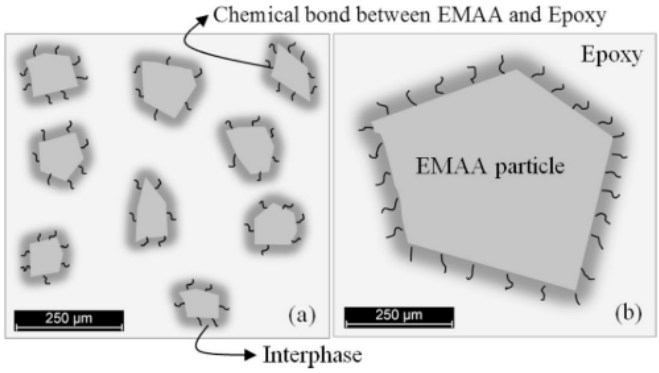

Figure 27 - Schema of EMAA-epoxy interphase according to EMAA particle size: (a) ≤ 125 µm and (b) ≤ 425 µm [110].

Thermomechanical properties

In the case of **molecular interdiffusion thermoplastics** (Table 3), DMA runs can be used to evaluate if the thermoplastic is well dispersed throughout the epoxy network. Typical curves of thermoplastic modified epoxies are shown in Figure 28. The thermoplastic molecular dispersion can be observed through a decrease in temperature corresponding to *tan δ* peak and through a decrease in the onset of storage modulus (*E'*) (Figure 28a). Moreover, the effect of plasticization on epoxy matrix caused by the content of dissolved thermoplastic can also be observed by the broadening of *tan δ* peak (Figure 28b).

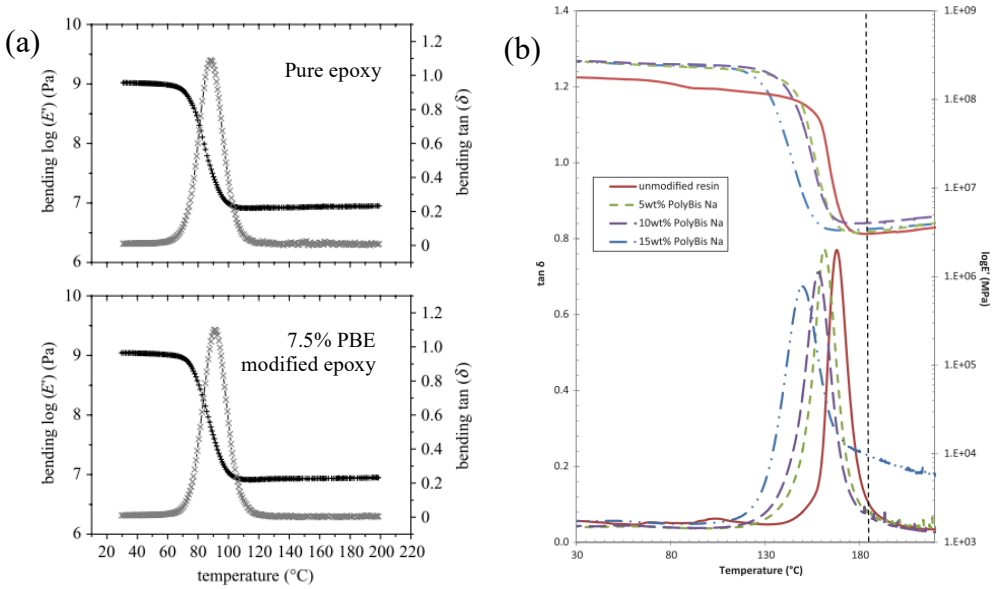

Figure 28 - Examples of DMA curves of PBE modified epoxy with (a) non-functionalized PBE (adapted from [82]) and (b) PBE-Na ionomer [83].

Thermomechanical analyses of modified epoxy by **polymerization-induced phase separated (PIPS) thermoplastic** (Table 3) are presented in Figure 29. A drop on storage modulus of PCL modified epoxy (Figure 29a) is observed at the melting temperature of the thermoplastic phase. Two *tan δ* peaks in modified systems is also an indicative of the phase-separated structure. Additionally, DMA curves provide information about the mechanical stability of epoxy-thermoplastic networks under a specific temperature. This information is necessary to confirm that healing events will not cause significant changes to the composite mechanical integrity. A typical example of the temperature effect on an epoxy-thermoplastic network is shown in Figure 29b.

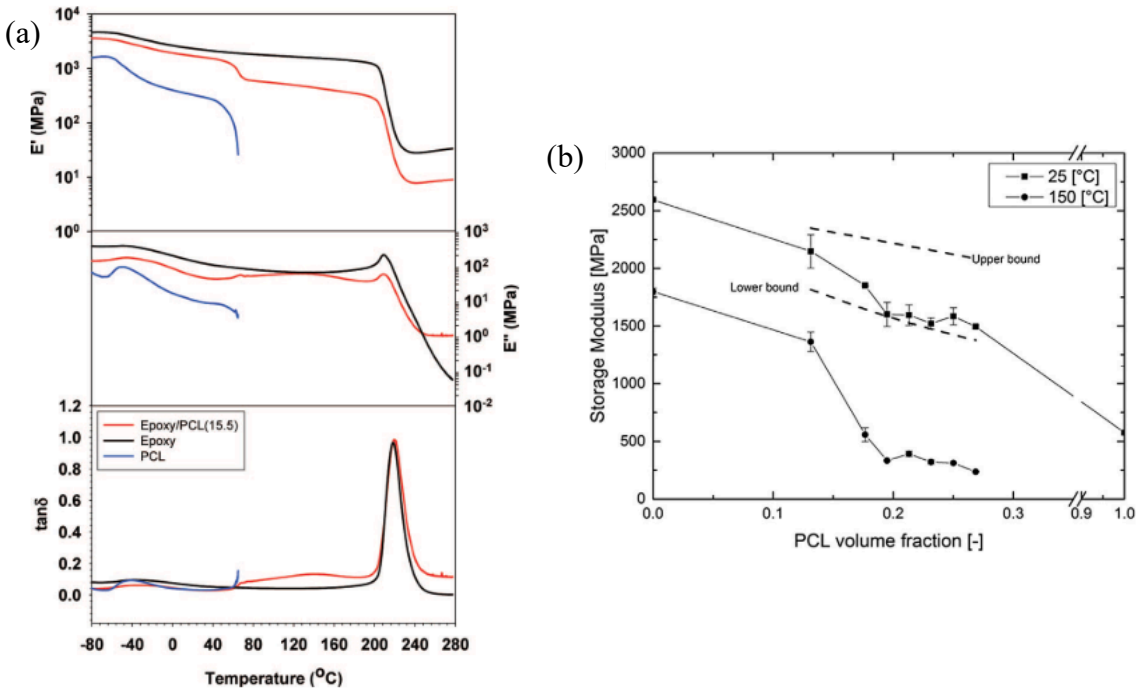

Figure 29 - DMA results of unmodified and PCL modified epoxy resin: (a) varying temperature runs [84] and isothermal results with varying PCL volume fraction (Adapted from [85]).

In the case of addition of **immiscible thermoplastics** (Table 3), thermomechanical analyses are commonly employed to observe network alterations caused by the addition of thermoplastic healing agents. The effect of the addition of different thermoplastic healing agents on epoxy matrix is presented in Figure 30. It can be observed that thermoplastics additions promoted a decrease in glass transition temperature (*Tg*) and a considerable broadening in *tan δ* peaks. In this case, authors [79] reported that despite immiscible, the presence of thermoplastic restricted the epoxy network formation because of the alterations in rheological conditions during mixture. It was also suggested that in the case of **thermally reactive flow polymers** (Table 3) the changes observed in thermomechanical analyses are also likely due to the interfacial chemical reactions, which lead to improvements in thermoplastic-epoxy adhesion.

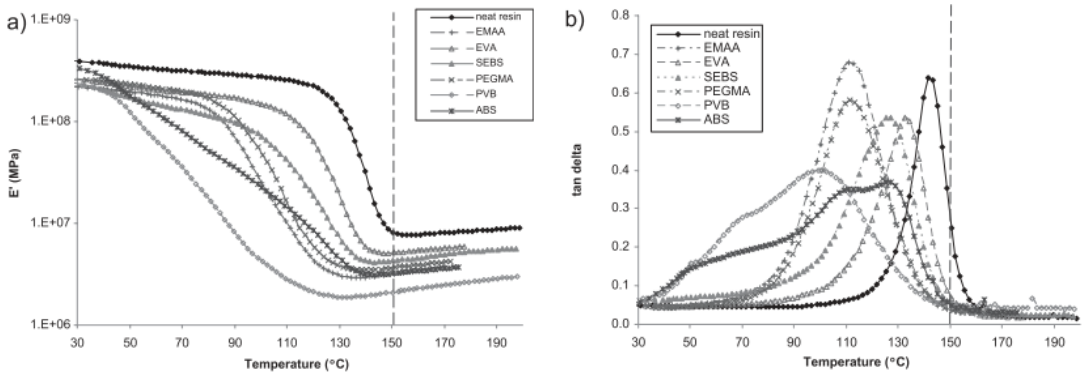

Figure 30 - DMA curves of modified epoxy systems with different thermoplastic healing agents: (a) storage modulus (E '), (b) tan δ [79].

Similar results were also reported by [103] and [78], whose studies considered the effect of the use of different EMAA molecular-weight and different high performance epoxy resins, respectively.

Fiber-matrix interactions

Fiber-matrix interactions play a crucial role in the mechanical properties of a composite, as it is through these interactions that load transfer from matrix to fiber is achieved. Thus, understanding the fiber-matrix interactions is fundamental to predict the integrity of a fiber reinforced composite.

Interface vs Interphase

Conceptually, the interface comprises a surface located in a common limiting region between reinforcing fiber and matrix, which is in intimate contact and allows the transfer of loads [111]. In addition, the contiguous region to the interface is called interphase. The interphase can be defined as a three-dimensional region of finite volume in which physical and mechanical properties gradually vary from the fiber to the matrix [111]. Figure 31 shows a schematic representation of interface and interphase definitions.

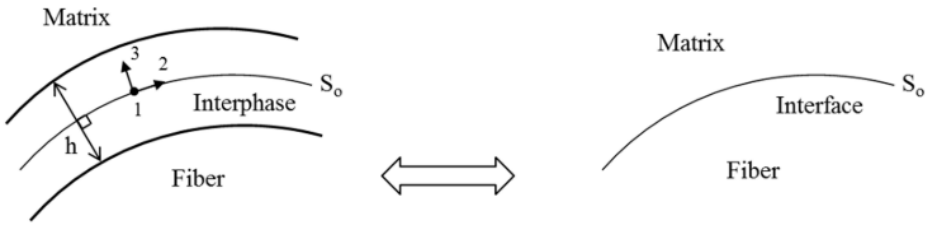

Figure 31 - Schematic illustration showing the difference between a three-dimensional interphase region (left) and a two-dimensional interface (right) [112].

Fiber-matrix interactions are known to play a determining role in the macromechanical properties of epoxy composites. Thus, the stronger is the interfacial bond, the more efficient will be the load transfer [111,113]. Interfacial adhesion is typically evaluated by its mechanical or chemical properties [111]. Mechanical evaluation normally comprises fracture toughness testing and interfacial micromechanical or interlaminar shear strength tests. Chemical evaluation analyzes chemical interactions between fiber and matrix considering the presence of functional groups or thermodynamic changes, for example.

Mechanisms of adhesion

Interface is promoted by different mechanisms of adhesion, which are commonly described by the theories of adhesion. Adhesion mechanisms include (1) adsorption and wetting (molecular

entanglement); (2) electrostatic attraction; (3) interdiffusion; (4) chemical bonding; (5) reaction bonding forming an intermediate component; and (5) mechanical interlocking (Figure 32). These mechanisms can occur individually or simultaneously. Other adhesion mechanisms may include hydrogen bonding, van der Waals forces and other low energy forces [111].

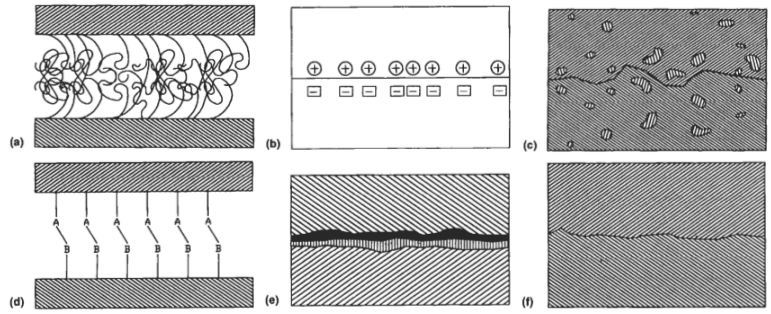

Figure 32 - Main interface bonding mechanisms: (a) chain entanglement; (b) electrostatic attraction; (c) interdiffusion; (d) chemical bonding; (e) reacting bonding and; (f) mechanical interlocking [111].

In order to provide a compatible interface and improve loading transfer between fiber and matrix, sizing is applied to fibrous reinforcements, such as glass or carbon-fiber [114]. Fiber sizing is a surface treatment in which chemical reactive groups are incorporated onto the virgin fiber surface. Generally, fiber sizing is specifically designed to react with traditional thermosetting matrices such as epoxy resins. Thus, any alteration either in epoxy network or fiber sizing composition may affect fiber-matrix interfacial properties.

Measuring fiber-matrix interfacial properties (micromechanical tests)

Mechanical properties of an epoxy-based composite are intimately associated to its interfacial fiber-matrix adhesion properties. Good adhesion can suppress problems under fatigue loading as well as in hostile service conditions. Interfacial shear properties can be appraised through micromechanical test methods that may indicate alterations in fiber-matrix adhesion, fiber surface treatments or modifications in the polymer matrix.

Micromechanical tests are of great interest because they can isolate one (or a few) embedded fiber in order to avoid influences from a macrostructure level. Thus, macromechanical effects, such as misalignment of fibers, uneven fiber-matrix packing or ineffective impregnation problems can be overpassed [115]. Following are some of the main micromechanical tests used to evaluate interfacial properties.

Fiber pull-out tests

The fiber pull-out test consists of partially embedding the fiber(s) length in a matrix bulk structure and applying tensile loads to promote fiber debonding. Some of the fiber-matrix test configurations are presented in Figure 33.

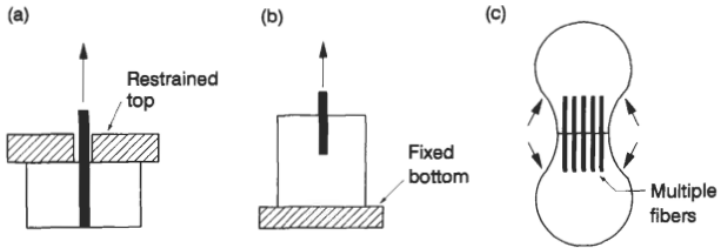

Figure 33 - Schematic configuration of different pull-out tests: (a) restrained top fiber; (b) fixed bottom fiber and; (c) double pull-out with multiple embedded fibers [111].

Theoretical calculations of interfacial shear strength ($IFSS$) consider the embedded fiber length (l), fiber diameter (d) and the applied force (F), as described in Eq. 5. Nevertheless, it is important to note that the equation presumes a uniform stress distribution along the fiber-matrix interface, which is not consistent to realistic conditions. For that reason, shear measurements are commonly referred to as "apparent" interfacial shear strength [116].

$$IFSS = \frac{F}{\pi d l} \qquad \text{(Eq. 5)}$$

A typical curve of a single fiber pull-out test is presented in Figure 34. In the first stage, the system is elastically loaded (F_{el}); some load drops are observed as the load increases indicating that debonding is taking place until the maximum load is reached (F_{max}) and the fiber is then completely detached, the load falls abruptly and only frictional forces (F_{fr}) are measured [111,116].

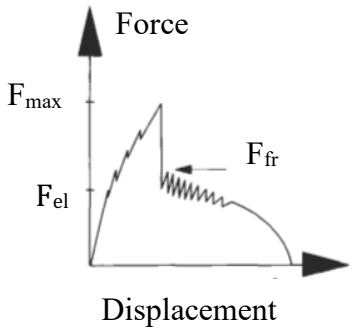

Figure 34 - Representative curve of a single fiber pull-out test (adapted from [111]).

Considering the theoretical interfacial shear strength equation (Eq. 5), higher shear strength is obtained for smaller embedded fiber length, as illustrated in Figure 35. This leads to a practical problem, which is associated with data reliability, as smaller embedded fiber lengths result in higher

data scatter. Further, this is even more challenging when dealing with thinner fiber, as carbon (8 μm diameter) or glass-fiber (up to 20 μm).

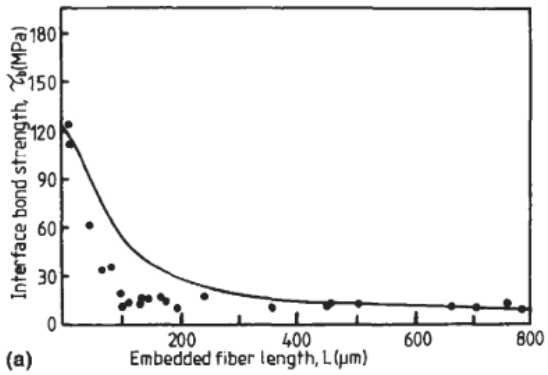

Figure 35 - Effect of the embedded fiber length on interface bond strength in a carbon fiber-acrylic matrix composite [111].

In Figure 35, a steady plateau can be observed after a given embedded fiber length. This is correlated to the shear-lag effect, which is a consequence of the stress transfer distribution along of the fiber-matrix interface.

Figure 36 shows that under a longitudinal deformation (ε) the matrix at the fiber ends is more affected by shear effects than the portion of the fiber away from the ends. Thus, above a limiting embedded fiber length, properties of the composites are mostly governed by fiber tensile strength and not by fiber-matrix interface, which gives the observed plateau. A diagram showing fiber longitudinal tensile and interface shear stresses according to the embedded length fiber is given in Figure 37.

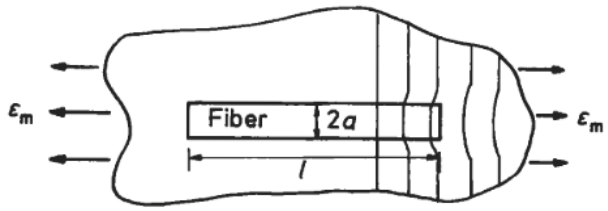

Figure 36 - Schematic illustration of deformation around a fiber embedded in a matrix under longitudinal tension [111].

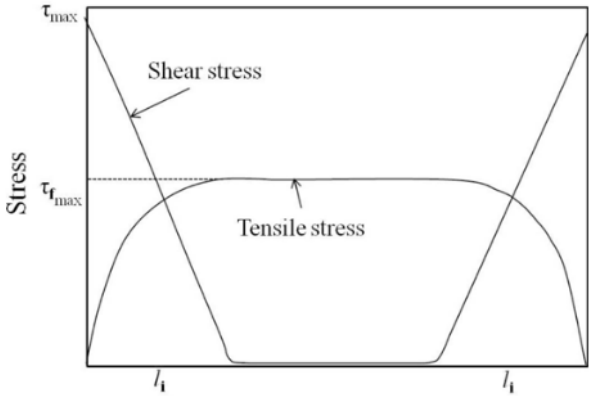

Figure 37 - Variations of fiber axial tension stress and interface shear strength (τ) throughout the embedded fiber length (l_i) [113].

Therefore, in IFSS tests, the embedded fiber length should not be too small to avoid catastrophic failure, in which typical interface effects may be masked. By increasing embedded fiber length, if the failure is not catastrophic, maximum forces recorded may be related to frictional energy dissipation. A further increase in the load may reach a maximum plateau, which is directly related to the bulk fiber-matrix properties, as illustrated in Figure 38.

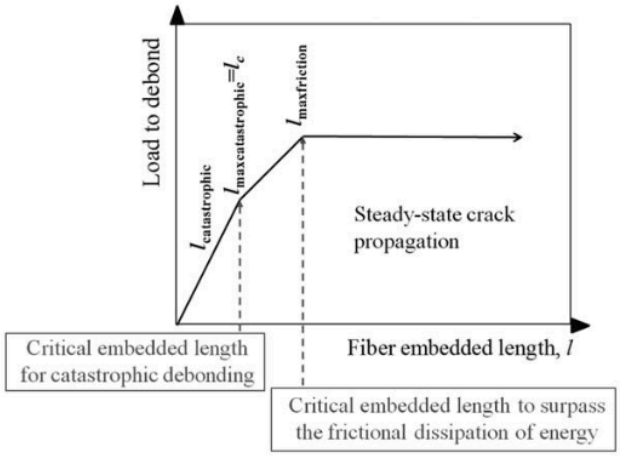

Figure 38 - Relationship between the embedded fiber length and the load to detach [113].

Studies using single fiber pull-out tests may provide a range of embedded fiber lengths and their respective debonding forces results. High standard deviations correlating debonding loads and embedded length may be associated to incorrect measurements or wrong choice of the applied loads [113].

Other limitations are related to the meticulous jig/fixture apparatus, which needs to be fabricated to hold the thin matrix blocks for every short-embedded fiber length. Breakage of high modulus fiber in grips are also of concern. Furthermore, the menisci formed around the fiber are also

of great concern, because they can create stress concentration sites making test results frequently unreliable [111].

Fiber push-in tests

The push-in tests or "microindentation tests" consist, as the name suggests, in employing a standard microindenter to assess fiber-matrix interfacial properties. A typical topography of an indented fiber is presented in Figure 39.

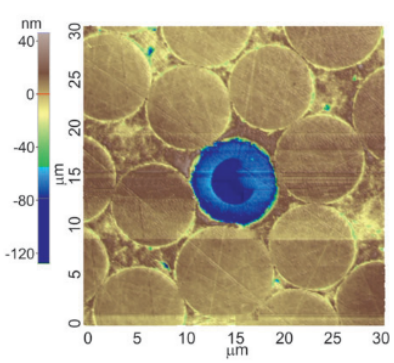

Figure 39 - Topography of a glass fiber microindented [117]

Fiber push-in test is a micromechanical test that enables *in situ* examination of interfaces in a realistic composite sample. Another advantage of this test is the relatively simple test specimen preparation, which only involves a surface polishing of the composite, perpendicularly to the fiber axis [111,113,115].

Fiber push-in tests are performed by loading a single fiber with a very thin flat-tip indenter of the order of a few micrometers. A pre-determined compressive load is applied onto the center of the fiber, allowing the fiber to slide along the fiber-matrix interface. A schematic configuration of a push-in test and its respective load-displacement curve are presented in Figure 40.

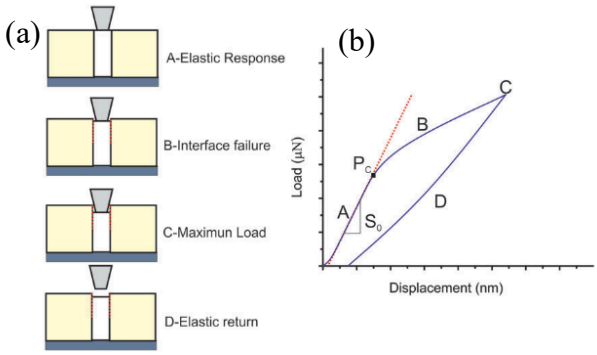

Figure 40 - (a) Stages of a push-in test and (b) the resulting load-displacement curve [117].

Typical load-displacement curves of single fiber push-in tests shows an S-shape (Figure 40b) [117]. The first stage of the curve is associated to the imperfect contact between indenter and fiber.

The second corresponds to the elastic regime (here identified by a slope, S_0), in which end is reached the critical interfacial load, P_c. As the load continues to be increased, a non-linear region is reached, which corresponds to interfacial debonding. The interfacial shear strength ($IFSS$) is then determined according to Eq. 6.

$$IFSS = \frac{nP_c}{2\pi r^2}$$

where r is the fiber radius and n is a parameter that takes into account elastic properties of the fibers and the matrix and also constraints effects caused by the surrounding fibers and can be obtained by Eq. 7.

$$n = \frac{S_0}{\pi r E_f} \quad \text{(Eq. 7)}$$

The main issues concerned with single fiber push-in tests are associated with the interpretation of experimental data. The constraining of enclosing fibers is not accurately taken into account and this may result in significant errors [118], especially in composites with large fiber volume fractions. Other drawbacks include breaking of fibers by sharper indenters and cracks within the matrix caused by the fiber-matrix debonding [111].

Fiber push-out tests

Similar to fiber push-in tests, in push-out tests a microindenter is also used to apply load onto a perpendicularly aligned fiber. However, in this test, a very thin and flat composite sample is required, from which fibers can be pushed out towards the opposite face of the applied load (Figure 41). In this test, it is also possible to inspect reinforced composites conventionally fabricated. Nevertheless, in contrast of push-in tests, the preparation of push-out test specimens may be laborious [113].

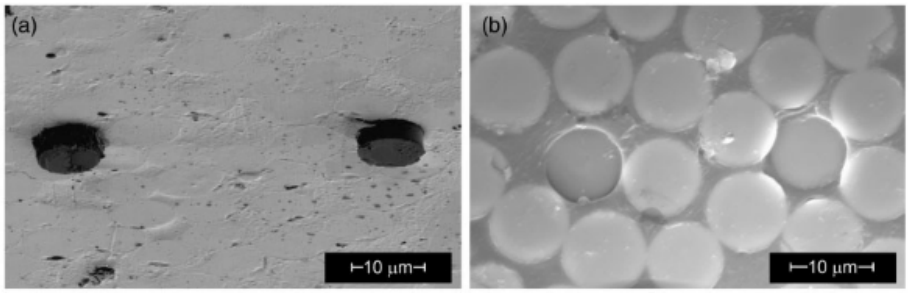

Figure 41 - Scanning electron micrographs of pushed-out glass fibers. (a) bottom surface, (b) top surface of the sheet [117].

The schematic representation of progressive debonding in push-out configuration and its respective load-displacement curve are shown in Figure 41. During the first stage of loading (A), the sheet sample is subjected to an elastic bending regime. The second stage corresponds to elastic deformation of the fiber (B) immediately followed by interfacial fracture load (C). After, frictional forces take place (D) and finally the indenter reaches the matrix (E). By measuring sample dimensions, as fiber diameter (D) and the embedded fiber length (i.e. the thickness of the sheet, H) and the applied load (F), the interfacial shear strength ($IFSS$) is determined as described in Eq. 8. No relevant constraints are related to this equation since the sample geometry can nearly isolate the fiber from its surrounding elements.

$$IFSS = \frac{F}{\pi DH} \qquad \text{(Eq. 8)}$$

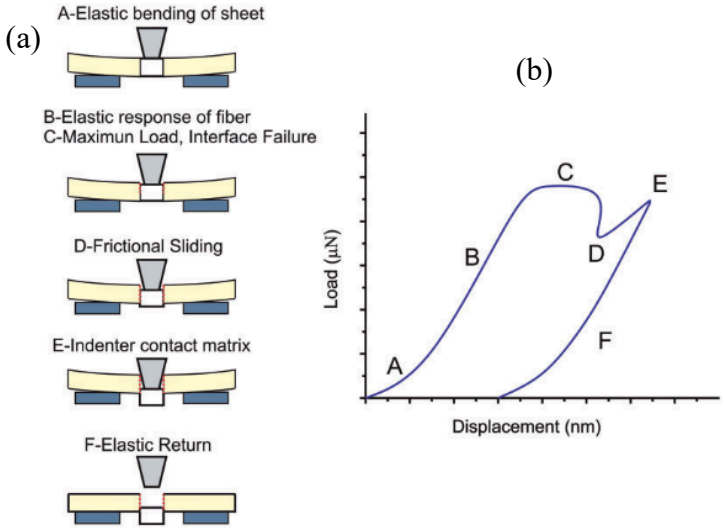

Figure 42 - (a) Stages of a push-out test and (b) the resulting load-displacement curve [117].

Overview

Micromechanical testing configurations to obtain interfacial shear strength were presented. Their results, however, may not be correlated because normal, shear and radial stresses related to fiber-matrix interface properties depends on various parameters intrinsically related to characteristics of each test. Varying embedded fiber length, fiber-matrix stiffness ratio, differences in local stresses, the presence of residual stresses and polymer crosslink density, just to name a few, play determining roles in these interfacial measurements. Therefore, results of interfacial shear strength from different test configurations may differ from one test to another [117,119].

In a previous study, single fiber push-in tests were carried out to determine the IFSS of a modified epoxy containing thermoplastic healing agent [99]. In this case, the **PIPS thermoplastic** (Table 3)**,** poly(ε-caprolactone) (PCL)**,** was investigated with varying the thermoplastic volume fraction content. Representative results of single fiber push-in tests are presented Figure 43. Fitting parameters were used to minimize the surrounding effects and inherent complexity of this type of test (Figure 43a). A typical indentation of a test specimen is shown in Figure 43b.

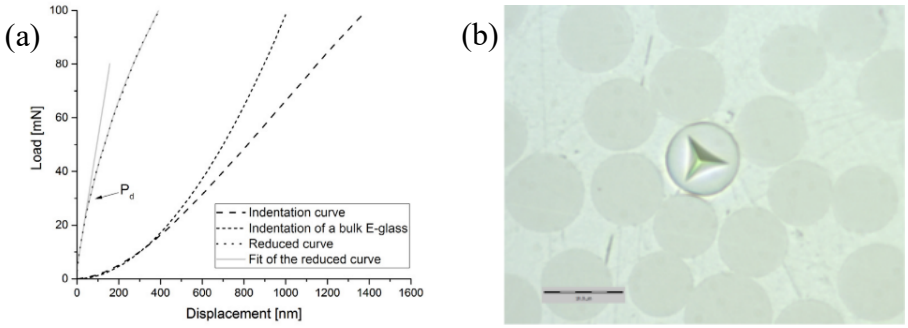

Figure 43 - Single fiber push-in: (a) load-displacement curves of a pure epoxy sample, along with the fitting curve; and (b) corresponding image of the indented test specimen [99].

Results reveal a tendency that the higher is the PCL content, the smaller is the IFSS (Figure 44). Inherent challenges of this type of test, such as variation of fiber diameter, difficulties for centering the indenter and fiber misalignment lead to large data scatter.

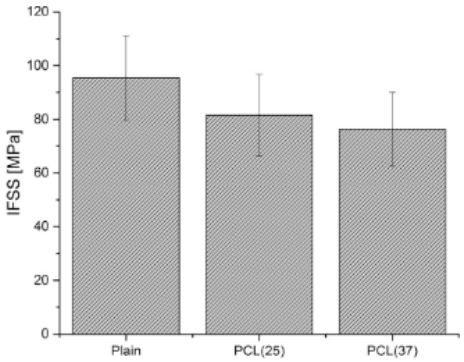

Figure 44 - IFSS results of pure and different PCL modified epoxy systems [99].

The authors also suggested that, despite the geometrical configuration favoring fiber-matrix contact, the decrease in IFSS is justified by the properties of the matrix surrounding the fiber. They stated that the higher PCL content lowers the overall elastic modulus of the epoxy matrix, so also lowering its IFSS.

3. Objectives

It is noteworthy that no records on interfacial properties of thermoplastic healing agents and reinforcing fiber in epoxy composites have been reported in literature. Moreover, there is still a lack of information concerning micromechanics of the most reported thermoplastic healing agent, poly(ethylene-co-methacrylic acid) (EMAA), from which the effect of healing on the fiber interfacial properties is also unknown. Furthermore, no methods using micromechanical testing to assess healing efficiency have been proposed in the literature.

Therefore, this research will:

- Study the effects of EMAA addition on epoxy network formation;
- Investigate the effect of EMAA addition on fiber-matrix interfacial properties of a glass fiber reinforced epoxy matrix composite;
- Study the potential for self-healing of an EMAA modified epoxy through micromechanical testing.

4. Preliminary studies

The effect of poly(ethylene-co-methacrylic acid) (EMAA) addition on chemical and thermomechanical properties of an epoxy system was preliminarily investigated. The objective was to determine the minimum thermoplastic content above which significant changes occur. Cured and post-cured epoxy samples containing (0, 5, 10 and 15) wt.% of EMAA were studied using dynamic mechanical analysis (DMA) and Fourier transform infrared spectroscopy (FTIR). In this preliminary study, the experiments used an epoxy system different from the main investigation because of supply issues regarding the same epoxy grade. These preliminary results aim to estimate a starting point for the main research topic. Thus, despite of different epoxy resin compositions, this study gives preliminary information of the addition of EMAA to an epoxy system.

Experimental

Materials

Epoxy resin, diglycidyl ether of Bisphenol A (DGEBA, *Araldite GY260*), was cured with an aliphatic amine, triethylenetetramine (TETA, *Aradur HY951*), using a 100:13 ratio by weight. The thermoplastic used was poly(ethylene-co-methacrylic acid) (EMAA) (14.5–15.5 wt% of methacrylic acid content) , supplied by *Sigma-Aldrich.* EMAA was cryogenically ground and its particles were sieved through a 425 μm pore-sized sieve and collected onto a 150 μm pore-sized sieve.

Sample preparation

Modified epoxy mixtures were performed by heating DGEBA monomer and EMAA particles at 65 ˚C under mechanical stirring (300 RPM) for 30 min. Then, the mixture was vacuum degassed for 25 min at room temperature. TETA hardener was poured into the mixture, stirred manually and degassed for 5 min. The mixture was then poured into silicon molds and allowed to curing for 24 h at room temperature. Samples were then post-cured in air circulating oven for 90 min at 50 ˚C, followed by 30 min at 150 ˚C. Curing and post-curing were performed according to the manufacturer recommendations. Pure epoxy samples were also produced following the same routine of EMAA modified epoxy compositions for comparison. All sample compositions are summarized in Table 6.

Table 6 – Formulations of epoxy samples (preliminary studies).

Pure epoxy (0 wt% EMAA)		**Modified epoxy (5 wt% EMAA)**		**Modified epoxy (10 wt% EMAA)**		**Modified epoxy (15 wt% EMAA)**	
Cured	Post-cured	Cured	Post-cured	Cured	Post-cured	Cured	Post-cured

Dynamic mechanical analysis (DMA)

Thermomechanical properties were obtained using a *Q800 Dynamic Mechanical Analyzer (TA Instruments)* in single cantilever configuration. Samples of 3.0 mm x 12.5 mm x 35 mm dimensions (thickness x width x length) were tested using 1 Hz frequency and a strain amplitude of 0.1 %. Temperature profile was ramped from room temperature to 200 ˚C with a heating rate of 2 ˚C/min. Tests were performed according to ASTM D7028 recommendations.

Fourier transform infrared (FTIR) spectroscopy

Chemical changes were investigated by comparing Fourier transform infrared (FTIR) spectra of pure and modified epoxy samples (Table 6). A *Shimadzu IRTracer – 100* spectrometer was used in Attenuated Total Reflectance (ATR) mode. The analysis procedure included 32 scans, over a range of 700 cm^{-1} to 4000 cm^{-1} with a 4 cm^{-1} resolution. An average of four spectra measured on the same sample was considered for each sample condition. Some spectra were shifted to better fit in the spectral window. Due to the ATR mode, changes in spectra analysis were examined for the existence of bands only, *i.e.,* signal intensity changes were not taken into account.

Preliminary results

Dynamic mechanical analysis (DMA)

An increase in Storage Modulus (E') at approximately 76 ˚C for all cured samples (Figure 45a) suggests residual crosslinking reactions, as observed in previous works [51,57]. Cured samples also presented two *tan δ* peaks (Figure 45b). Thus, glass transition temperature (*Tg*) for cured samples is compatible with a two-part component. For post-cured samples, one single drop in *E'* (Figure 45c) along with one *tan δ* peak (Figure 45d) were observed, indicating a complete crosslinked network.

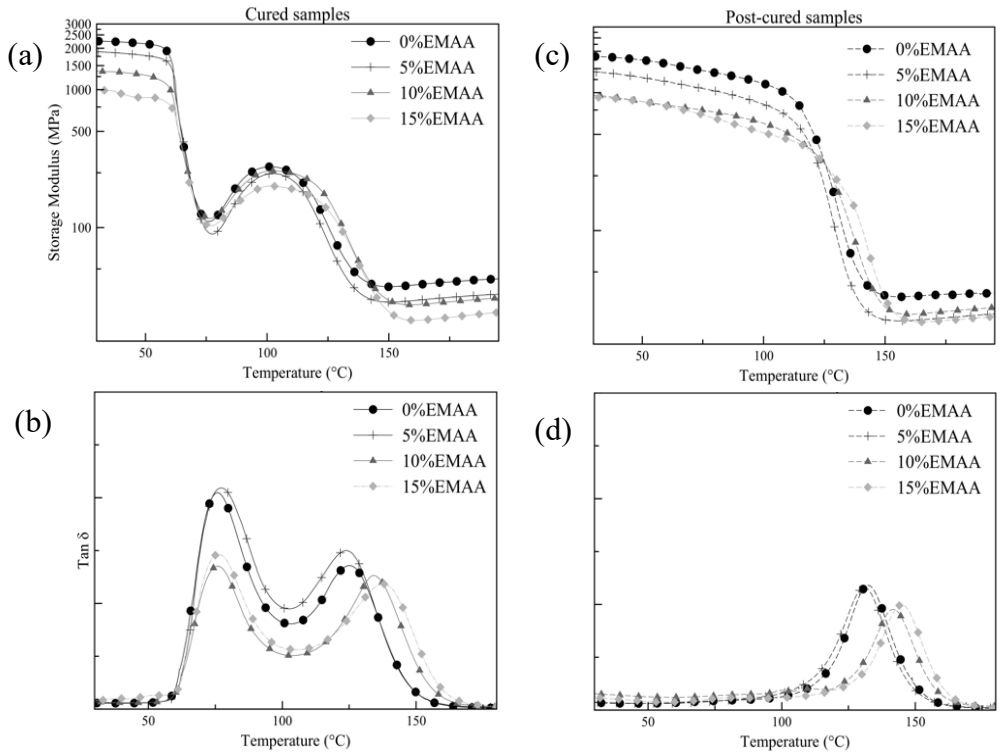

Figure 45 - Storage Modulus and *tan δ* curves of cured (a,b) and post-cured (c,d) of epoxy systems (preliminary studies).

In both cured and post-cured conditions, thermoplastic modification did not lead to any additional *tan δ* peak or minor *β*-relaxations slopes. The EMAA used in this work is likely above its *Tg* (12˚C [120]) and its melting temperature (*Tm*) (89˚C [120]) is in the same range as epoxy *Tg*, when the test was carried out. Therefore, it is reasonable to assume that the thermoplastic second phase is cohesively integrated into the epoxy network.

Table 7 summarizes the *Tgs* obtained from *tan δ* peaks. All cured samples (second column) show similar *Tg* values, suggesting the presence of EMAA did not affect the first stage of curing. However, modified epoxies with an EMAA content of 10 wt.% or higher showed a significant increase in *Tg* of post-cured samples (third column). This indicates that the EMAA in such concentration may alter post-curing, as observed in previous investigations [66,110]. The changes of *Tg* may be explained by the formation of an interphase surrounding EMAA particles that constrains epoxy network relaxations [110]. Further, it supports the evidence that EMAA effects on epoxy are most relevant at higher temperatures [86,88].

Table 7 - Glass transition temperature (*Tg*) obtained from *tan δ* peaks of cured and post-cured epoxy formulations (preliminary studies).

Epoxy formulation	***Tg* (1st peak) Cured (˚C)**	***Tg* (2nd/single peak) Post-cured (˚C)**
0 wt% EMAA – cured	75.9	125.1
0 wt% EMAA – post-cured	-	132.2
5 wt% EMAA – cured	77.2	123.8
5 wt% EMAA – post-cured	-	130.8
10 wt% EMAA – cured	76.0	134.1
10 wt% EMAA – post-cured	-	141.6
15 wt% EMAA – cured	76.1	137.7
15 wt% EMAA – post-cured	-	144.8

Fourier transform infrared (FTIR) spectroscopy

FTIR spectra of epoxy formulations and pure EMAA are presented in Figure 46. The carboxylic acid dimer peak at 1697 cm^{-1} [88] (Figure 46b) from pure EMAA thermoplastic disappeared indicating that this chemical group has reacted with the epoxy chemical structure, as observed in previous works [88,107]. Consequently, the peak related to amine salt of carboxylic acid (1570 cm^{-1} [88]) increase in intensity as the EMAA content is increased. These peaks are already noticed in concentrations of 5 wt.% of EMAA, in both cured and post-cured conditions.

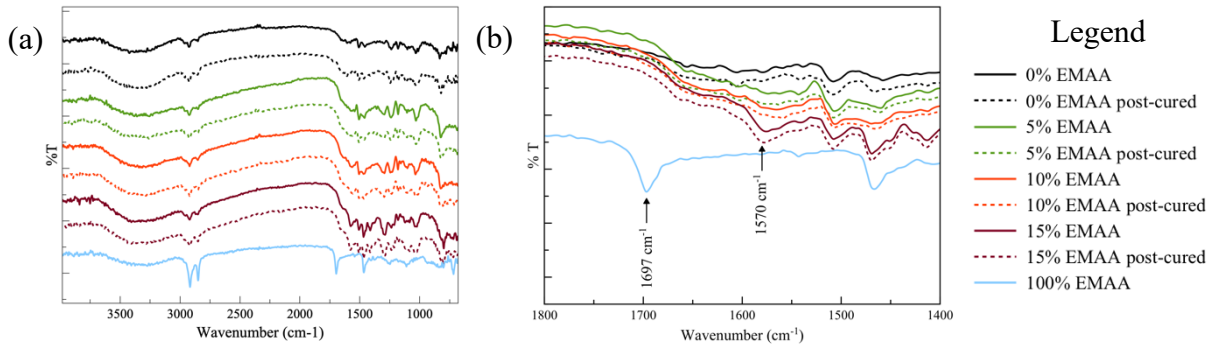

Figure 46 - FTIR spectra of epoxy formulations, along with spectrum of pure EMAA thermoplastic: (a) full spectral range and (b) (1800-1400) cm^{-1} interval range (preliminary studies).

Conclusions of the preliminary work

A preliminary investigation of the effect of EMAA addition on the epoxy network was conducted. Results indicated that a content up from 10 wt.% of EMAA was sufficient to alter the thermomechanical properties of epoxy, which is also associated to the changes observed in infrared spectroscopy analyses. EMAA content in works previously published in the literature varies up to 20 wt.%, but the preliminary results showed that chemical and thermomechanical alterations occur at lower contents. Thus, the proposed investigation will be focused on modified epoxy containing 10 wt.% of EMAA particles.

5. Paper: Microscale evaluation of epoxy matrix composites containing thermoplastic healing agent

Contents lists available at ScienceDirect

Composites Science and Technology

journal homepage: www.elsevier.com/locate/compscitech

Microscale evaluation of epoxy matrix composites containing thermoplastic healing agent

Érick S.S. Guerra [a,*], Bruna L. Silva [a], José D.D. Melo [a], Gerhard Kalinka [b], Ana P.C. Barbosa [a]

[a] Department of Materials Engineering, Federal University of Rio Grande do Norte, Av. Senador Salgado Filho 3000, CEP 59078-970, Natal, RN, Brazil
[b] BAM 5.3, Federal Institute for Materials Research and Testing, Unter den Eichen 87, D-12205, Berlin, Germany

ARTICLE INFO

Keywords:
Interfacial strength
Fiber/matrix bond
Self-healing
Polymer-matrix composites (PMC)

ABSTRACT

Among the strategies to produce healable thermosetting systems is their modification by the addition of thermoplastic particles. This work investigates the influence of poly(ethylene-*co*-methacrylic acid) (EMAA) on fiber-matrix interfacial properties of a glass fiber reinforced epoxy matrix composite. Epoxy-EMAA interactions were evaluated using differential scanning calorimetry (DSC) and infrared spectroscopy. The effects of EMAA on the epoxy network formation were evidenced by changes in glass transition temperature, cure kinetics and alteration of chemical groups during cure. Interfacial shear strength (IFSS) measurements obtained by single fiber pull-out tests indicate similar interfacial properties for pure and EMAA modified epoxy. Additionally, the potential for self-healing ability of an EMAA modified epoxy was demonstrated. However, IFSS after a healing cycle for the EMAA modified epoxy was lower as compared to the pure epoxy, because of the lower fiber-EMAA interfacial shear strength. So, thermoplastic healing agents has not only to fill cracks in the matrix material, but also have to be optimized regarding its interface properties to the reinforcing fibers.

1. Introduction

Poly(ethylene-*co*-methacrylic acid) (EMAA) is one of the most reported thermoplastic healing agents used in epoxy thermosetting matrices [1–8]. The healing mechanism is normally performed using heat, which allows the thermoplastic phase within the epoxy matrix to flow into a contiguous microcrack area, restoring partially – or in some cases even fully – mechanical properties [9,10]. The chemical interaction between EMAA and epoxy also produces volatiles at the thermoplastic-epoxy interface that tends to expand under higher temperature and force the molten EMAA to flow further into microcracks – a process called "pressure delivery mechanism" [11].

Nevertheless, the presence of immiscible – but reactive – thermoplastic healing agents in the liquid resin affects the formation of the epoxy network during the cure process. As a consequence, alterations on glass transition temperature [4–8], chemical structure [2,3,5–8] and cure reactions [3,5,7,8] of the epoxy network have been observed. Additionally, single fiber tests reveals that the fiber-matrix interfacial shear strength (IFSS) may vary under different temperature processing conditions [12], and different amine:epoxy stoichiometry [13]. In another work [14], a thermoplastic healing agent (poly-ε-caprolactone) (PCL) was demonstrated to decrease IFSS as more thermoplastic is added into epoxy.

Therefore, the goal of this work was to determine the microscale properties of an epoxy system modified with the addition of EMAA as a self-healing agent. EMAA modified and pure epoxy samples were characterized using infrared (IR) spectroscopy, and differential scanning calorimetry (DSC). Alterations in the cure kinetics due to the addition of thermoplastic particles were also investigated using DSC. Finally, a study about fiber-matrix interactions for EMAA-modified epoxy compared to the pure epoxy network was performed using single fiber pull-out tests. Moreover, fiber-matrix interfacial properties of pure EMAA were also addressed. As a result, a new method for the evaluation of healing mechanism and efficiency based on optically monitored single fiber pull-out tests was proposed.

2. Experimental

2.1. Materials

Epoxy resin (RIMR135, Hexion, Germany) was cured with a mixture of polyamines (RIMH137, Hexion, Germany) in an epoxy:hardener

* Corresponding author.
E-mail address: erickssguerra@gmail.com (É.S.S. Guerra).

https://doi.org/10.1016/j.compscitech.2022.109843
Received 4 April 2022; Received in revised form 7 November 2022; Accepted 11 November 2022
Available online 21 November 2022

weight ratio of 100:30. The cure was performed for 48 h at room temperature, followed by a post-cure at 80 °C for 15 h.

Poly(ethylene-*co*-methacrylic acid) (EMAA) (Sigma-Aldrich, Germany) containing 14.5–15.5% of methacrylic acid was supplied in the pellet form. Thermoplastic particles were obtained grinding the pellets in a cryogenic mill *IKA, model A11 basic*. Particles were then sieved using a 450 μm pore size sieve and collected onto a 315 μm pore size sieve.

Two types of glass fiber were used in this work. For the single fiber pull-out tests, fibers of 17–20 μm diameter (Advantex® *SE 2020)* were used. For the optically monitored (OM) single fiber pull-out tests, optical fibers of 125 μm diameter (*Corning*® *SMF-28e+* ®) were used. The coating of optical fibers was removed using a professional fiber plier followed by ketone rinsing. Before the embedding, the optical fibers were cut perpendicularly using a cleaver designed for cutting this type of fiber.

2.2. Polymer samples

Modified resin samples were produced by manual mixing the epoxy monomer and EMAA particles (10 wt%) for 15 min, followed by vacuum degassing until all bubbles disappeared. After, the hardener was poured into the mixture, and the liquid was agitated for an additional 15 min. The mixture was degassed again and allowed to cure partially for 2 h. After this, the viscosity was still low, allowing the mixture to be stirred and degassed again, and finally poured into a metal mold of 260 mm × 260 mm x 4 mm (length x width x thickness) dimensions. Cured samples were cut from the middle region of the plate, discarding upper and lower portions at 45 mm along the length (see Fig. S1 in supporting information). Pure epoxy samples were also produced by the same processing routine. Modified and pure epoxy samples were further investigated by X-ray microtomography, Differential Scanning Calorimetry (DSC) and infrared spectroscopy.

2.3. X-ray microtomography

A sample of EMAA modified epoxy of 4 mm × 4 mm x 55 mm size was imaged in 3D employing a commercial X-ray microscope device (*ZEISS Xradia 620 Versa*). For imaging, an X-ray tube acceleration voltage of 80 kV, a tube power of 10 W, a *LE1* X-ray spectrum filter, and a detector exposure time of 1 s were used. The distances tube-sample (25 mm) and tube-detector (170 mm), as well as an optical detector magnification led to an effective voxel size of approximately 10 μm. The amount and volumetric measurements of bubbles and EMAA particles were estimated by the *Avizo* modules label analysis in 3D. Material statistics were obtained by 'area per slice' in 2D throughout the sample's longitudinal axis. An equivalent diameter of the irregular shaped of EMAA particles was adopted.

2.4. Infrared spectroscopy

Chemical alterations were monitored using near-infrared (NIR) spectroscopy. A NIR spectrometer *Nicolet 8700* was used in transmission mode with a spectral range of 4500–7000 cm^{-1}. NIR spectra were obtained in a resolution of 4 cm^{-1} and with a number of 32 scans were used. Samples of 4 mm thickness were placed perpendicularly to the laser beam. The effect of EMAA addition on the formation of the epoxy network was investigated using cured and post-cured samples. The effect of healing conditions was also investigated in post-cured samples. Some infrared spectra were y-axis shifted to better fit into the spectra window.

2.5. Differential scanning calorimetry (DSC)

Dynamic scanning calorimetry (DSC) was used (1) to trace the energy flow profile during a healing cycle, and (2) to investigate the kinetics during the cure of the resin. All DSC runs were performed using a *Hitachi DSC 7020* calorimeter under a nitrogen atmosphere (30 mL/min purging) with sample weight of 2–5 mg. Parameters of the DSC runs are summarized in Table 1. In the case of (1), closed aluminum pans containing post-cured epoxy samples were used. On the other hand, in (2), all the runs containing liquid resin were performed in open aluminum pans. The isotherms at (1) were performed to simulate a healing event. Glass transition temperature (Tg) was determined according to ASTM D7426.

For the isothermal experiments (2), a dynamic run from 35 °C to 250 °C at a heating rate of 10 °C/min was performed to determine the residual heat of cure when the isothermal DSC thermogram leveled off to the baseline.

A period of time of 30 min between mixing and starting the DSC run was adopted for all uncured samples. The area under the exothermic cure peak of the DSC results was used to calculate the total heat of cure (ΔH_{total} – J/g) by the trapezoidal rule. The degree of cure (χ) was calculated from $\chi = \Delta H_i/\Delta H_{total}$, where ΔH_i is the partial heat of reaction at a certain time. The kinetic reactions studied in this work follow the model proposed by Kamal and Sourour [15] (Eq. (1)),

$$\frac{d\chi}{dt} = (k_1 + k_2.\chi^m)(1-\chi)^n \quad (1)$$

where k_1 is the rate constant for the catalytic reaction and k_2 is the autocatalytic rate constant, and m and n are kinetic exponents of the reaction. The constants k_1 and k_2 are assumed to follow the Arrhenius equation ($k_i = A_i \exp(-E_{ai}/RT)$), where A_i is the Arrhenius frequency factor, E_{ai} is the activation energy, R is the ideal gas constant (8.314 J mol^{-1} K^{-1}) and T is the temperature. To determine the kinetic parameters, a nonlinear estimation using the algorithm of Quasi-Newton and simplex was employed, coupling with the least square method available in the software *Statistica*.

2.6. Single fiber pull-out tests

The effect of the addition of a thermoplastic phase on the fiber-matrix interface shear strength (IFSS) was assessed by single fiber pull-out tests, following methodologies presented in previous studies [16,17].

For resin sample preparation, one end of a single fiber fixed on a magnetic holder, was perpendicularly aligned over a small blind hole (1 mm diameter) in a small aluminum block. A period of time of 30 min between mixing and starting the embedding of the fiber was adopted for all the epoxy samples. A small amount of the mixture was then carefully poured into the blind hole using a syringe needle. After, the other end of the fiber was dunked into the resin droplet. A variation of embedding length ranging from 50 to 200 μm was achieved by a motorized stage. After placing the fiber, samples were allowed to cure for 48 h at room temperature followed by post-cure at 80 °C for 15 h.

For the preparation of embedding fibers in pure EMAA substrate, a single particle of the thermoplastic of approximately 5 mm diameter was placed onto a small aluminum block. After heating up and holding at 150 °C for a minimum of 30 min, the thermoplastic melts and forms a liquid droplet. The fiber embedding follows the same process as for epoxy resin samples. Pure EMAA samples were then allowed to cool down to room temperature for at least 24 h. After the embedding process, the partially embedded fiber was cut free from the magnetic holder,

Table 1
Parameters used in the DSC runs.

Measurement	Parameters
(1) Energy profile (during a healing cycle)	Heating up: 30°C-150 °C (rate of 20 °C/min) Isotherms: 150 °C for 30 min Cooling down: 150°C-30 °C (rate of 20 °C/min)
(2) Kinetics of cure	Isotherm: 100 °C; 110 °C and 120 °C for 80 min.

creating thus a new free end.

For the single fiber pull-out test, the free end of the fiber was glued onto a pad coupled to the force transducer of the pull-out device. After the cure of the glue, the fiber was pulled at a rate of 1.0 μm/s. Force and displacement were continuously recorded until the fiber-matrix interface is broken and the fiber is completely pulled out from the polymer droplet. Fiber diameter (d_{fiber}) and fiber embedded length (l_e) were measured using an optical microscope. The interfacial shear strength (τ_{app}) was obtained according to $\tau_{app}=F_{max}/A$, where F_{max} is the maximum pull-out force and A corresponds to the fiber embedded area ($A = d_{fiber} \times \pi \times l_e$). More than 25 samples containing 0 wt% EMAA (pure epoxy), 10 wt% EMAA and 100 wt% EMAA (pure EMAA) for each condition were tested and analyzed.

After the pull-out, the roughness profile of the surface of the embedded fiber area was evaluated using a confocal laser microscope *Keyence VK-X100*. From the 3D profile, a roughness profile was calculated using a *ZEN Imaging Software*. A tilt correction was applied throughout a user-defined straight line on the embedded fiber region.

2.7. Healing at microscale

The healing efficiency of EMAA modified epoxy was assessed by optically monitored (OM) single fiber pull-out tests. Additionally, the healing mechanism was assumed to be the visible changes occurring in a single fiber composite sample. To enable a better observation, thick fibers (125 μm) were used. The fibers were impregnated in between two thin microscope slides containing the matrix material in the middle forming a fiber "sandwiched" sample (see Fig. S2 in supporting information). This sandwich was glued to a flat pad. The free fiber end was then bonded on another microscope slide and glued onto other flat pad. Both pads were then clamped to a piezo actuator. To produce an interface failure, cyclic loads with a displacement increment of 1 μm and a ramp speed of 10 μm/s were applied. This loading regime was stopped when a drop in force of at least 1 N was observed. After this, the clamps were moved to their initial position. Polarized light was used to track the interface failure by changes in the strain field of the matrix during the test, thus allowing *in situ* monitoring of the fiber-matrix debonding.

After documentation of the broken interface, a healing cycle was applied. For this purpose, the samples were heated up at 150 °C for 30 min. Afterwards, the healed fiber-matrix interface was photographed again, and a second pull-out test was performed using the same sample and the same test parameters.

Healing efficiency (η) was assessed comparing the maximum force achieved before ($F_{original}$) and after healing (F_{healed}), according to $\eta = F_{original}/F_{healed}$. Due to the nature of powder filling, the local arrangement of particles in relation the fiber vary from one sample to another.

3. Results and discussion

3.1. X-ray microtomography

The distribution of EMAA particles throughout a representative sample is shown in Fig. 1a and b. Bubbles occupy a negligible surface area per slice throughout the sample as shown in Fig. 1c. In addition to this, the cumulative volume fraction of 50% (D50) of EMAA particle size was 350 μm, whilst D50 of bubble was 70 μm (see Fig. S3 in supporting information). The presence of bubbles can be related to EMAA-epoxy nucleation or trapped air during processing. However, the negligible amount and the small volume size would not affect significantly the mechanical properties of the material.

3.2. Infrared spectroscopy

The objective of IR spectroscopy was to monitor the effects of EMAA addition on epoxy formation considering three conditions: as cured, as post-cured, and after a healing cycle (*i.e.*, as healed). Near Infrared (NIR) spectrum of cured modified epoxy revealed that the primary and secondary amine spectral region (6500 cm^{-1}) [7,18] and the oxirane peak (4530 cm^{-1}) [7,18] remained unreacted and were only consumed after post-cure (Fig. 2). This indicates that EMAA particles may have altered cure reactions. Moreover, post-cure demonstrated to be sufficient to allow epoxy-amine consumption to take place, as no noteworthy difference between both post-cured modified and pure epoxy spectra were observed in their respective band length.

Full NIR spectra can be observed in support information (Fig. S4).

3.3. Energy profile

A broad exothermic peak (96 °C – 141 °C) in the 1st heating of the pure epoxy curve (Fig. 3a) indicates that reminiscent cure reaction was

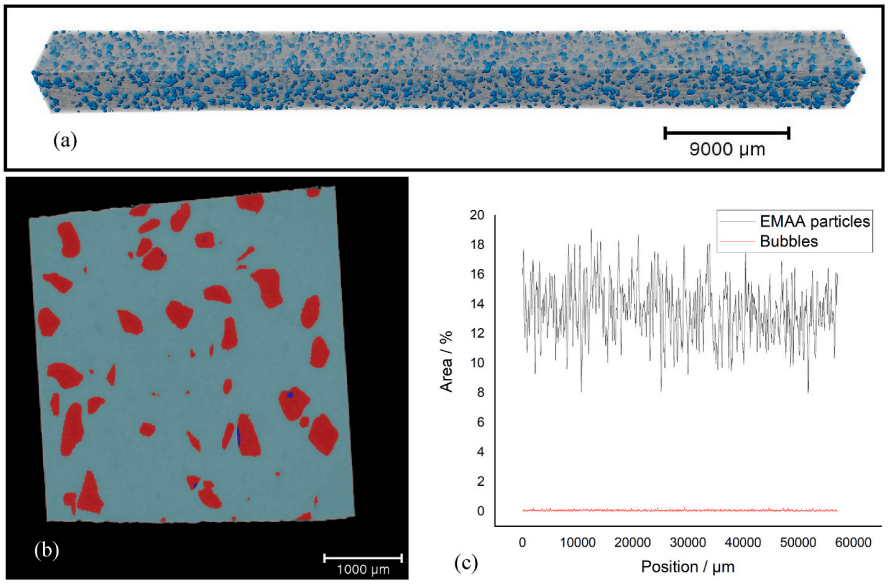

Fig. 1. Particle distribution throughout epoxy sample: (a) 3D sample overview; (b) a random perpendicular slice plan and; (c) EMAA particles and bubbles occupied area per slice position.

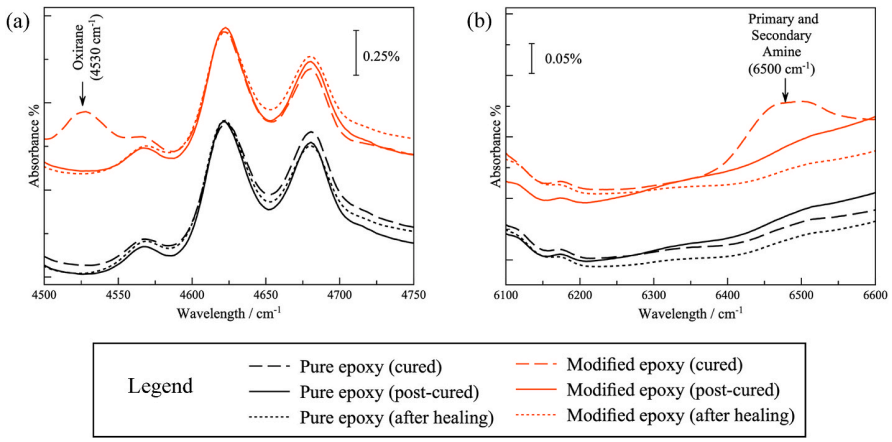

Fig. 2. NIR spectra of pure and modified epoxy samples along with their cured and post-cured conditions: (a) 4500-4750 cm^{-1} interval, and (b) 6100-6600 cm^{-1} interval.

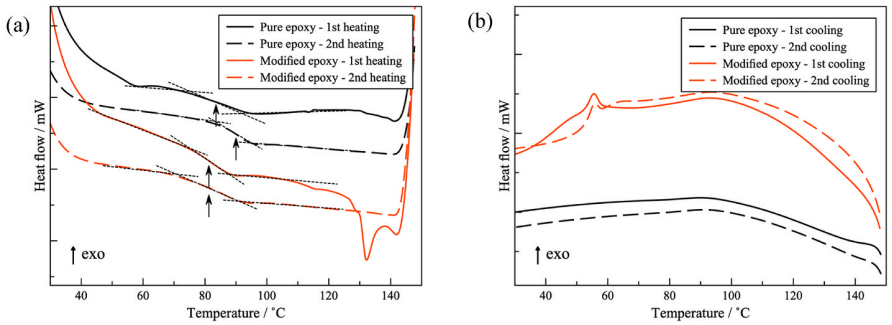

Fig. 3. DSC runs of pure and modified epoxy at the (a) 1st and 2nd heating and (b) 1st and 2nd cooling ramps.

still occurring. This can also be observed by the increase of 6.5 °C in the glass transition temperature (Tg) between the 1st and 2nd heating. In contrast to pure epoxy samples, EMAA modified systems showed no alteration in Tg, even after a healing event (dashed line), indicating that EMAA particles may have altered the formation of the epoxy network. Glass transition temperature can be found in supporting information (Table S5). Furthermore, the glass transition temperature of epoxy may have masked the observation of melting of EMAA (65 °C – 92 °C [5,6]) in both heating curves, as they occur in the same range of temperature, although the EMAA crystallization endothermic peak at 55 °C could be identified in the cooling run (Fig. 3b).

An endothermic event during the first heating curve of modified epoxy (110 °C – 150 °C) may indicate chemical reactions between EMAA and epoxy at later stages of cure (*i.e.* at higher temperatures), as also reported in Refs. [2,7,11]. Moreover, this endothermic event did not occur during the second heating ramp, indicating that the chemical reactions occur in the first healing cycle only. Exothermic peaks from reminiscent cure reactions in EMAA modified epoxy may have been masked by the effect of endothermic event at the end of the 1st heating curve.

3.4. Kinetics of cure

Results of 100 °C isotherm revealed that 80 min was sufficient to observe no reminiscent exothermic peak during the dynamic ramp (see Fig. S6 in supporting information).

The variation of the cure rate ($d\chi/dt$) for 100 °C, 110 °C, and 120 °C isotherms of pure and modified epoxy are presented in Fig. 4. The difference between 100 °C and 110 °C curve behavior of modified epoxy shows that at 100 °C, the thermoplastic does not present high mobility,

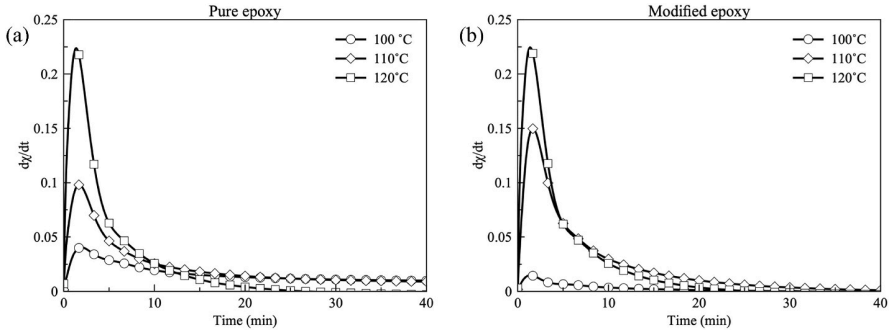

Fig. 4. Cure rate ($d\chi/dt$) throughout the time for (a) pure and (b) 10 wt% EMAA modified epoxy.

whilist at 110 °C the thermoplastic have gained sufficient mobility so its interaction within the resin system have facilitated cure reactions to take place.

The curves presented in Fig. 5 were adjusted using Kamal's model [15], which demonstrated good agreement with the experimental data. Again, the difference between 100 °C and 110 °C curves for both modified and pure epoxy systems may indicate that the EMAA acts in the different stages of cure. First, the EMAA at low cure temperatures (100 °C) may hinder the first stage of cure to take place. However, during the second stage of cure (110 °C) EMAA increases the rate of conversion (χ), suggesting a higher interaction with epoxy constituents. Results also suggest an oxirane-carboxylic acid reaction catalyzed by the tertiary amine present during the later stages of the cure reaction for the EMAA modified epoxy at higher temperatures. NIR spectra also support this result, showing the consumption of primary and secondary amines only after post-cure for EMAA modified epoxy. The delayed formation of tertiary amine for modified systems indicates that this group may have catalyzed post-cure reactions. Furthermore, as a large amount of tertiary amine was postponed and only created at the later stages of the cure for modified epoxy, the extension of this reaction may have been considerably affected at higher temperatures. Other relevant information is that at 120 °C modified and pure epoxy samples presented very analogous kinetics of cure behavior. This may be explained by the rate of reaction occurring so quickly that the presence of EMAA particles does not have enough time to participate in the cure reactions.

Curves of the extension of reaction at 120 °C for pure and modified epoxy, along with the curve of 110 °C for modified epoxy showed a nonmonotonic form compared to other curves. It means that under these conditions, the curing process develops as an nth-order reaction at the expense of an autocatalytic reaction. Moreover, it also shows that EMAA acted in the later stages of the cure, accelerating it.

The activation energy for the pure epoxy system was 65.4 ± 0.2 kJ/mol, whilst modified systems reached 68.9 ± 7.6 kJ/mol. This indicates that molecules in the EMAA modified epoxy move faster than in the pure epoxy system. Full kinetic parameters can be found in supporting information (Table S7).

3.5. Single fiber pull-out tests

Force-displacement curves of pull-out tests of pure epoxy, EMMA modified, and pure EMAA were sorted according to the embedded fiber length and are presented in Fig. 6a, b, and c, respectively. The curves suggest that, in addition to adhesion, friction occurs in the later stages of debonding after the debonding peak. The relationship between the maximum force and the minimum embedded length is directly related to a strong interfacial shear strength (IFSS). In epoxy samples (Fig. 6a and b), the embedded fiber length varied equivalently for all corresponding maximum forces, indicating similar IFSS property. On the other hand, in Pure EMAA curves (Fig. 6c), fiber embedded lengths were longer than 150 μm (maximum displacement of the actuator) for most of the samples. Consequently, the combination between long embedded length and low forces indicates lower values of IFSS for pure EMAA compared to pure and modified epoxy curves.

3.5.1. Influence of EMAA

The interfacial shear strength (IFSS) results for pure and modified epoxy samples (Fig. 6a and b) indicate that the presence of 10 wt% EMAA did not affect significantly fiber-matrix adhesion. This can be explained by the geometrical situation, that is although the volume content of EMAA is nearly 10%, a much lower fraction of the fiber surface is in point contact to EMAA particles. On the other hand, a full contact EMAA-fiber (Fig. 6c) leads to a significant lower IFSS. Glass fibers typically contain polar groups, such as OH, on their surface to improve adhesion with epoxy polar constituents (such as hydroxyls, amines, or oxirane rings) [13]. On the other hand, EMAA contains in its chain a predominant part of nonpolar ethylene mer, which may explain its weaker interaction with the fibers. Expanded force-displacement curves sorted in embedded fiber intervals are available in supporting information (Fig. S8).

3.5.2. Adhesion behavior

A steeper slope in adhesion behavior curves (Fig. 7a) for pure and modified epoxy trendlines reveals a significantly stronger adhesion as compared to pure EMAA results. Furthermore, average results of IFSS tests (Fig. 7b) indicate that epoxy samples (pure or modified) presented 3 to 6.5 x higher IFSS than pure EMAA.

3.5.3. Surface of the pulled-out fibers

The contact area of the fiber after pull-out from EMAA (Fig. 8a) substrate shows a more irregular surface profile, indicating then that part of the EMAA remained attached to the fiber surface (red circle area). The presence of EMAA substrate on the fiber surface also indicates that EMAA-fiber IFSS was higher than inner EMAA intermolecular bond strength. On the other hand, pulled out fibers of pure and modified epoxy samples (Fig. 8b and c) showed a smoother surface in the laser microscopy images. Therefore, this suggests that the fiber-matrix IFSS was smaller than inner epoxy intermolecular bonding. Furthermore, this may also indicate that the fiber-epoxy fracture occurred abruptly and presented a brittle behavior.

Roughness measurements (see Fig. S9 in supporting information) also revealed that a larger fracture surface was created during the debonding process of pure EMAA substrate, suggesting an improvement in fracture toughness, as reported in Refs. [3–5]. Nevertheless, it is important to note that the tests were performed at room temperature. Therefore, EMAA was in its glass transition region (−20 °C to 70 °C) [19], whilst epoxy was in the glassy state, which could also be a reason for the different patterns on the fiber surface.

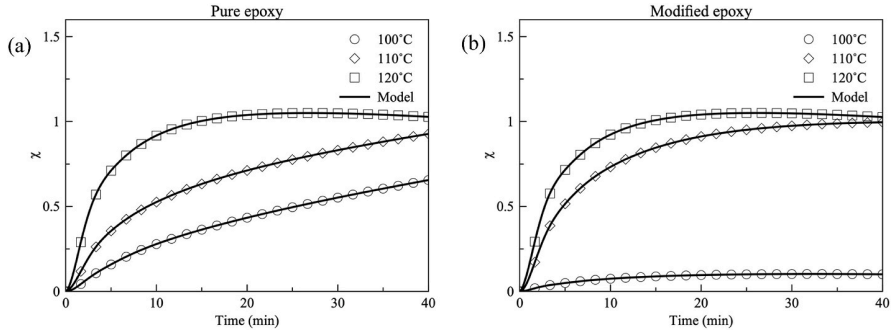

Fig. 5. Extent of reaction (χ)-time curves of pure (a) and modified (b) epoxy.

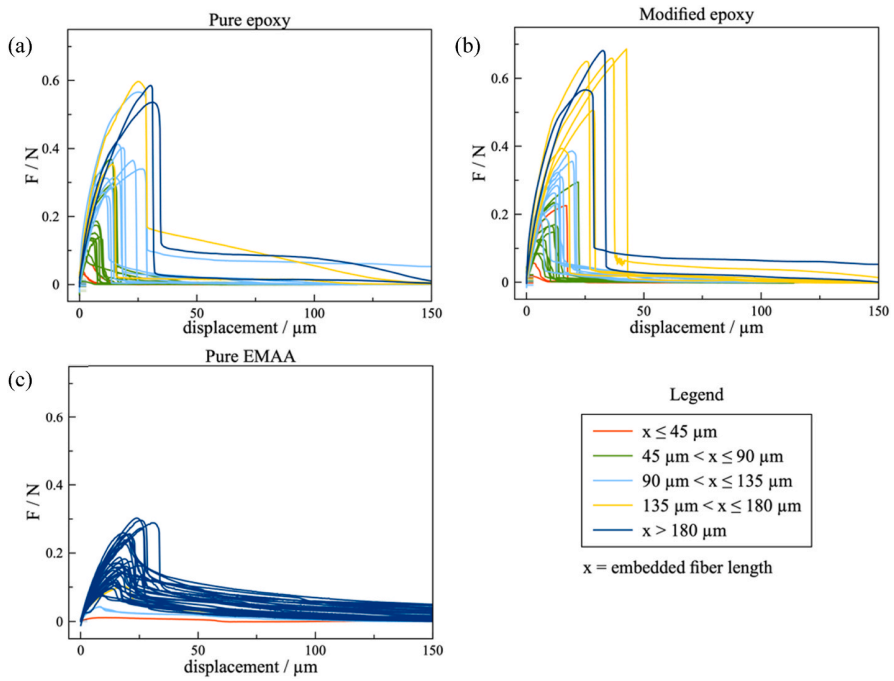

Fig. 6. Single fiber pull-out force-displacement curves: (a) pure epoxy, (b) 10 wt% EMAA modified epoxy, (c) pure EMAA.

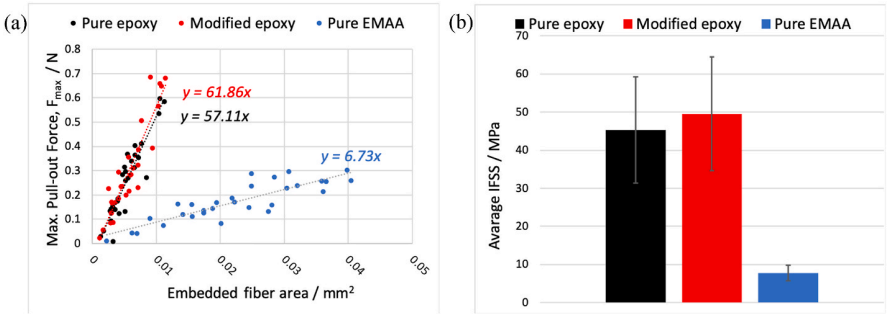

Fig. 7. (a) Maximum pull-out force *vs.* embedded fiber area; (b) Average and standard variation of IFSS for pure epoxy, 10 wt% EMAA modified epoxy, and pure EMAA.

3.6. Healing at microscale

Original and healed samples were sorted in groups according to the healing efficiency (η) (Fig. 9). All tests in original condition revealed the same behavior of IFSS tests (see Figs. S10 and S11 in supporting information), indicating a similar fiber-matrix interaction. However, after healing, the fiber interfacial properties for pure and EMAA modified expoxy varied significantly from one condition to another. It should be noted that experiments considered only the interfacial fiber shear strength (IFSS) of the composite samples as a parameter to assess the healing efficiency. Thus, results focus on the fiber micromechanics instead of the macro performance of a healed material. As previously mentioned, EMAA-modified epoxy composites are well-established self-healing materials. Therefore, the purpose of the IFSS tests was to shed light on the thermoplastic behavior and interaction with fibers during a healing cycle.

3.6.1. Healing in pure epoxy

Most of the pure epoxy tested samples reached a η higher than 50%, sometimes even higher than 100%. This could be explained by physical and chemical phenomena as observed by Ref. [20]. Other factor is that the healing temperature may have promoted cure shrinkage reactions [21], leading to extra mechanical interlocking in the fiber-matrix interface.

3.6.2. Healing in EMAA modified epoxy

EMMA modified epoxy revealed a significant decrease in η, as compared to pure epoxy samples. This may be related to a lower mechanical interlocking effect, which is attenuated by the presence of the EMAA, because the thermoplastic was in the rubbery state during the test [19]. Additionally, the area between fiber and matrix may have been affected by the thermoplastic addition then decreasing the IFSS, as observed by the lower IFSS of the fiber-EMMA. Moreover, it is possible that EMAA limited the epoxy matrix to promote further chemical reactions, as suggested by DSC and IR spectroscopic results.

3.7. Optically monitored tests – pure epoxy

Images taken during a pull-out test performed with a pure epoxy sample (Fig. 10) show the process of debonding of before (I-III) and after (IV-VI) healing. Videos of the full time sequence can be found in supporting information.

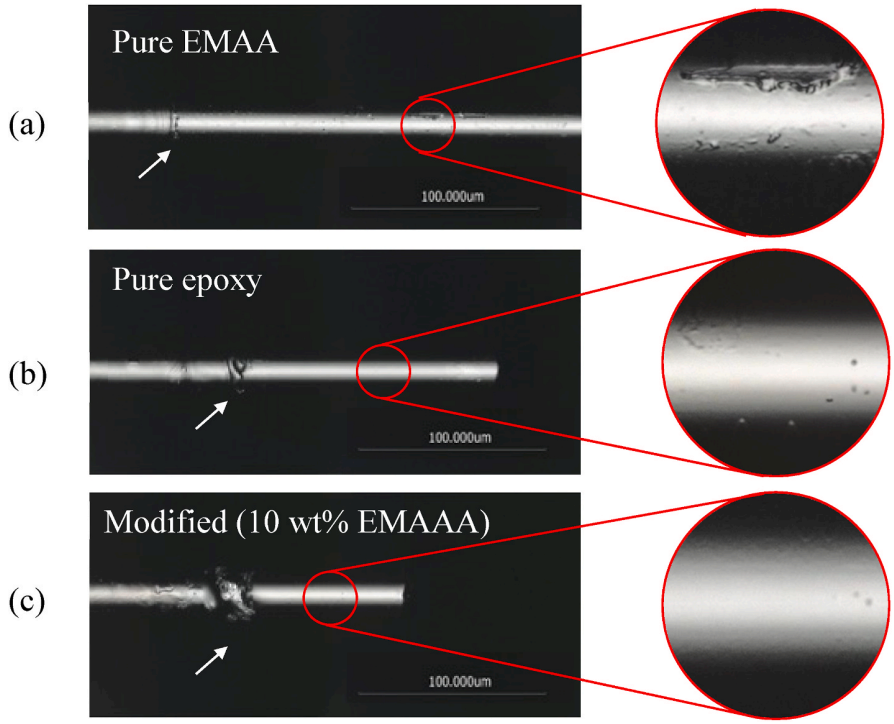

Fig. 8. Laser scanning microscopy images of fibers after pull-out: (a) pure EMAA, (b) pure epoxy; (10 wt% EMAA) and pure EMAA. Arrows indicate the menisci. Red circles indicate detailed areas in higher resolution.

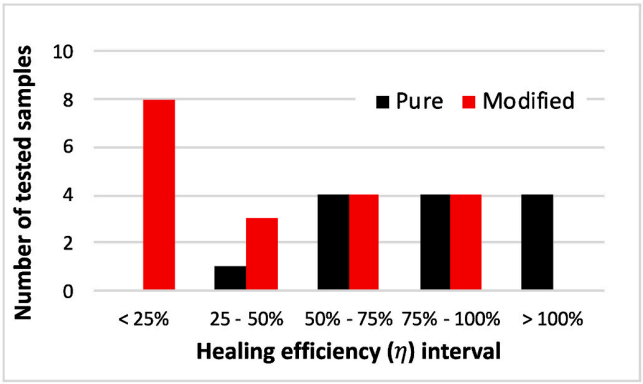

Fig. 9. Distribution of healing efficiency (η) according to the number of tested samples.

Supplementary videos related to this article can be found at https://doi.org/10.1016/j.compscitech.2022.109843

3.7.1. Before healing

The stage (I) indicates the beginning of the test when no stress was applied. Polarized light highlights alterations in the yielding field around the fiber as the fiber is pulled (II). When the fiber was completely detached and replaced to its original position (III), the stressed light field returned to its initial condition, in which no significant stress in the fiber surroundings was observed.

3.7.2. After healing

After healing, no evident difference between (III) and (IV) was observed. As the test restart (V), the stress field in the matrix was significantly lower, indicating that the fiber-matrix interface was also lower, as compared to the original condition (before healing). Continuing the test, it was evidenced an abrupt hue alteration (arrow indicated in VI) on the yielding stress field, which may indicate the break of a new epoxy-fiber interfacial bonding.

3.8. Optically monitored tests – EMAA modified epoxy

Time sequence images of an EMAA modified sample during a pull-out test before (I-III) and after (IV-VI) a healing cycle are presented in Fig. 11. Videos of the full time sequence are provided in supporting information.

3.8.1. Before healing

Polarized light indicates that in stage (I) and (III) no stress along the embedded fiber was present, which indicate respectively the begin and the end of the test. However, under increasing pull-out stress (II), a visible alteration of the light pattern was observed. Still in stage (II), the fiber starts to detach from the matrix, being completely detached in stage (III), when the test was stopped.

3.8.2. After healing

After heating, some detached interface areas (arrows indicated in III) were filled with EMAA (arrows indicated in IV), showing the healing mechanism. As the test proceeds, the stress throughout the fiber presents a lower light intensity change, similarly as that observed in pure epoxy samples. However, the yielding stress was differently distributed in the matrix surroundings (V and VI). This could be related to the lower EMAA-fiber IFSS, from which only epoxy-fiber regions maintained a certain adhesion.

4. Conclusions

The influence of poly(ethylene-*co*-methacrylic acid) (EMAA) addition on fiber-matrix interfacial properties of a glass fiber reinforced epoxy matrix composite was investigated. Alterations in the epoxy network formation due to the presence of EMAA were evidenced by

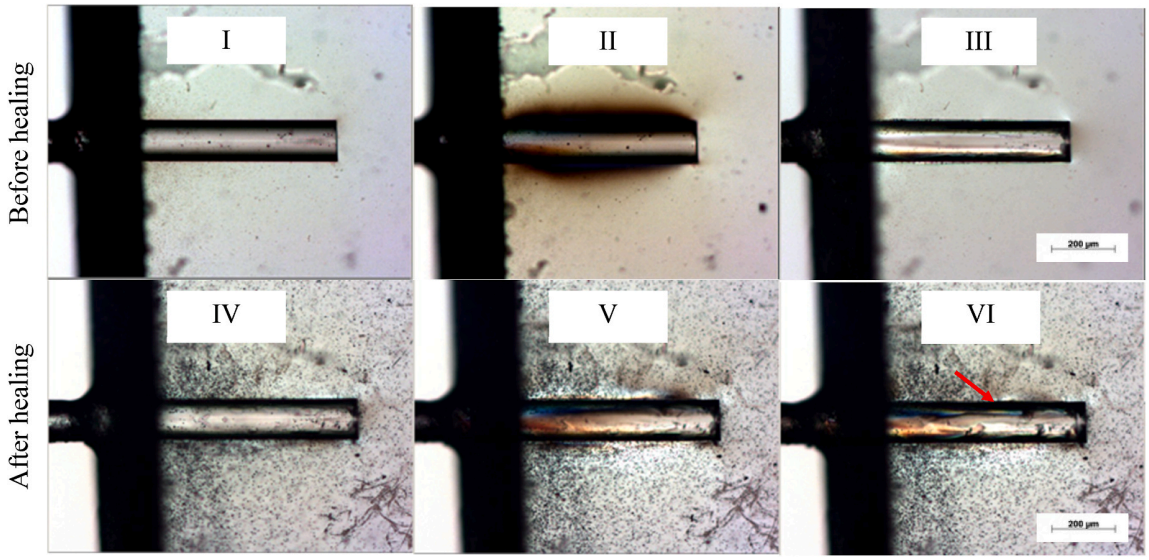

Fig. 10. Time sequence images of OM single fiber pull-out tests of a pure epoxy sample before (I-III) and after (IV-VI) healing.

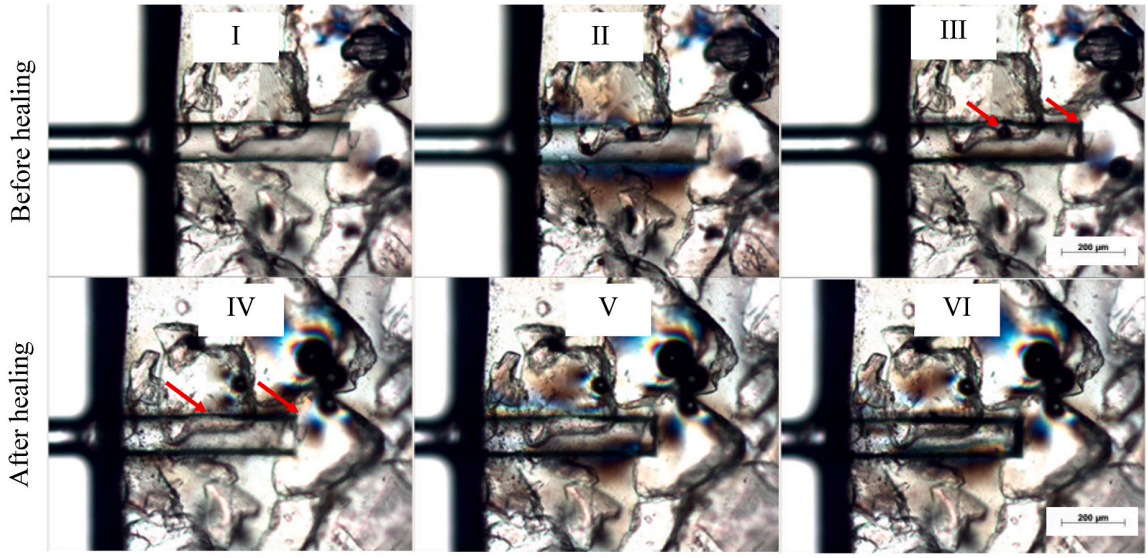

Fig. 11. Time sequence images of OM single fiber pull-out tests of a modified epoxy sample before (I-III) and after (IV-VI) healing.

infrared spectroscopy, DSC and kinetics of cure analysis. However, post-cure proved to be sufficient to reach a suitable crosslinked network, as evidenced by IFSS results. The results also suggest that restoration may be held by the inherent fiber interfacial recovering ability and by the thermoplastic healing mechanism. However, EMAA modified epoxy demonstrated smaller healing efficiency, which can be explained by two complementing events: (1) weaker EMAA-fiber interactions, as compared to epoxy-fiber and, (2) alterations during the formation of the epoxy network. Therefore, the healing ability reported in the literature is most likely held by EMAA-matrix or fiber-matrix interactions, but not to EMAA-fiber interactions. Consequently, to optimize the healing ability of EMAA-epoxy composites, fiber interfacial properties have to be optimized to promote better adhesion to the thermoplastic phase.

Authorship statement

All people who meet authorship criteria are listed as authors, and all authors certify that they have participated sufficiently in the work to take public responsibility for the content, including participation in the concept, design, analysis, writing, or revision of the manuscript. Furthermore, each author certifies that this material or similar material has not been and will not be submitted to or published in any other publication before its appearance in the *Composites Science and Technology*.

Authorship contributions.

É.S.S. Guerra: Methodology, Formal Analysis, Investigation, Writing – Original Draft, Visualization;

B.L. Silva: Formal Analysis, Writing – Review & Editing;

J.D.D. Melo: Conceptualization, Writing – Review & Editing, Project Administration, Funding Acquisition;

G. Kalinka: Conceptualization, Methodology, Resources, Writing – Review & Editing, Supervision;

A.P.C. Barbosa: Conceptualization, Methodology, Writing – Review & Editing, Supervision.

Declaration of competing interest

The authors declare that they have no known competing financial interests or personal relationships that could have appeared to influence the work reported in this paper.

Data availability

Data will be made available on request.

Acknowledgement

This study was financed in part by the Coordenação de Aperfeiçoamento de Pessoal de Nível Superior - Brasil (CAPES) - Code 001. The authors are also thankful to to Martina Bistritz and to Alexander Funk, whose technical expertise were essential to perform IFSS tests and X-ray microtomography analyses respectively.

Appendix A. Supplementary data

Supplementary data to this article can be found online at https://doi.org/10.1016/j.compscitech.2022.109843.

References

[1] S. Meure, S. Furman, S. Khor, Poly[ethylene-co-(methacrylic acid)] healing agents for mendable carbon fiber laminates, Macromol. Mater. Eng. 295 (5) (2010) 420–424.
[2] S. Meure, D.-Y. Wu, S.A. Furman, FTIR study of bonding between a thermoplastic healing agent and a mendable epoxy resin, Vib. Spectrosc. 52 (1) (Jan. 2010) 10–15.
[3] S. Meure, R.J. Varley, D.Y. Wu, S. Mayo, K. Nairn, S. Furman, Confirmation of the healing mechanism in a mendable EMAA-epoxy resin, Eur. Polym. J. 48 (3) (2012) 524–531.
[4] K. Pingkarawat, T. Bhat, D.A. Craze, C.H. Wang, R.J. Varley, A.P. Mouritz, Healing of carbon fibre-epoxy composites using thermoplastic additives, Polym. Chem. 4 (2013) 5007–5015.
[5] K. Pingkarawat, C. Dell'Olio, R.J. Varley, A.P. Mouritz, Poly(ethylene-co-methacrylic acid) (EMAA) as an efficient healing agent for high performance epoxy networks using diglycidyl ether of bisphenol A (DGEBA), Polymer (United Kingdom) 92 (2016) 153–163.
[6] A. Azevedo do Nascimento, F. Fernandez, F.S. da Silva, E.P.C. Ferreira, J.D. D. Melo, A.P. Cysne Barbosa, Addition of poly (ethylene-co-methacrylic acid) (EMAA) as self-healing agent to carbon-epoxy composites, Compos. Appl. Sci. Manuf. 137 (February) (Oct. 2020), 106016.
[7] C.D. Olio, Q. Yuan, R.J. Varley, Epoxy/poly (ethylene- co -methacrylic acid) blends as thermally activated healing agents in an epoxy/amine network, Macromol. Mater. Eng. 300 (2014) 70–79.
[8] B.L. Silva, C. Gomes de Moura Filho, J.D. Diniz Melo, A.P. Cysne Barbosa, The role of poly (ethylene-co-methacrylic acid) (EMAA) on cure kinetics and thermomechanical properties of epoxy, Polym. Bull. (2021), 0123456789.
[9] D.Y. Wu, S. Meure, D. Solomon, Self-healing polymeric materials: a review of recent developments, Prog. Polym. Sci. 33 (5) (2008) 479–522.
[10] M.Q. Zhang, M.Z. Rong, Self-healing Polymers and Polymer Composites, John Wiley & Sons, Inc., 2011.
[11] S. Meure, D.Y. Wu, S. Furman, Polyethylene-co-methacrylic acid healing agents for mendable epoxy resins, Acta Mater. 57 (14) (2009) 4312–4320.
[12] A. Gao, Y. Gu, Q. Wu, C. Yuan, M. Li, Z. Zhang, Influence of processing temperature on interfacial behavior of HKT800 carbon fiber with BMI and epoxy matrices, Chin. J. Aeronaut. 28 (4) (2015) 1255–1262.
[13] J.L. Thomason, L. Yang, D. Bryce, R. Minty, An exploration of the relationship of chemical and physical parameters in the micromechanical characterisation of the apparent interfacial strength in glass fibre epoxy systems, IOP Conf. Ser. Mater. Sci. Eng. 139 (1) (Jul. 2016), 012048.
[14] A. Cohades, V. Michaud, Thermal mending in E-glass reinforced poly (ε-caprolactone)/epoxy blends, Compos. Appl. Sci. Manuf. 99 (Aug. 2017) 129–138.
[15] M.R. Kamal, S. Sourour, Kinetics and thermal characterization of thermoset cure, Polym. Eng. Sci. 13 (1) (Jan. 1973) 59–64.
[16] M. Sahin, et al., Tailoring the interfaces in glass fiber-reinforced photopolymer composites, Polymer 141 (2018) 221–231.
[17] M.Q. Tran, K.K.C. Ho, G. Kalinka, M.S.P. Shaffer, A. Bismarck, Carbon fibre reinforced poly(vinylidene fluoride): impact of matrix modification on fibre/polymer adhesion, Compos. Sci. Technol. 68 (7–8) (2008) 1766–1776.
[18] M. Erdmann, V. Trappe, H. Sturm, U. Braun, E. Duemichen, Cure conversion of structural epoxies by cure state analysis and in situ cure kinetics using nondestructive NIR spectroscopy, Thermochim. Acta 650 (2017) 8–17.
[19] S. Deschanel, et al., Rate dependent finite deformation stress-strain behavior of an ethylene methacrylic acid copolymer and an ethylene methacrylic acid butyl acrylate copolymer, Polymer 50 (1) (Jan. 2009) 227–235.
[20] M. Peñas-Caballero, M. Hernández Santana, R. Verdejo, M.A. Lopez-Manchado, Measuring self-healing in epoxy matrices: the need for standard conditions, React. Funct. Polym. 161 (2020) 2021. November.
[21] C. Kim, S.P. Phansalkar, H.S. Lee, B. Han, Measurement of effective cure shrinkage of epoxy-based molding compound by fiber Bragg grating sensor using two-stage curing process, J. Appl. Polym. Sci. 139 (6) (2022) 1–10.

7. Complementary tests

Additional tests were performed to better understand and characterize the epoxy network properties and to investigate the effect of the healing temperature on chemical and interfacial properties of the material.

Experimental

Materials

Epoxy resin (RIMR135, Hexion, Germany) was cured with a mixture of polyamines (RIMH137, Hexion, Germany) in an epoxy:hardener weight ratio of 100:30. Curing was performed for 48 h at room temperature, followed by a post-curing at 80 ˚C for 15 h. Curing and post-curing were performed according to the manufacturer recommendations.

Poly(ethylene-co-methacrylic acid) (EMAA) (Sigma-Aldrich, Germany) containing 14.5-15.5% of methacrylic acid was supplied in the pellet form. Thermoplastic particles were obtained by cryogenic grinding of pellets in a *IKA* mill*, model A11 basic*. Particles were then sieved into sizes between 450 µm and 315 µm.

Glass fibers of 17-20 µm diameter (Advantex® *SE 2020)* were used for the single fiber pull-out tests.

Polymer samples

Modified resin samples were prepared by manually mixing the epoxy monomer and EMAA particles (10 wt.%) for 15 min, followed by vacuum degassing until all bubbles disappeared. Then, the hardener was poured into the mixture, and the liquid was agitated for additional 15 min. The mixture was degassed again and allowed to curing partially for 2 h. After this, the viscosity was still low, allowing the mixture to be stirred and degassed again, and finally poured into a metal mold of 260 mm x 260 mm x 4 mm (length x width x thickness) dimensions. The material was allowed to curing for 48 h, at room temperature. Cured samples were cut from the middle region of the plate, discarding upper and lower portions at 45 mm along the length (Fig. S1 in Appendix A). Pure epoxy samples were also produced by the same processing routine. Samples were analyzed using dynamic mechanical analysis (DMA) and Fourier transform infrared (FTIR) spectroscopy.

Dynamic mechanical analysis (DMA)

The effects of EMAA addition on viscoelastic properties of epoxy were assessed using a *DMA Q800* analyzer. Cured and post-cured samples with dimensions of 60 mm x 12 mm x 4 mm (length x width x thickness) were tested in dual cantilever configuration using a frequency of 1.0 Hz and strain amplitude of 0.1 %. A temperature profile ranging from 30˚C to 200˚C at a heating rate of 2 ˚C/min was adopted according to ASTM D5418 recommendations. Glass transition temperature (*Tg*) was determined by the peak value of loss modulus (E'').

Kinetics of curing using non-isothermal method

Differential scanning calorimetry (DSC) was used to investigate the kinetics of curing of pure and modified epoxy systems using a *Hitachi DSC 7020* calorimeter. Non-isothermal runs using four heating rates (*ß*) (2.5, 5.0, 10.0 and 20.0) ˚C/min were employed, over temperature ranges of 20 ˚C to 250 ˚C, under nitrogen atmosphere (30 mL/min). DSC runs were performed in open aluminum pans containing liquid resin (2-5 mg). A time period of 30 min was observed between mixing and starting the DSC run for all liquid samples.

The curing kinetics was described using following Kissinger's [121] method (Eq. 10):

$$ln\left(\frac{\beta}{T_p^2}\right) = ln\left(\frac{AR}{E_a}\right) - \frac{E_a}{RT_p} \quad \text{(Eq. 10)}$$

where T_p is the peak temperature (K) of the exothermic event during curing, A is the pre-exponential factor (min^{-1}), R is the gas constant (8.314 J / mol K) and E_a is the activation energy (J / mol). The linear slope of the graph obtained by $ln(ß/T_p^2)$ and $1/T_p$ was used to determine E_a. The area under the DSC heat flow curves was used to determine the heat of the reaction (ΔH), which was necessary to calculate the curing conversion (α), by an accumulating function.

FTIR spectroscopy of healed samples

The effect of a healing cycle on epoxy chemical structure was investigated through Fourier transform infrared (FTIR) spectroscopy. Cured and post-cured samples were subjected to a healing cycle for 30 min at 150 ˚C and spectra were compared to the original samples (Table 8). An FTIR spectrometer Shimadzu *IRTracer-100* was used in Attenuated Total Reflectance (ATR) mode covering a 600-4000 cm^{-1} interval, using a 4 cm^{-1} resolution and a number of 40 scans. Samples of 4 mm thick were perpendicularly placed to the laser beam and spectra were averaged from four different measurements of the sample surface. FTIR spectra were also baselined and normalized according to the aromatic peak at 1508 cm^{-1}.

Table 8 - Sample designations for FTIR measurements (complementary tests).

Pure epoxy		**Modified epoxy**	
PC	Cured	**MC**	Cured
PCH	Cured and healed	**MCH**	Cured and healed
PPC	Post-cured	**MPC**	Post-cured
PPCH	Post-cured and healed	**MPCH**	Post-cured and healed

Interfacial shear strength (IFSS) of healed samples

The effect of a healing cycle on the fiber-matrix interfacial shear strength (IFSS) was evaluated by single fiber pull-out tests. Sample preparation and tests parameters can be found in *Section 5 – Single fiber pull-out tests*. Before testing, healing was performed at temperature of 150 ˚C for 30 min followed by cooling down to room temperature, which is maintained for at least a 24 h before testing. The number of samples for each condition is presented in Table 9.

Table 9 - Number of IFSS samples for each condition tested (complementary tests).

Pure epoxy	29 samples	**Modified epoxy**	30 samples
Pure epoxy - healed	13 samples	**Modified epoxy - healed**	17 samples

Results

Dynamic mechanical analysis (DMA)

Storage modulus (E') curves of cured samples (Figure 47a) presented an accentuated drop, whilst post-cured samples demonstrated a more gradual decrease. This may indicate that the network of cured samples was not completely interlocked, due to incomplete crosslinking. Thus, with fewer crosslink bonds anchoring the epoxy network, the transition region from a glassy to a rubbery solid was easily overpassed.

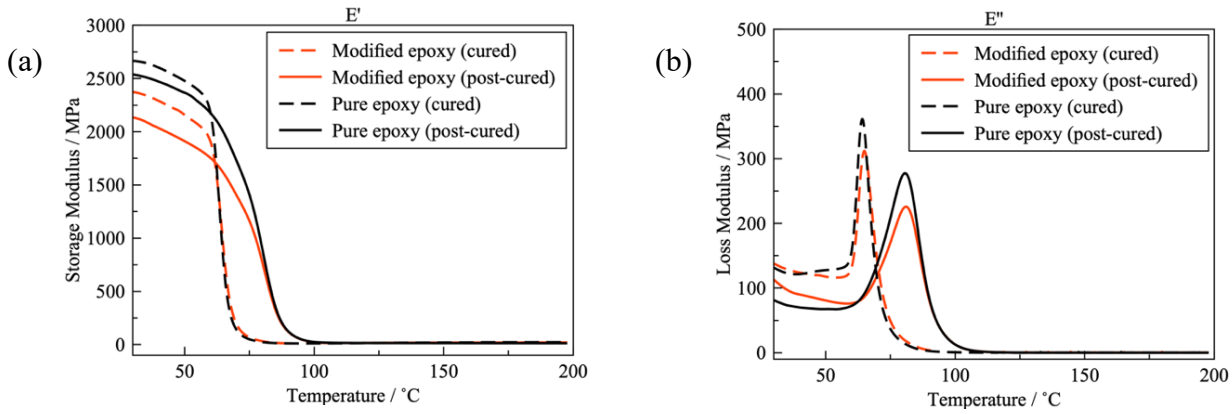

Figure 47 - DMA curves of pure and modified epoxy systems: (a) Storage Modulus and (b) Loss Modulus (complementary tests).

A single drop in *E'* and single peak in loss modulus (*E"*) observed in the curves are also relevant. Despite the melting temperature (*Tm*) of this type of EMAA (89˚C [120]) being in the range of epoxy glass transition temperature (*Tg*) (Figure 47b), it did not change the curves for cured or post-cured systems. In fact, this is an indication that EMAA and epoxy network are two separated phases acting cohesively due to their strong chemical affinity.

The crosslinking effect could also be verified by the *Tg* in *E"* curves (Figure 47b). The addition of EMAA did not a *Tg* in either cured or post-cured conditions. This is an indicative that EMAA did not alter significantly viscoelastic properties of the epoxy network, as similarly observed in a previous work [110].

Kinetics of curing using non-isothermal method

All DSC curves show a single exothermic peak for all heating rates (β) (Figure 48). Peak temperature (T_p) and the area under the curve (ΔH) shifted towards higher values as (β) increases (Table 10). Comparing both epoxy systems, a decrease in ΔH values was observed for all modified curves, except for the 20˚C/min heating ramp, which instead revealed an increase (Table 10). This may indicate that EMAA effects on epoxy network formation varies when a certain sample processing condition is achieved.

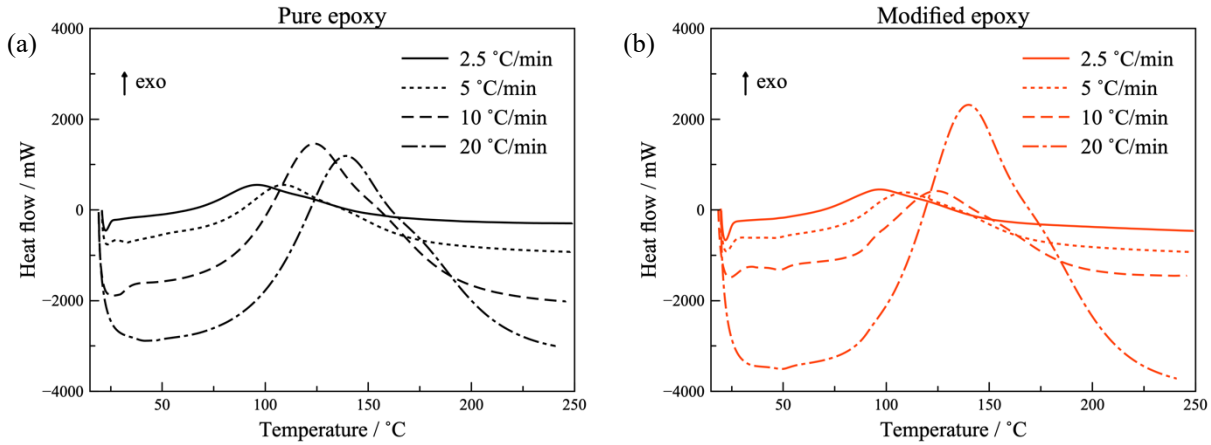

Figure 48 - Non-isothermal DSC curves for (a) pure epoxy and (b) modified epoxy systems (complementary tests).

Table 10 - DSC data of pure and modified epoxy systems (complementary tests).

Pure epoxy					
β (°C/min)	T_p (K)	$ln\ \beta$	$1 / T_p$ ($\times 10^3$ K^{-1})	$- ln\ (\beta/T_p^2)$	$-\Delta H$ (J/g)
2.5	369.2	0.916	2.708	-10.907	51.4
5	382.4	1.609	2.614	-10.284	91.3
10	397.1	2.302	2.517	-9.666	208.3
20	412.2	2.996	2.426	-9.048	315.6
Modified epoxy					
β (°C/min)	T_p (K)	$ln\ \beta$	$1 / T_p$ ($\times 10^3$ / K^{-1})	$- ln\ (\beta/T_p^2)$	$-\Delta H$ (J/g)
2.5	370.2	0.916	2.701	-10.912	41.9
5	382.5	1.609	2.614	-10.284	77.6
10	397.7	2.302	2.514	-9.669	107.1
20	413.1	2.996	2.420	-9.052	408.7

Activation energy (E_a) was obtained from the slope of the Kissinger model plots (Figure 49). A linear fitting (R^2) higher than 0.999 for pure and modified systems was found. No relevant

differences in E_a for pure epoxy (E_a = 54.5 KJ/mol) and modified epoxy (E_a = 54.7 KJ/mol) were observed. This may indicate that both systems need to overpass the same activation energy to curing.

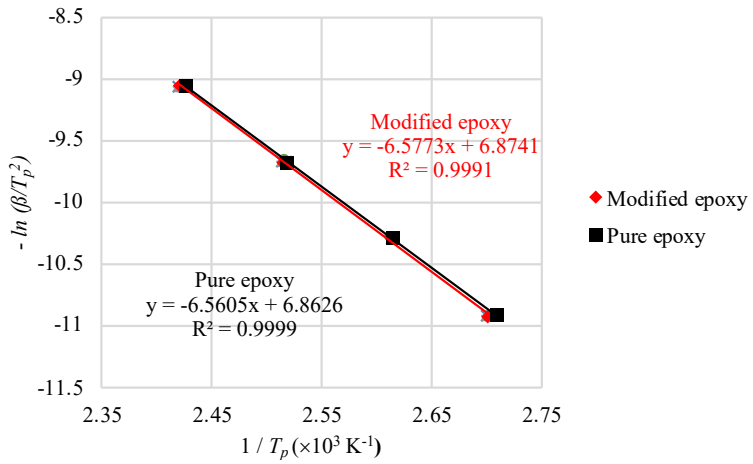

Figure 49 - Slopes of $-ln(\beta/T_p^2)$ vs $1/T_p$ for pure and modified epoxy (complementary tests).

Curing conversion (α) over temperature plots (Figure 50) for pure and modified epoxy suggest that EMAA addition lead to two different behaviors. First, at lower temperatures, modified epoxy showed slower curing conversion compared to pure epoxy. However, at higher temperatures, the thermoplastic modification increases conversion, overpassing that of pure epoxy curves, which was also observed in the paper presented in this document and in previous investigations [110]. Furthermore, the effect of accelerating and slowing the curing rate conversion may be due to the similar E_a found in both epoxy systems, because of their opposite and combining effects.

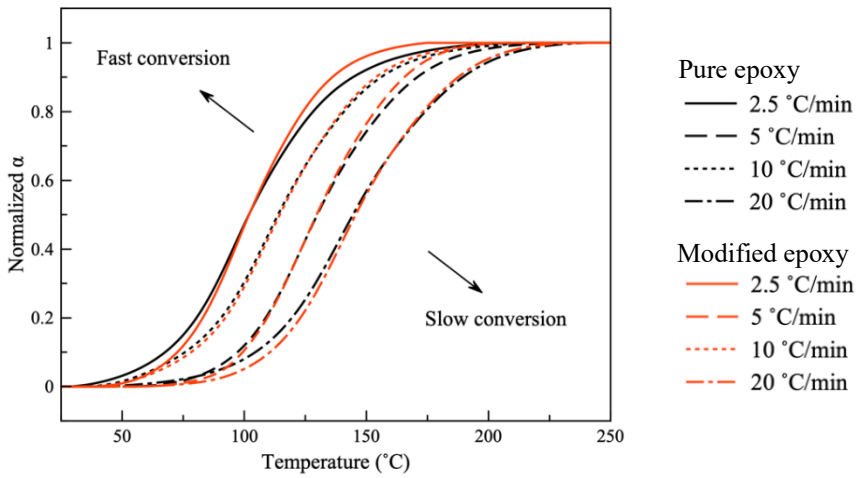

Figure 50 – Normalized curing conversion (α) over temperature for pure and modified epoxy (complementary results).

FTIR spectroscopy of healed samples

FTIR spectra of all analyzed samples are presented in Figure 51. The presence of carbonyl peak (1730 cm^{-1}) (Figure 51b) can be due to two reasons: (1) oxidation of epoxy structure [29,31] and (2) carboxyl group from EMAA molecule [88]. In this regard, PCH revealed a significant increase in carbonyl peak, as compared to PC spectrum. This may be an indicative that not post cured pure epoxy is more susceptible to oxidation, suggesting that only part of the chemical structure is crosslinked, thus allowing unreacted sites of the epoxy chain to be oxidized.

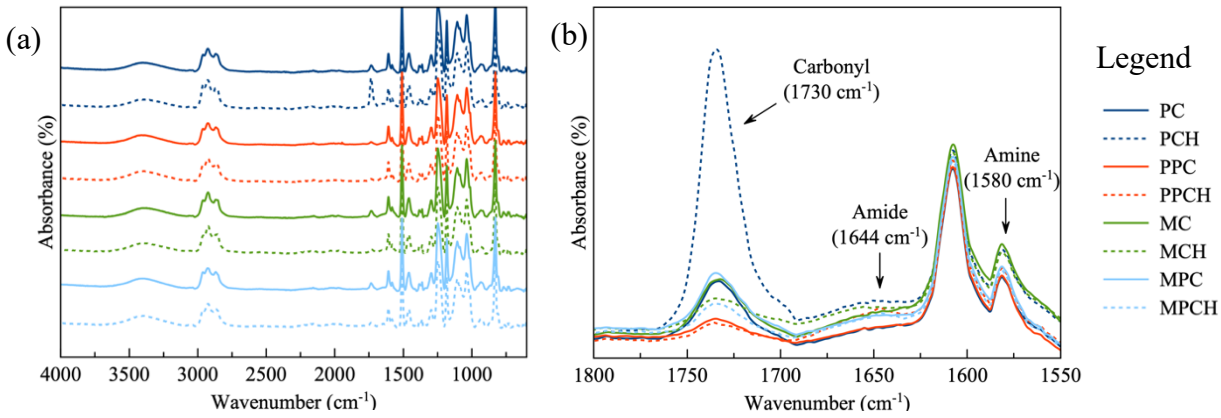

Figure 51 - FTIR spectra of all samples: (a) full range spectra and (b) 1800-1550cm^{-1} interval (complementary tests).

MCH (Figure 51b) presented an opposite response when compared to MC samples, that is a decrease of intensity of carbonyl peak after healing. This trend was also observed in MPCH (in comparison to MPC) and may be an indicative of two events: (1) consumption of carboxyl groups from EMAA chain during healing and (2) alteration of epoxy oxidation susceptibility. Oxidation was also observed in PPCH samples, and in lower extent in PCH and MCH by the amide (1644cm^{-1}) [32,88] peak rising.

Remaining amine groups (1580cm^{-1}) in the spectra of MC and MCH suggests that EMAA changed the epoxy-amine consumption, as observed in previous works [20,88]. This suggests that the healing cycle was not sufficient to promote further epoxy-amine reactions, because of other competing reactions, such as oxidation and carboxyl consumption.

Interfacial shear strength (IFSS) of healed samples

Force-displacement curves (Figure 52) for all tested conditions reveal the same mechanical response concerning adhesion followed by friction forces. This may indicate that healing does not significantly affect interfacial properties of neat or modified epoxy systems. A larger number of healed samples is needed to confirm such assumptions.

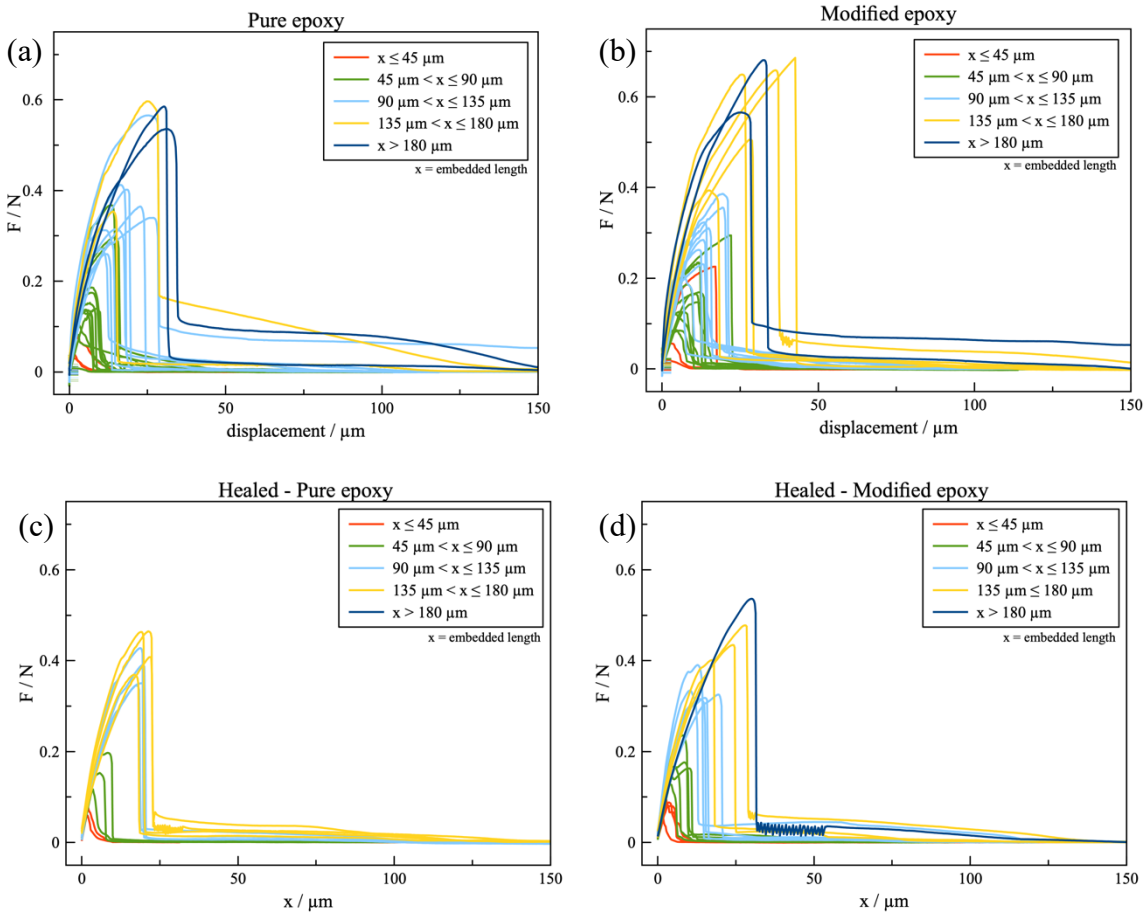

Figure 52 - Single fiber pull-out force-displacement curves: (a) pure epoxy, (b) 10 wt.% EMAA modified epoxy, (c) pure epoxy healed, and (d) modified epoxy healed (complementary tests).

Analyses of the fiber-matrix interfacial data of cured and post-cured (before and after healing) samples are presented in Figure 53. Considering the standard deviation scattering, average values of IFSS (Figure 53a) were quite similar. A small error bar of healed samples may be related either to more precise measurements or to the lower number of samples.

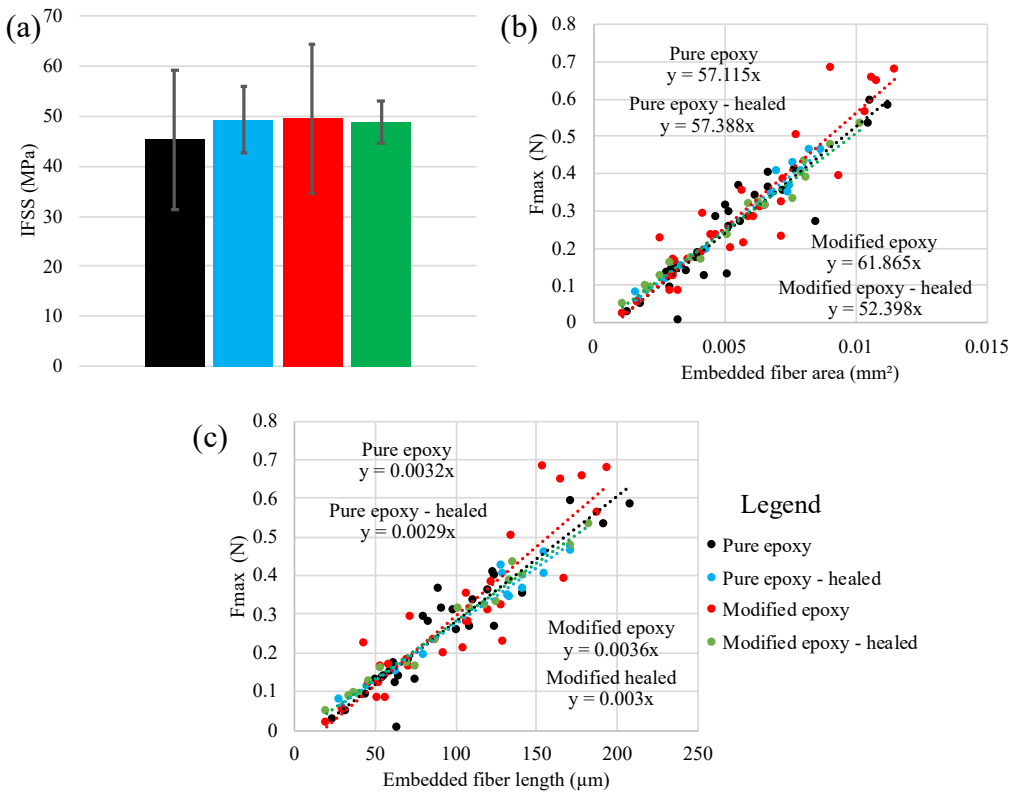

Figure 53 - Analyses of pull-out test results for epoxy systems: (a) Average and standard deviation of IFSS values, (b) Maximum force (F_{max}) *vs* Embedded fiber area and (c) Embedded fiber length plot (complementary tests).

The adhesion behavior (Figure 53b) also revealed a similar tendency for all pure epoxy samples (*y-slopes*). However, modified epoxy systems showed a decrease in *y-slope*, when comparing original (y = 61.9x) and healed (y = 52.4x) data. Two possible reasons could explain this behavior: (1) the lower number of samples and (2) change in IFSS due to a healing cycle in modified epoxy systems. Due to the lack of standardization, it is appropriate to perform more than 30 single-fiber pull-out tests per sample condition to obtain results which are more representative of the properties measured. Similar tendency was found when comparing fiber embedded length (Figure 53c).

8. Conclusions

The micromechanics of an epoxy with self-healing ability was investigated. For this, the effects of the addition of the thermoplastic healing agent, poly(ethylene-co-methacrylic acid) (EMAA), on the epoxy network formation were studied. In fact, the main results revealed alterations in the kinetics of curing and thermomechanical properties of modified epoxy systems, which were also confirmed by preliminary and complementary studies. Nevertheless, the changes did not demonstrate to be crucial to the interfacial properties of an EMAA modified epoxy, which presented similar and satisfactory values of interfacial shear strength (IFSS) even after a healing cycle.

The interfacial properties between fiber and EMAA, on the other hand, revealed a significantly lower IFSS, as compared to epoxy samples. This suggests that healing ability is most likely performed by fiber-matrix or EMAA-matrix and not by fiber-EMAA interactions.

A new approach to assess healing efficiency was achieved using micromechanical tests. In this case, pure and modified epoxy systems were capable of restore interfacial properties. Pure epoxy systems presented higher healing efficiency than modified epoxy ones. The promotion of new chemical bonds and matrix shrinkage are the main reasons that explain the higher efficiency of pure epoxy samples. Additionally, the lower IFSS of fiber-EMAA and the chemical alterations observed after a healing cycle are among the reasons for the lower healing efficiency of modified epoxy systems.

9. Suggestions for future works

Single-lap shear test: EMAA-epoxy interaction

Once fiber-matrix and fiber-thermoplastic interactions were already scrutinized, measuring thermoplastic-matrix interactions can provide a complete view about the mechanism of healing. In this perspective, single-lap shear tests with thermoplastic substrates can be greatly useful.

A typical single-lap shear test specimen is shown in Figure 54. In this test, a common area (shear area) is bonded using an epoxy resin. Interaction of different substrates with epoxy can be stipulated by pulling each extremity of the test specimen (area in-test grips). Full test recommendations can be found in ASTM D3163.

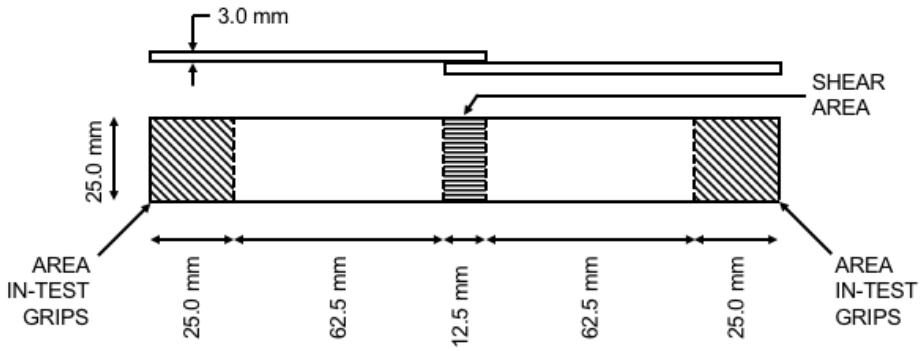

Figure 54 - Arrangement and dimensions of a single-lap shear specimen test.

Effect of multiple healings on epoxy

One characteristic of intrinsic healing mechanism is the ability to perform multiple healings, which can vary from 1 to 5 healing cycles [90,92,93,122,123]. Multiple healings can be performed to evaluate chemical and thermomechanical alterations in the epoxy network. In this perspective, dynamic mechanical analysis (DMA) and infrared spectroscopy can be very useful for understanding alterations caused by healing cycles in epoxy systems. Furthermore, these tests can also reveal the effects of aging caused by multiple healing events.

Effect of multiple healings on interfacial properties

The effect of multiple healings can also be assessed by single fiber pull-out tests. In this case, interfacial shear strength (IFSS) measurements can elucidate the tendency of multiple healing cycles and then predict the composite mechanical properties.

Appendix A – Supporting information

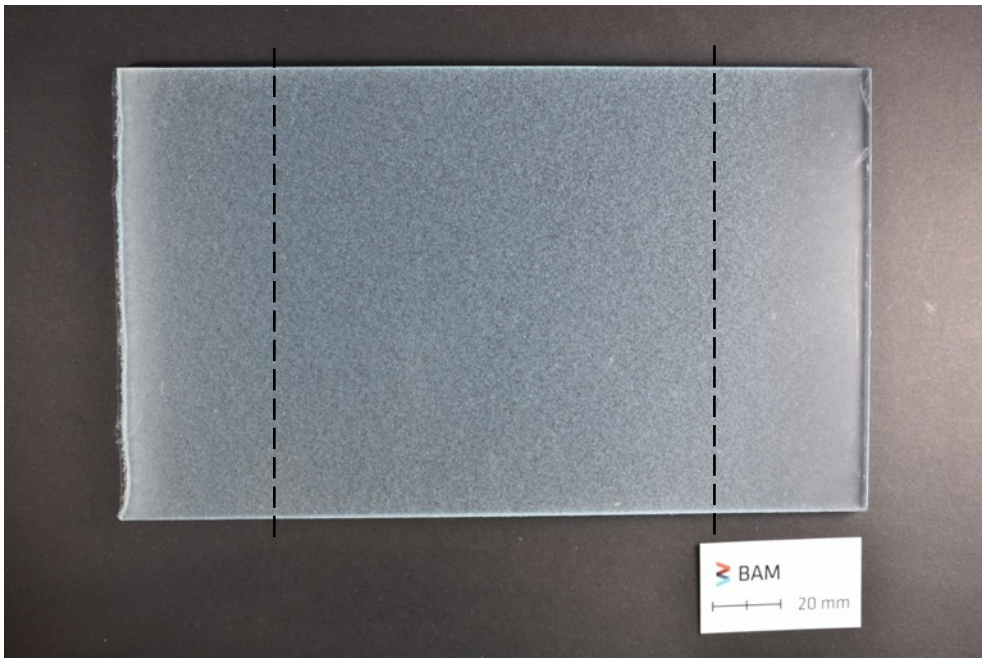

Figure S1 – Modified epoxy plate. Dashed lines delimitate de middle region, 45 mm from the upper and lower edges.

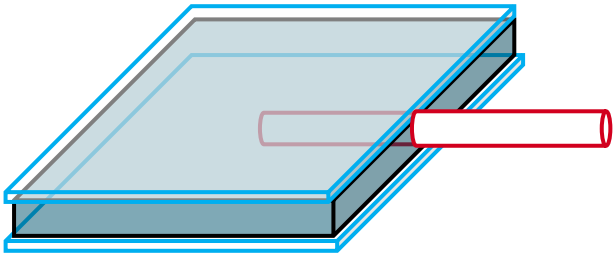

Figure S2 – Schema of the optically monitored test specimen.

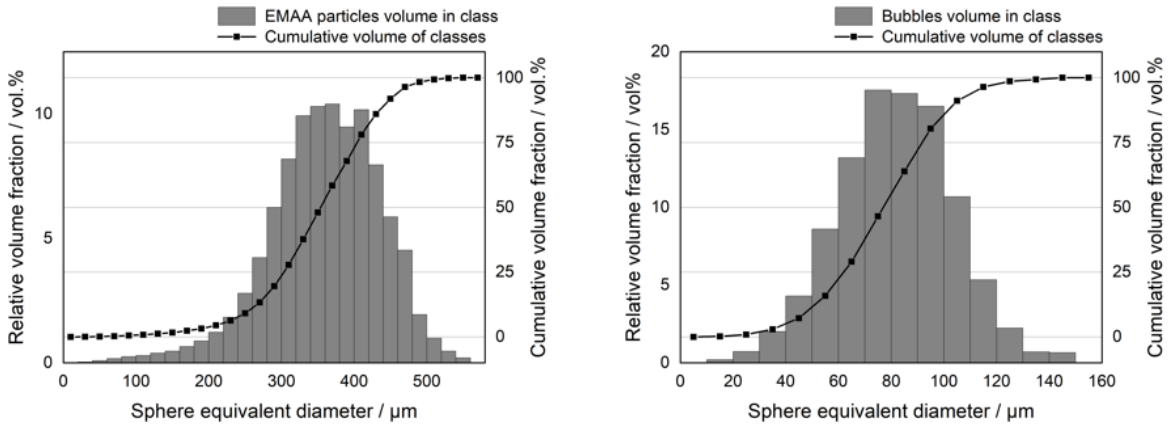

(a) (b)

Figure S3 - Volume size distribution of (a) EMAA particles and (b) bubbles.

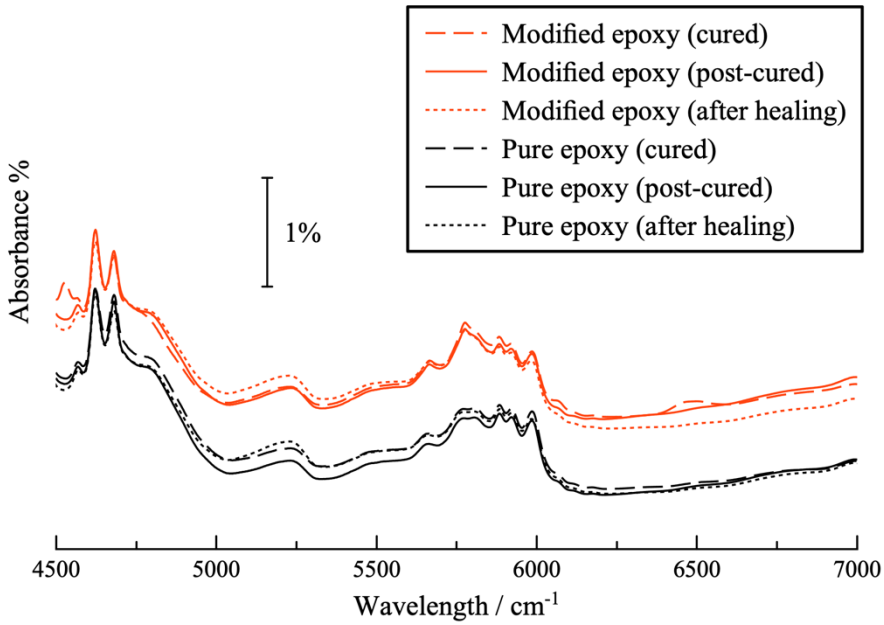

Figure S4 - NIR full spectra of pure and modified epoxy samples along with their cured and post-cured conditions.

Table S5 - Glass transition temperature (*Tg*) of pure and modified epoxy samples.

Sample	**Glass transition temperature (*Tg*)**
Pure epoxy – 1st heating	83.5 ˚C
Pure epoxy – 2nd heating	90.0 ˚C
Modified epoxy – 1st heating	81.2 ˚C
Modified epoxy – 2nd heating	81.0 ˚C

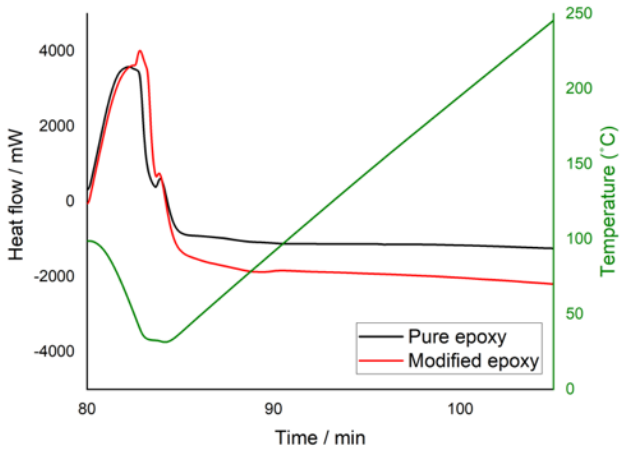

Figure S6 - DSC runs of pure and modified epoxy after an 80 min isotherm at 100˚C.

Table S7 - Kinetics parameters of pure and modified epoxy samples.

Sample	T (°C)	m	n	k_1	k_2	E_{a1} (kJ mol^{-1})	E_{a2}(kJ mol^{-1})
Pure epoxy	100	0.24	2.48	3.71	65.44	65.66	41.26
	110	1.00	1.00	0.41	33.41	65.34	35.94
	120	1.00	1.00	0.04	406.9	65.34	27.77
					Average	**65.4 ±0.2**	**35.0 ±6.8**
Modified epoxy	100	1.51	1.00	0.43	33.07	65.18	35.97
	110	0.34	1.85	0.22	360.5	77.78	38.68
	120	0.18	1.00	0.64	313.5	63.89	36.14
					Average	**68.9 ±7.6**	**36.9 ±1.5**

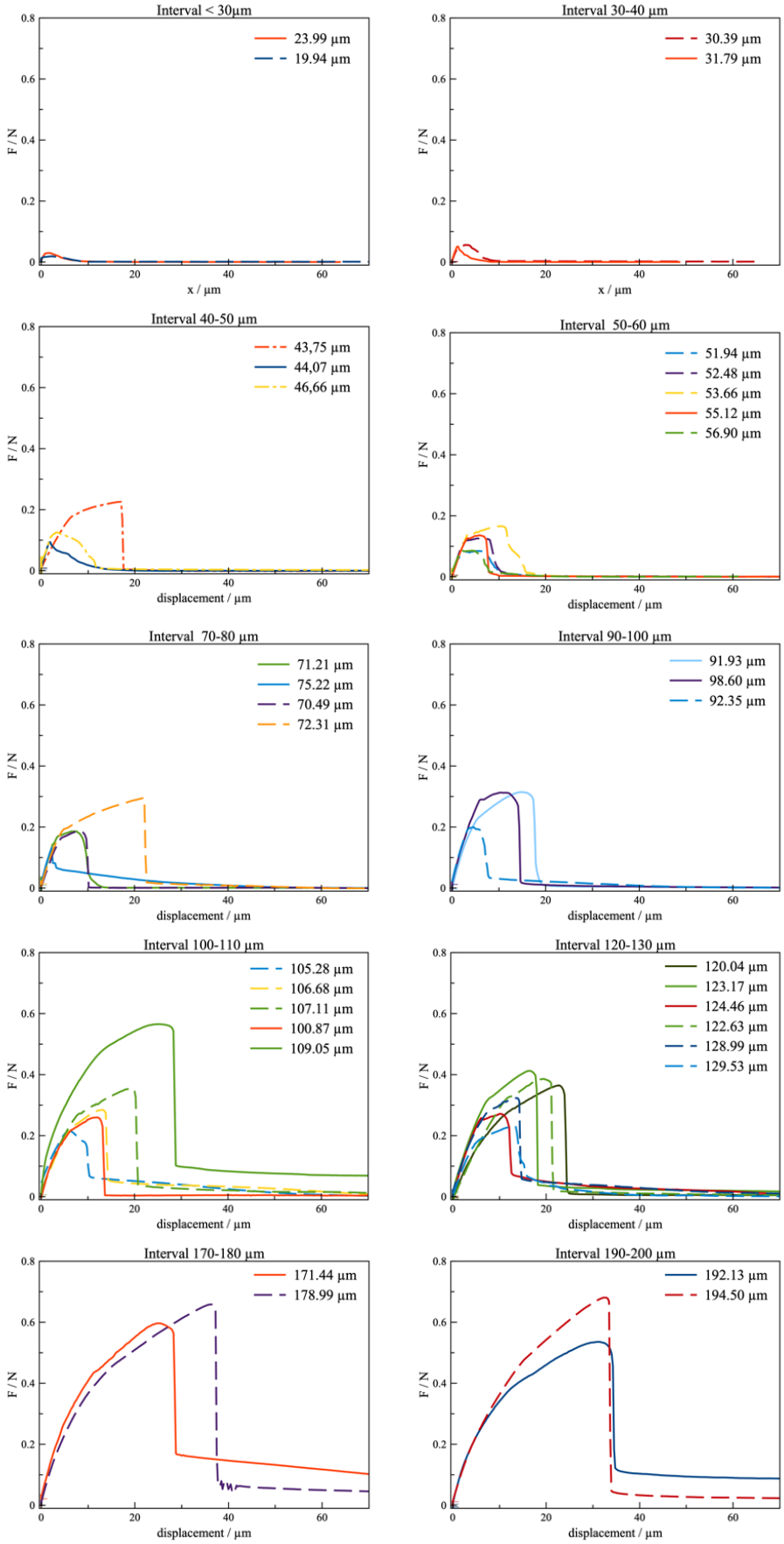

Figure S8 - Force-displacement curves of pure (solid line) and modified (dashed line) epoxy systems according to the interval of fiber embedding length.

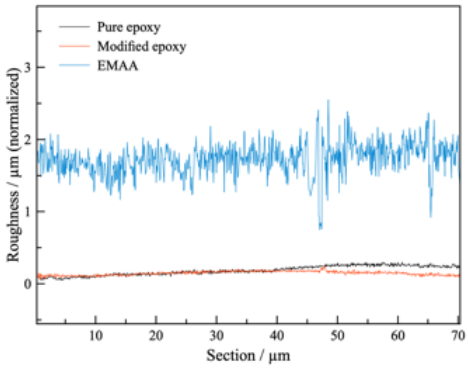

Figure S9 - Roughness profile of embedded fiber area of Pure epoxy, Modified (10 wt% EMAA) and Pure EMAA samples.

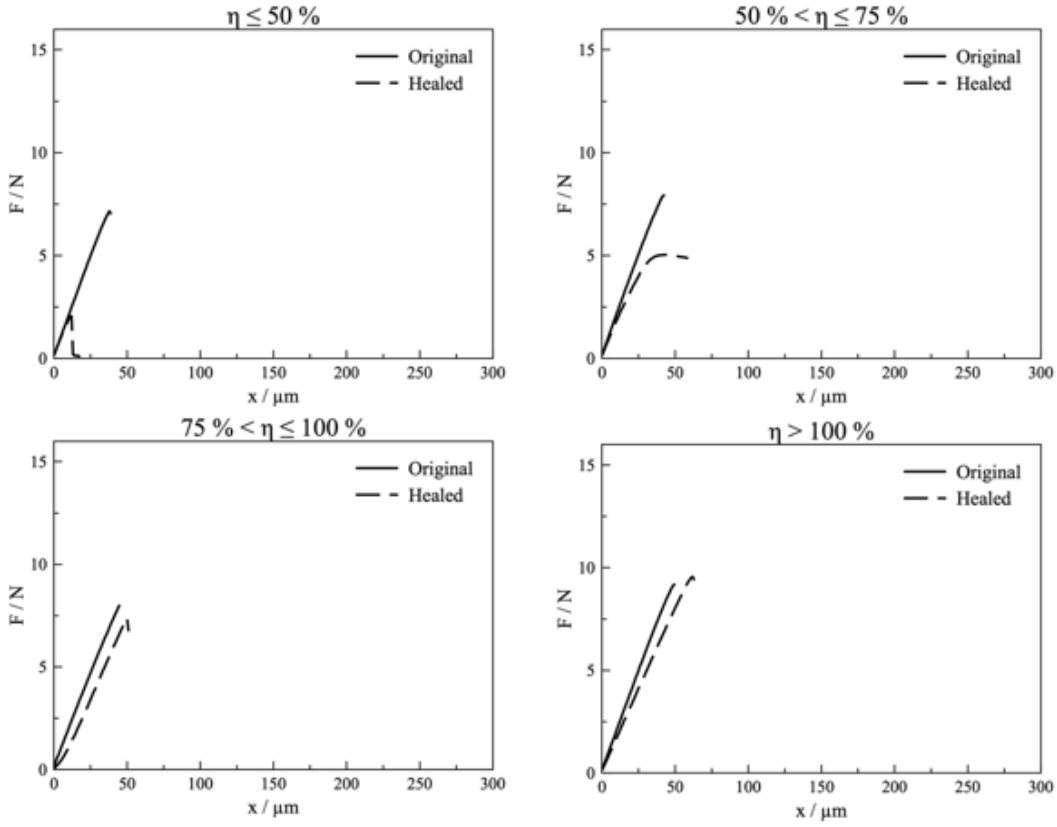

Figure S10 - Typical curves of OM pull-out tests of pure epoxy samples grouped according to the healing efficiency (η).

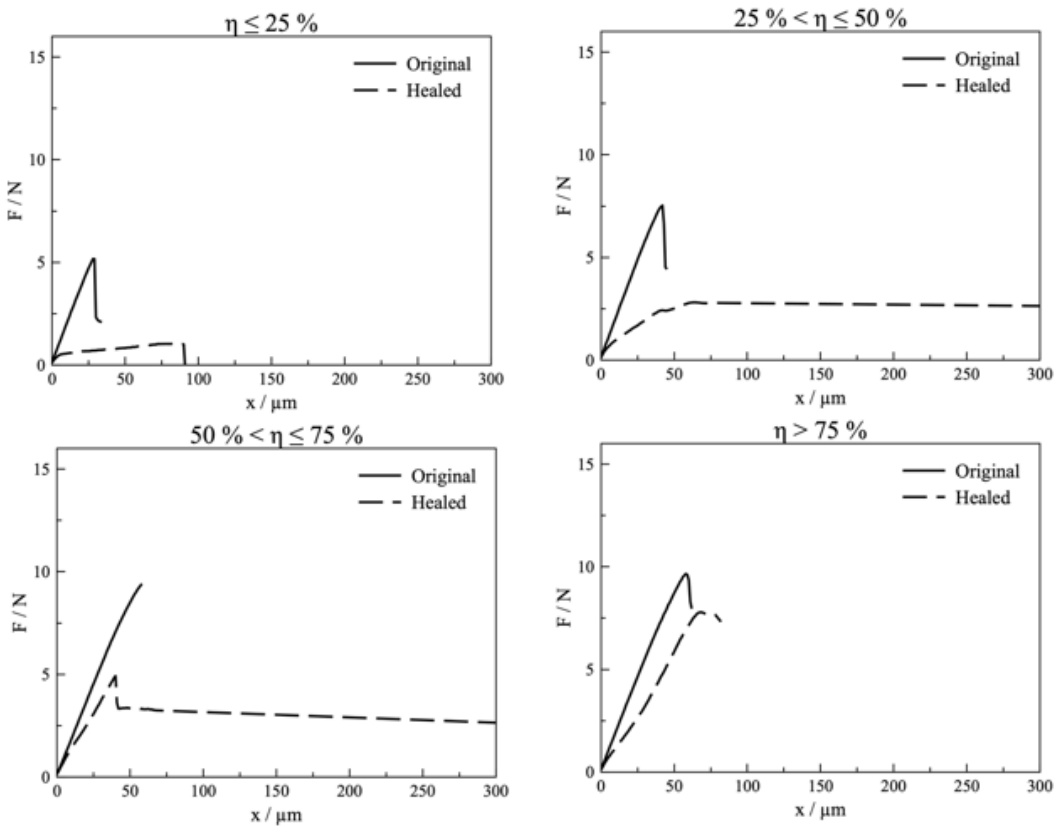

Figure S11 – Typical curves of OM pull-out tests of modified epoxy samples grouped according to the healing efficiency (η).

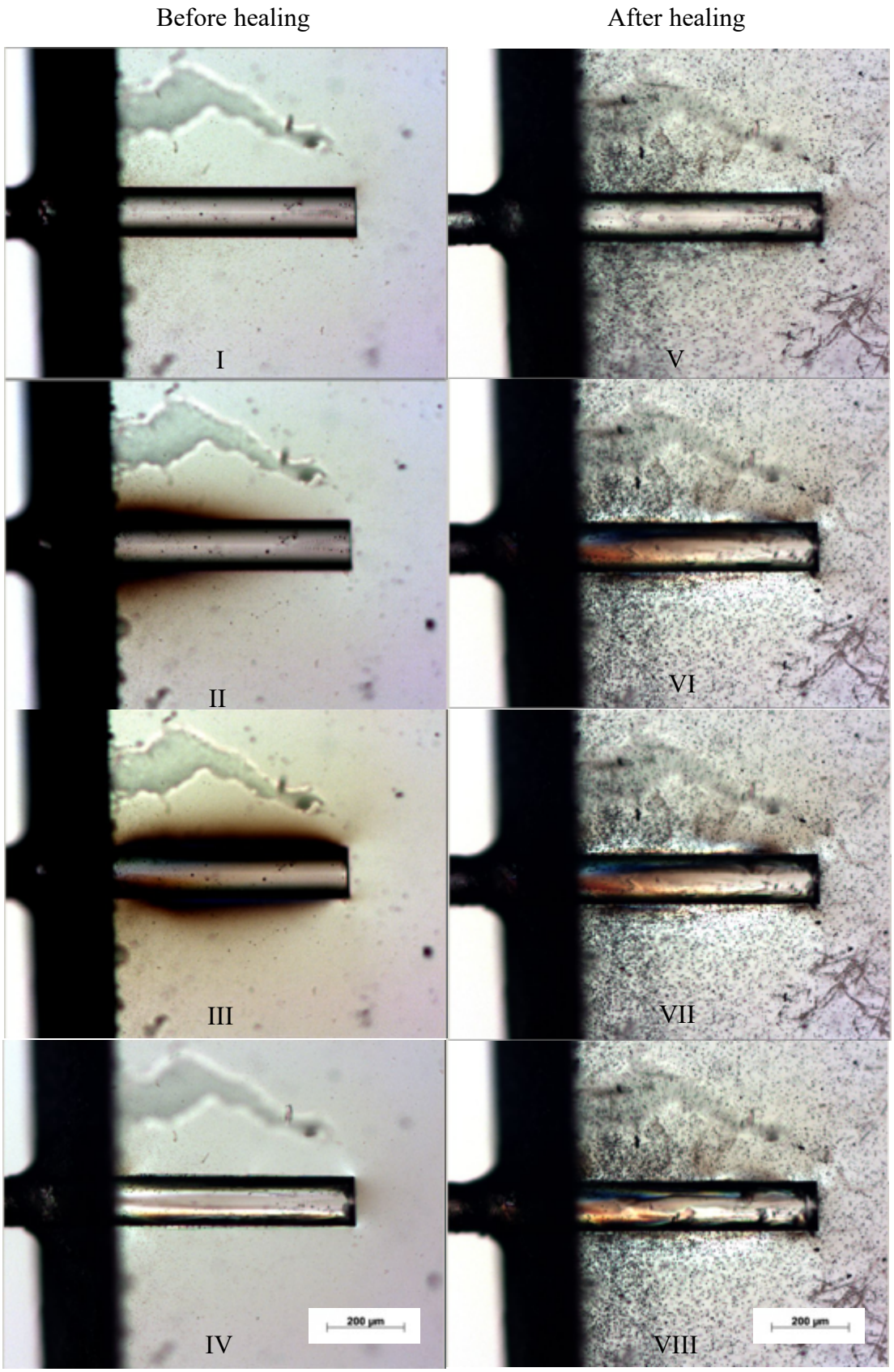

Videos S12 and S13 - Time lapse images of OM single fiber pull-out tests of a pure epoxy sample before (S12 – I to IV) and after (S13 – V to VIII) healing.

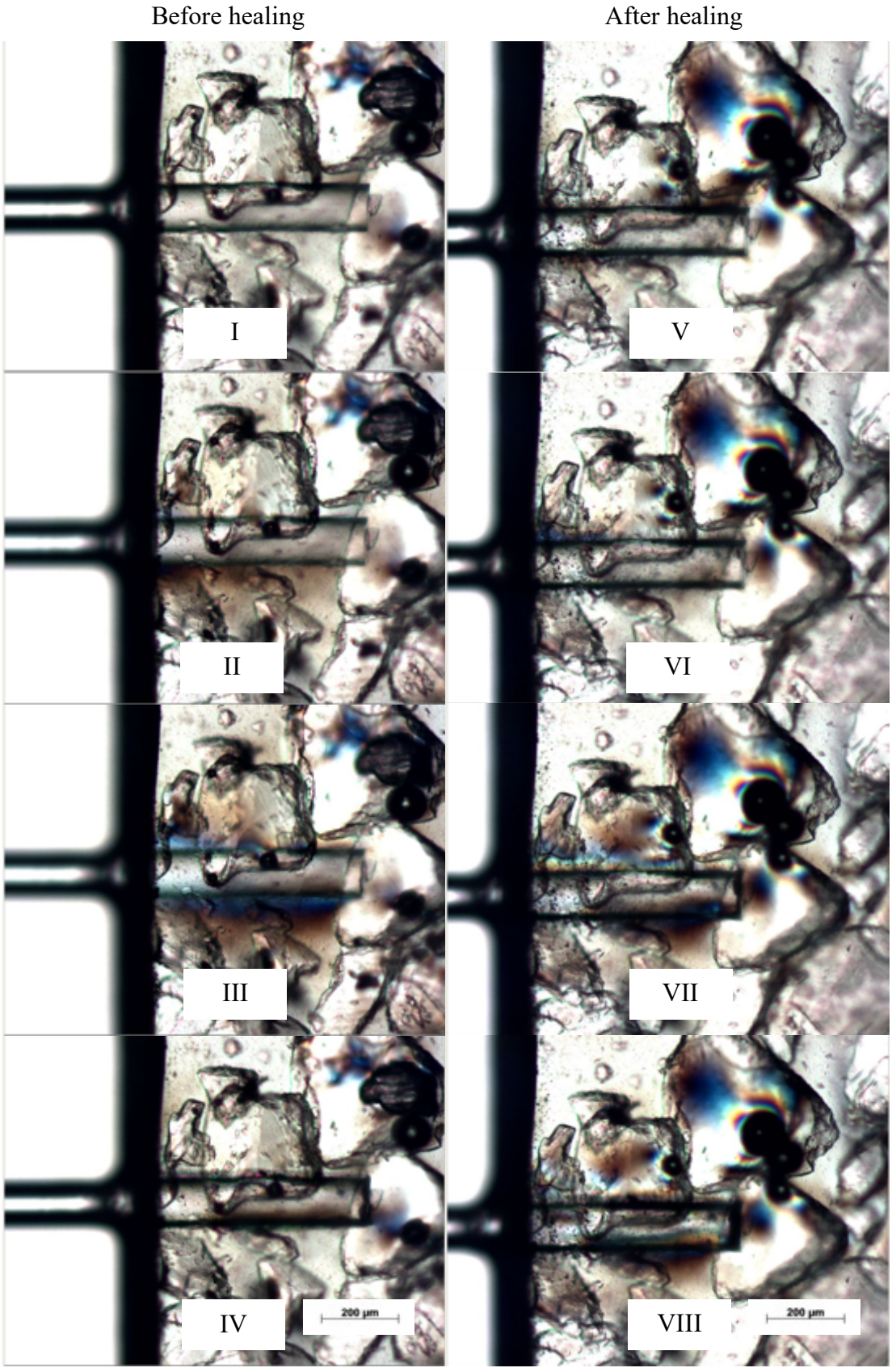

Videos S14 and S15 - Time lapse images of OM single fiber pull-out tests of a EMAA modified epoxy sample before (S14 – I to IV) and after (S15 – V to VIII) healing.

References

[1] **W. D. Callister and D. G. Rethwisch**, *Materials science and engineering: an introduction*, 8th ed. John Wiley and Sons, 2009.

[2] **J. K. Fink**, *Reactive Polymers Fundamentals and Applications: Epoxy Resins*. 2013.

[3] **C. Li and A. Strachan**, "Free volume evolution in the process of epoxy curing and its effect on mechanical properties," *Polymer*, vol. 97, pp. 456–464, 2016.

[4] **V. Authors**, *Epoxy resins: Chemistry and technology*, 2nd ed. Marcel Dekker, Inc, 1988.

[5] **H. J. White**, "Amine curing agents for epoxy resins," *Journal of Protective Coatings and Linings*, vol. 6, no. 8, pp. 47–56, 1989.

[6] **E. W. Flick**, *Epoxy Resins, Curing Agents, Compounds, and Modifiers: an Industrial Guide*, 2nd ed. Noyes Publication, 1992.

[7] **N. R. Paluvai, S. Mohanty, and S. K. Nayak**, "Synthesis and Modifications of Epoxy Resins and Their Composites: A Review," *Polymer-Plastics Technology and Engineering*, vol. 53, no. 16, pp. 1723–1758, 2014.

[8] **A. Srikanth, J. Vergara, G. Palmese, and C. F. Abrams**, "The effect of alkyl chain length on material properties of fatty-acid-functionalized amidoamine-epoxy systems," *European Polymer Journal*, vol. 89, pp. 1–12, 2017.

[9] **A. Cerit, M. E. Marti, U. Soydal, S. Kocaman, and G. Ahmetli**, "Effect of Modification with Various Epoxide Compounds on Mechanical, Thermal, and Coating Properties of Epoxy Resin," *International Journal of Polymer Science*, vol. 2016, 2016.

[10] **V. Authors**, *Epoxy Resin Chemistry*. American Chemical Society, 1979.

[11] **O. Cakiroglu, L. Arda, C. Boyraz, and O. A. Sacli**, "Electrical Characterizations of MgO-ZrO2 High Temperature Sol-Gel Insulations Coatings on Different Types of Epoxies," *IEEE Transactions on Applied Superconductivity*, vol. 18, no. 2, pp. 1398–1401, Jun. 2008.

[12] **A. Burkanudeen and P. Ramesh**, "Novel latent epoxy curing agent for secondary insulation in electrical rotors and stators," *IEEE Transactions on Dielectrics and Electrical Insulation*, vol. 19, no. 5, pp. 1791–1798, 2012.

[13] **S. Komori and Y. Sakamoto**, "Development Trend of Epoxy Molding Compound for Encapsulating Semiconductor Chips," in *Materials for Advanced Packaging*, D. Lu and C. P. Wong, Eds. Boston, MA: Springer US, 2009, pp. 339–363.

[14] **C.-H. Lin, W.-T. Whang, C.-H. Chen, S.-C. Huang, and K.-C. Chen**, "Novel Siloxane-Modified Epoxy Resins as Promising Encapsulant for LEDs," *Polymers*, vol. 12, no. 1, p. 21, Dec. 2019.

[15] **F. L. Jin, X. Li, and S. J. Park**, "Synthesis and application of epoxy resins: A review," *Journal of Industrial and Engineering Chemistry*, vol. 29, pp. 1–11, 2015.

[16] **C. Pommer and M. Sinapius**, "A Novel Approach to Monitoring the Curing of Epoxy in Closed Tools by Use of Ultrasonic Spectroscopy," *Sensors*, vol. 18, no. 1, p. 96, Dec. 2017.

[17] **D. G. Lee and H. G. Kim**, "Non-isothermal in situ dielectric cure monitoring for thermosetting matrix composites," *Journal of Composite Materials*, vol. 38, no. 12, pp. 977–993, 2004.

[18] **R. Montanini and L. D'Acquisto**, "Simultaneous measurement of temperature and strain in glass fiber/epoxy composites by embedded fiber optic sensors: I. Cure monitoring," *Smart Materials and Structures*, vol. 16, no. 5, pp. 1718–1726, 2007.

[19] **C. M. Sahagun, K. M. Knauer, and S. E. Morgan**, "Molecular network development and evolution of nanoscale morphology in an epoxy-amine thermoset polymer," *Journal of Applied Polymer Science*, vol. 126, no. 4, pp. 1394–1405, Nov. 2012.

[20] **M. González-González, J. C. Cabanelas, and J. Baselga**, *Infrared Spectroscopy - Materials Science, Engineering and Technology*, vol. 2. InTech, 2012.

[21] **J. D. McCoy *et al.***, "Cure mechanisms of diglycidyl ether of bisphenol A (DGEBA) epoxy with diethanolamine," *Polymer (United Kingdom)*, vol. 105, pp. 243–254, 2016.

[22] **G. Nikolic, S. Zlatkovic, M. Cakic, S. Cakic, C. Lacnjevac, and Z. Rajic**, "Fast Fourier Transform IR Characterization of Epoxy GY Systems Crosslinked with Aliphatic and Cycloaliphatic EH Polyamine Adducts," *Sensors*, vol. 10, no. 1, pp. 684–696, Jan. 2010.

[23] **N. Poisson, G. Lachenal, and H. Sautereau**, "Near- and mid-infrared spectroscopy studies of an epoxy reactive system," *Vibrational Spectroscopy*, vol. 12, no. 2, pp. 237–247, 1996.

[24] **J. Mijovic and S. Andjelic**, "A Study of Reaction Kinetics by Near-Infrared Spectroscopy. 1. Comprehensive Analysis of a Model Epoxy/Amine System," 1995.

[25] **D. A. Janzen, M. F. Diniz, J. B. Azevedo, J. R. A. Pinto, N. B. Sanches, and R. D. C. L. Dutra**, "Qualitative and quantitative evaluation of epoxy systems by fourier transform infrared spectroscopy and the flexibilizing effect of mercaptans," *Anais da Academia Brasileira de Ciencias*, vol. 93, no. 2, pp. 1–20, 2021.

[26] **S. Yoshida**, "Quantitative evaluation of an epoxy resin dispersion by infrared spectroscopy,"

Polymer Journal, vol. 46, no. 7, pp. 430–434, 2014.

[27] **M. Erdmann, V. Trappe, H. Sturm, U. Braun, and E. Duemichen**, "Cure conversion of structural epoxies by cure state analysis and in situ cure kinetics using nondestructive NIR spectroscopy," *Thermochimica Acta*, vol. 650, pp. 8–17, 2017.

[28] **E. Duemichen *et al.***, "Analyzing the network formation and curing kinetics of epoxy resins by in situ near-infrared measurements with variable heating rates," *Thermochimica Acta*, vol. 616, pp. 49–60, 2015.

[29] **A. Doblies, B. Boll, and B. Fiedler**, "Prediction of thermal exposure and mechanical behavior of epoxy resin using artificial neural networks and Fourier transform infrared spectroscopy," *Polymers*, vol. 11, no. 2, 2019.

[30] **S. Yousef, J. Eimontas, N. Striūgas, and M. A. Abdelnaby**, "Influence of carbon black filler on pyrolysis kinetic behaviour and TG-FTIR-GC–MS analysis of glass fibre reinforced polymer composites," *Energy*, vol. 233, 2021.

[31] **S. Yousef, J. Eimontas, N. Striūgas, M. Praspaliauskas, and M. A. Abdelnaby**, "Pyrolysis kinetic behaviour of glass fibre-reinforced epoxy resin composites using linear and nonlinear isoconversional methods," *Polymers*, vol. 13, no. 10, pp. 1–18, 2021.

[32] **A. P. Cysne Barbosa *et al.***, "Accelerated aging effects on carbon fiber/epoxy composites," *Composites Part B: Engineering*, vol. 110, pp. 298–306, 2017.

[33] **A. P. P. Fulco, A. M. de Medeiros, M. L. P. Tonatto, S. C. Amico, R. Talreja, and J. D. D. Melo**, "Fatigue damage and fatigue life diagrams of a carbon/epoxy cross ply laminate aged by hygrothermal exposure," *Composites Part A: Applied Science and Manufacturing*, vol. 127, no. May, p. 105628, 2019.

[34] **S. Zhou, Y. X. Jia, L. Xu, L. Wang, and L. Hui**, "Study on the damage behavior of carbon fiber composite after low-velocity impact under hygrothermal aging," *Journal of Applied Polymer Science*, vol. 138, no. 17, pp. 1–10, 2021.

[35] **V. Ollier-Dureault and B. Gosse**, "Photooxidation of anhydride-cured epoxies: FTIR study of the modifications of the chemical structure," *Journal of applied polymer*, vol. 70, pp. 1221–1287, 1998.

[36] **S. Vyazovkin and N. Sbirrazzuoli**, "Mechanism and kinetics of epoxy-amine cure studied by differential scanning calorimetry," *Macromolecules*, vol. 29, no. 6, pp. 1867–1873, 1996.

[37] **R. Hardis**, "Cure kinetics characterization and monitoring of an epoxy resin for thick composite structures," 2012.

[38] **J. Ding, W. Peng, T. Luo, and H. Yu**, "Study on the curing reaction kinetics of a novel epoxy system," *RSC Advances*, vol. 7, no. 12, pp. 6981–6987, 2017.

[39] **X. Yu, S. Chen, and Y. Xu**, "Curing Kinetics and Properties of Epoxy Resin with 1, 4-bis (2, 4-diaminophenoxy)benzene," *Journal of Wuhan University of Technology-Mater. Sci. Ed.*, vol. 33, no. 5, pp. 1256–1262, Oct. 2018.

[40] **H. Ma, X. Zhang, F. Ju, and S.-B. Tsai**, "A Study on Curing Kinetics of Nano-Phase Modified Epoxy Resin," *Scientific Reports*, vol. 8, no. 1, p. 3045, Dec. 2018.

[41] **M. Javdanitehran, D. C. Berg, E. Duemichen, and G. Ziegmann**, "An iterative approach for isothermal curing kinetics modelling of an epoxy resin system," *Thermochimica Acta*, vol. 623, pp. 72–79, 2016.

[42] **A. Bernath, L. Kärger, and F. Henning**, "Accurate cure modeling for isothermal processing of fast curing epoxy resins," *Polymers*, vol. 8, no. 11, pp. 1–19, 2016.

[43] **H. Cai *et al.***, "Curing kinetics study of epoxy resin/flexible amine toughness systems by dynamic and isothermal DSC," *Thermochimica Acta*, vol. 473, no. 1–2, pp. 101–105, 2008.

[44] **L. Núñez, F. Fraga López, L. Fraga Grueiro, and J. A. Rodriguez Añón**, "Activation energies and rate constants for an epoxy/cure agent reaction: Variation in peak exotherm temperature," *Journal of Thermal Analysis*, vol. 47, no. 3, pp. 743–750, 1996.

[45] **ASTM International**, "E1356 - Standard Test Method for Assignment of the Glass Transition Temperatures by Differential Scanning Calorimetry." pp. 1–4, 2008.

[46] **M. R. Kamal and S. Sourour**, "Kinetics and thermal characterization of thermoset cure," *Polymer Engineering and Science*, vol. 13, no. 1, pp. 59–64, Jan. 1973.

[47] **S. Patra, P. M. Ajayan, and T. N. Narayanan**, "Dynamic mechanical analysis in materials science: The Novice's Tale," *Oxford Open Materials Science*, vol. 1, no. 1, Nov. 2020.

[48] **N. Saba, M. Jawaid, O. Y. Alothman, and M. T. Paridah**, "A review on dynamic mechanical properties of natural fibre reinforced polymer composites," *Construction and Building Materials*, vol. 106, pp. 149–159, 2016.

[49] **C. A. May and F. E. Weir**, "Dynamic mechanical properties of epoxy resins," *Polymer Engineering & Science*, vol. 2, no. 3, pp. 207–212, 1962.

[50] **B. S. Kim and T. Inoue**, "Dynamic mechanical and Fourier-transform infra-red analyses on the very late stage of the cure process in thermoset/thermoplastic blends: trifunctional epoxy/poly(ether sulfone)," *Polymer*, vol. 36, no. 10, pp. 1985–1989, 1995.

[51] **J. M. Cuevas, J. M. Laza, M. Correa, J. L. Vilas, M. Rodríguez, and L. M. León**, "Determination of the rheological behavior of epoxy-amine thermosets by dynamic mechanical analysis: Isothermal methods versus nonisothermal methods," *Journal of Polymer Science, Part B: Polymer Physics*, vol. 41, no. 17, pp. 1965–1977, 2003.

[52] **M. Sánchez-Cabezudo, R. M. Masegosa, C. Salom, and M. G. Prolongo**, "Correlations between the morphology and the thermo-mechanical properties in poly(vinyl acetate)/epoxy thermosets," *Journal of Thermal Analysis and Calorimetry*, vol. 102, no. 3, pp. 1025–1033, Dec. 2010.

[53] **N. Zheng, G. Fang, Z. Cao, Q. Zhao, and T. Xie**, "High strain epoxy shape memory polymer," *Polymer Chemistry*, vol. 6, no. 16, pp. 3046–3053, 2015.

[54] **L. Kehrer, D. Wicht, J. T. Wood, and T. Böhlke**, "Dynamic mechanical analysis of pure and fiber-reinforced thermoset- and thermoplastic-based polymers and free volume-based viscoelastic modeling," *GAMM Mitteilungen*, vol. 41, no. 1, pp. 1–16, 2018.

[55] **M. S. Chattha, R. A. Dickie, and K. R. Carduner**, "Epoxy-modified diallylbisphenol A and bis(maleimidophenyl)methane thermoset compositions: composition and dynamic mechanical thermal analysis," *Industrial & Engineering Chemistry Research*, vol. 28, no. 9, pp. 1438–1441, Sep. 1989.

[56] **B. Guo and D. Jia**, "Effects of epoxy content on dynamic mechanical behaviour of PEI-toughened dicyanate-novolac epoxy blends," *Polymer International*, vol. 53, no. 9, pp. 1378–1381, 2004.

[57] **W. Stark, H. Goering, U. Michel, and H. Bayerl**, "Online monitoring of thermoset post-curing by dynamic mechanical thermal analysis DMTA," *Polymer Testing*, vol. 28, no. 6, pp. 561–566, Sep. 2009.

[58] **A. Lavoratti, A. J. Zattera, and S. C. Amico**, "Mechanical and dynamic-mechanical properties of silane-treated graphite nanoplatelet/epoxy composites," *Journal of Applied Polymer Science*, vol. 135, no. 45, pp. 1–10, 2018.

[59] **A. Shabeer, A. Garg, S. Sundararaman, K. Chandrashekhara, V. Flanigan, and S. Kapila**, "Dynamic mechanical characterization of a soy based epoxy resin system," *Journal of Applied Polymer Science*, vol. 98, no. 4, pp. 1772–1780, 2005.

[60] **A. Chatterjee**, "Thermal degradation analysis of thermoset resins," *Journal of Applied Polymer Science*, vol. 114, no. 3, pp. 1417–1425, 2009.

[61] **S. E. Zeltmann, B. Chen, and N. Gupta**, "Thermal expansion and dynamic mechanical

analysis of epoxy matrix–borosilicate glass hollow particle syntactic foams," *Journal of Cellular Plastics*, vol. 54, no. 3, pp. 463–481, 2018.

[62] **J. A. Nairn**, "Matrix Microcracking in Composites," in *Comprehensive Composite Materials*, vol. 2, R. Talreja and J.-A. Månson, Eds. Elsevier, 2000, pp. 403–432.

[63] **J. A. Nairn and S. Hu**, "Matrix Microcracking," in *Damage Mechanics of Composite Materials*, vol. 1, R. Talreja, Ed. Elsevier, 1994, pp. 1–46.

[64] **M. Naebe, M. M. Abolhasani, H. Khayyam, A. Amini, and B. Fox**, "Crack damage in polymers and composites: A review," *Polymer Reviews*, vol. 56, no. 1, pp. 31–69, 2016.

[65] **D. K. Hsu, V. Dayal, M. Gerken, A. Subramanian, K.-H. Im, and D. J. Barnard**, "A Study of Microcracks and Delaminations in Composite Laminates," in *Nondestructive Testing of Materials and Structures*, vol. 6, no. February, O. Güneş and Y. Akkaya, Eds. Dordrecht: Springer Netherlands, 2013, pp. 661–667.

[66] **Y. X. He *et al.***, "Micro-crack behavior of carbon fiber reinforced thermoplastic modified epoxy composites for cryogenic applications," *Composites Part B: Engineering*, vol. 44, no. 1, pp. 533–539, 2013.

[67] **D. Y. Wu, S. Meure, and D. Solomon**, "Self-healing polymeric materials: A review of recent developments," *Progress in Polymer Science*, vol. 33, no. 5, pp. 479–522, 2008.

[68] **I. L. Hia, V. Vahedi, and P. Pasbakhsh**, "Self-Healing Polymer Composites: Prospects, Challenges, and Applications," *Polymer Reviews*, vol. 56, no. 2, pp. 225–261, 2016.

[69] **N. Jee Kanu, E. Gupta, U. Kumar Vates, and G. Kumar Singh**, "Self-healing composites: A state-of-the-art review," *Composites Part A: Applied Science and Manufacturing*, vol. 121, no. April, pp. 474–486, 2019.

[70] **C. Dry**, "Procedures developed for self-repair of polymer matrix composite materials," *Composite Structures*, vol. 35, no. 3, pp. 263–269, Jul. 1996.

[71] **S. R. White *et al.***, "Autonomic healing of polymer composites.," *Nature*, vol. 409, pp. 794–797, 2001.

[72] **X. Chen *et al.***, "New Thermally Remendable Highly Cross-Linked Polymeric Materials.," *Macromolecules*, vol. 36, pp. 1802–1807, 2003.

[73] **J. S. Park, T. Darlington, A. F. Starr, K. Takahashi, J. Riendeau, and H. Thomas Hahn**, "Multiple healing effect of thermally activated self-healing composites based on Diels-Alder reaction," *Composites Science and Technology*, vol. 70, no. 15, pp. 2154–2159, 2010.

[74] **B. J. Adzima, C. J. Kloxin, and C. N. Bowman**, "Externally triggered healing of a thermoreversible covalent network via self-limited hysteresis heating," *Advanced Materials*, vol. 22, no. 25, pp. 2784–2787, 2010.

[75] **D. H. Turkenburg and H. R. Fischer**, "Diels-Alder based, thermo-reversible cross-linked epoxies for use in self-healing composites," *Polymer (United Kingdom)*, vol. 79, pp. 187–194, 2015.

[76] **M. Zako and N. Takano**, "Intelligent material systems using epoxy particles to repair microcracks and delamination damage in GFRP," *Journal of Intelligent Material Systems and Structures*, vol. 10, pp. 836–841, 1999.

[77] **K. Pingkarawat, T. Bhat, D. A. Craze, C. H. Wang, R. J. Varley, and A. P. Mouritz**, "Healing of carbon fibre–epoxy composites using thermoplastic additives," *Polymer Chemistry*, vol. 4, pp. 5007–5015, 2013.

[78] **K. Pingkarawat, C. Dell'Olio, R. J. Varley, and A. P. Mouritz**, "Poly(ethylene-co-methacrylic acid) (EMAA) as an efficient healing agent for high performance epoxy networks using diglycidyl ether of bisphenol A (DGEBA)," *Polymer (United Kingdom)*, vol. 92, pp. 153–163, 2016.

[79] **R. J. Varley, D. A. Craze, A. P. Mouritz, and C. H. Wang**, "Thermoplastic Healing in Epoxy Networks: Exploring Performance and Mechanism of Alternative Healing Agents," *Macromolecular Materials and Engineering*, vol. 298, no. 11, pp. 1232–1242, Nov. 2013.

[80] **K. Pingkarawat, C. H. Wang, R. J. Varley, and A. P. Mouritz**, "Mechanical properties of mendable composites containing self-healing thermoplastic agents," *Composites Part A: Applied Science and Manufacturing*, vol. 65, pp. 10–18, 2014.

[81] **S. A. Hayes, F. R. Jones, K. Marshiya, and W. Zhang**, "A self-healing thermosetting composite material," *Composites Part A: Applied Science and Manufacturing*, vol. 38, no. 4, pp. 1116–1120, 2007.

[82] **S. A. Hayes, W. Zhang, M. Branthwaite, and F. R. Jones**, "Self-healing of damage in fibre-reinforced polymer-matrix composites," *Journal of The Royal Society Interface*, vol. 4, no. 13, pp. 381–387, 2007.

[83] **R. J. Varley, B. Dao, C. Pillsbury, S. J. Kalista, and F. R. Jones**, "Low-molecular-weight thermoplastic modifiers as effective healing agents in mendable epoxy networks," *Journal of Intelligent Material Systems and Structures*, vol. 25, no. 1, pp. 107–117, Jan. 2014.

[84] **X. Luo, R. Ou, D. E. Eberly, A. Singhal, W. Viratyaporn, and P. T. Mather**, "A

thermoplastic/thermoset blend exhibiting thermal mending and reversible adhesion," *ACS Applied Materials and Interfaces*, vol. 1, no. 3, pp. 612–620, 2009.

[85] **A. Cohades, E. Manfredi, J.-C. Plummer, and V. Michaud**, "Thermal mending in phase-separated Poly(ε-caprolactone)/epoxy blends.," *European Polymer Journal*, vol. 81, pp. 114–128, 2016.

[86] **S. Meure, D. Y. Wu, and S. Furman**, "Polyethylene-co-methacrylic acid healing agents for mendable epoxy resins," *Acta Materialia*, vol. 57, no. 14, pp. 4312–4320, 2009.

[87] **S. Meure, S. Furman, and S. Khor**, "Poly[ethylene-co-(methacrylic acid)] healing agents for mendable carbon fiber laminates," *Macromolecular Materials and Engineering*, vol. 295, no. 5, pp. 420–424, 2010.

[88] **S. Meure, D.-Y. Wu, and S. A. Furman**, "FTIR study of bonding between a thermoplastic healing agent and a mendable epoxy resin," *Vibrational Spectroscopy*, vol. 52, no. 1, pp. 10–15, Jan. 2010.

[89] **S. Meure, R. J. Varley, D. Y. Wu, S. Mayo, K. Nairn, and S. Furman**, "Confirmation of the healing mechanism in a mendable EMAA-epoxy resin," *European Polymer Journal*, vol. 48, no. 3, pp. 524–531, 2012.

[90] **K. Pingkarawat, C. H. Wang, R. J. Varley, and A. P. Mouritz**, "Self-healing of delamination fatigue cracks in carbon fibre-epoxy laminate using mendable thermoplastic," *Journal of Materials Science*, vol. 47, no. 10, pp. 4449–4456, 2012.

[91] **C. H. Wang, K. Sidhu, T. Yang, J. Zhang, and R. Shanks**, "Interlayer self-healing and toughening of carbon fibre/epoxy composites using copolymer films," *Composites Part A: Applied Science and Manufacturing*, vol. 43, no. 3, pp. 512–518, 2012.

[92] **T. Yang, C. H. Wang, J. Zhang, S. He, and A. P. Mouritz**, "Toughening and self-healing of epoxy matrix laminates using mendable polymer stitching," *Composites Science and Technology*, vol. 72, no. 12, pp. 1396–1401, 2012.

[93] **K. Pingkarawat, C. H. Wang, R. J. Varley, and A. P. Mouritz**, "Self-healing of delamination cracks in mendable epoxy matrix laminates using poly[ethylene-co-(methacrylic acid)] thermoplastic," *Composites Part A: Applied Science and Manufacturing*, vol. 43, no. 8, pp. 1301–1307, Aug. 2012.

[94] **K. Pingkarawat, C. H. Wang, R. J. Varley, and A. P. Mouritz**, "Healing of fatigue delamination cracks in carbon-epoxy composite using mendable polymer stitching," *Journal of Intelligent Material Systems and Structures*, vol. 25, no. 1, pp. 75–86, 2014.

[95] **M. Q. Zhang and M. Z. Rong**, *Self-healing Polymers and Polymer Composites*. John Wiley & Sons, Inc., 2011.

[96] **R. S. Trask, H. R. Williams, and I. P. Bond**, "Self-healing polymer composites: mimicking nature to enhance performance.," *Bioinspiration & biomimetics*, vol. 2, no. 1, pp. 1–9, 2007.

[97] **Y. C. Yuan, T. Yin, M. Z. Rong, and M. Q. Zhang**, "Self healing in polymers and polymer composites. Concepts, realization and outlook: A review," *Express Polymer Letters*, vol. 2, no. 4, pp. 238–250, 2008.

[98] **E. B. Murphy and F. Wudl**, "The world of smart healable materials," *Progress in Polymer Science (Oxford)*, vol. 35, no. 1–2, pp. 223–251, 2010.

[99] **A. Cohades and V. Michaud**, "Thermal mending in E-glass reinforced poly(ε-caprolactone)/epoxy blends," *Composites Part A: Applied Science and Manufacturing*, vol. 99, pp. 129–138, Aug. 2017.

[100] **R. P. Wool and K. M. O'Connor**, "Time Dependence of Crack Healing," *Polymer letters edition*, vol. 20, no. 13, pp. 7–16, 1982.

[101] **ASTM International**, "D5045 - Standard Test Methods for Plane-Strain Fracture Toughness and Strain Energy Release Rate of Plastic Materials 1." pp. 1–9, 2013.

[102] **E. N. Brown**, "Use of the tapered double-cantilever beam geometry for fracture toughness measurements and its application to the quantification of self-healing," *Journal of Strain Analysis for Engineering Design*, vol. 46, no. 3, pp. 167–186, 2011.

[103] **C. D. Olio, Q. Yuan, and R. J. Varley**, "Epoxy / Poly (ethylene- co -methacrylic acid) Blends as Thermally Activated Healing Agents in an Epoxy / Amine Network," *Macromolecular Materials and Engineering*, vol. 300, pp. 70–79, 2014.

[104] **V. Authors**, *Self-healig Polymers: From Principles to Applications*. Wiley-VCH, 2013.

[105] **K. Pingkarawat, C. D. Olio, R. J. Varley, and a P. Mouritz**, "Thermally Activated Healing in High Performance Carbon Fibre / Epoxy Composites," no. July, pp. 19–24, 2015.

[106] **R. J. Varley and F. Charve**, "EMAA as a healing agent for mendable high temperature epoxy amine thermosets," *Composites Part A: Applied Science and Manufacturing*, vol. 43, no. 7, pp. 1073–1080, 2012.

[107] **A. Azevedo do Nascimento, F. Fernandez, F. S. da Silva, E. P.C. Ferreira, J. D. D. Melo, and A. P. Cysne Barbosa**, "Addition of poly (ethylene-co-methacrylic acid) (EMAA) as self-healing agent to carbon-epoxy composites," *Composites Part A: Applied Science and*

Manufacturing, vol. 137, no. February, p. 106016, Oct. 2020.

[108] **S. C. Garcea, Y. Wang, and P. J. Withers**, "X-ray computed tomography of polymer composites," *Composites Science and Technology*, vol. 156, pp. 305–319, Mar. 2018.

[109] **R. Pyrz**, "Application of X-Ray Microtomography to the Study of Polymer Composites," in *SAE Technical Papers*, 1999.

[110] **B. L. Silva, C. Gomes de Moura Filho, J. D. Diniz Melo, and A. P. Cysne Barbosa**, "The role of poly (ethylene-co-methacrylic acid) (EMAA) on cure kinetics and thermomechanical properties of epoxy," *Polymer Bulletin*, no. 0123456789, 2021.

[111] **J. Kim and Y. Mai**, *Engineered Interfaces in Fiber Reinforced Composites*, 1 st editi. Elsevier, 1998.

[112] **R. dos S. Escarpini Filho and S. P. C. Marques**, "A Model for Homogenization of Linear Viscoelastic Periodic Composite Materials with Imperfect Interface," *Latin American Journal of Solids and Structures*, vol. 13, no. 14, pp. 2706–2735, 2016.

[113] **S.-J. Park and M.-K. Seo**, *Interface Science and Composites*, First edit. 2011.

[114] **F. R. Jones**, "A Review of Interphase Formation and Design in Fibre-Reinforced Composites," *Journal of Adhesion Science and Technology*, vol. 24, no. 1, pp. 171–202, Jan. 2010.

[115] **G. Kalinka, A. Leistner, and A. Hampe**, "Characterisation of the fibre/matrix interface in reinforced polymers by the push-in technique," *Composites Science and Technology*, vol. 57, no. 8, pp. 845–851, 1997.

[116] **M. Sahin *et al.***, "Tailoring the interfaces in glass fiber-reinforced photopolymer composites," *Polymer*, vol. 141, pp. 221–231, 2018.

[117] **C. Medinam, J. M. Molina-Aldareguía, C. González, M. F. Melendrez, P. Flores, and J. Llorca**, "Comparison of push-in and push-out tests for measuring interfacial shear strength in nano-reinforced composite materials," *Journal of Composite Materials*, vol. 50, no. 12, pp. 1651–1659, 2016.

[118] **M. Rodríguez, J. M. Molina-Aldareguía, C. González, and J. Llorca**, "A methodology to measure the interface shear strength by means of the fiber push-in test," *Composites Science and Technology*, vol. 72, no. 15, pp. 1924–1932, 2012.

[119] **A. Hampe, G. Kalinka, S. Meretz, and E. Schulz**, "An advanced equipment for single-fibre pull-out test designed to monitor the fracture process," *Composites*, vol. 26, no. 1, pp. 40–46, 1995.

[120] **K. Wakabayashi and R. A. Register**, "Micromechanical interpretation of the modulus of ethylene–(meth)acrylic acid copolymers," *Polymer*, vol. 46, no. 20, pp. 8838–8845, Sep. 2005.

[121] **H. E. Kissinger**, "Reaction Kinetics in Differential Thermal Analysis," *Analytical Chemistry*, vol. 29, no. 11, pp. 1702–1706, 1957.

[122] **T. Yang, J. Zhang, A. P. Mouritz, and C. H. Wang**, "Healing of carbon fibre-epoxy composite T-joints using mendable polymer fibre stitching," *Composites Part B: Engineering*, vol. 45, no. 1, pp. 1499–1507, 2013.

[123] **K. Hargou, K. Pingkarawat, A. P. Mouritz, and C. H. Wang**, "Ultrasonic activation of mendable polymer for self-healing carbon-epoxy laminates," *Composites Part B: Engineering*, vol. 45, no. 1, pp. 1031–1039, 2013.